



FORSCHUNGSZENTRUM JÜLICH GmbH

Institut für Sicherheitsforschung und Reaktortechnik

EXPERIMENTAL INVESTIGATION OF CORROSION OF IG-110 GRAPHITE BY STEAM

H.-K. Hinssen

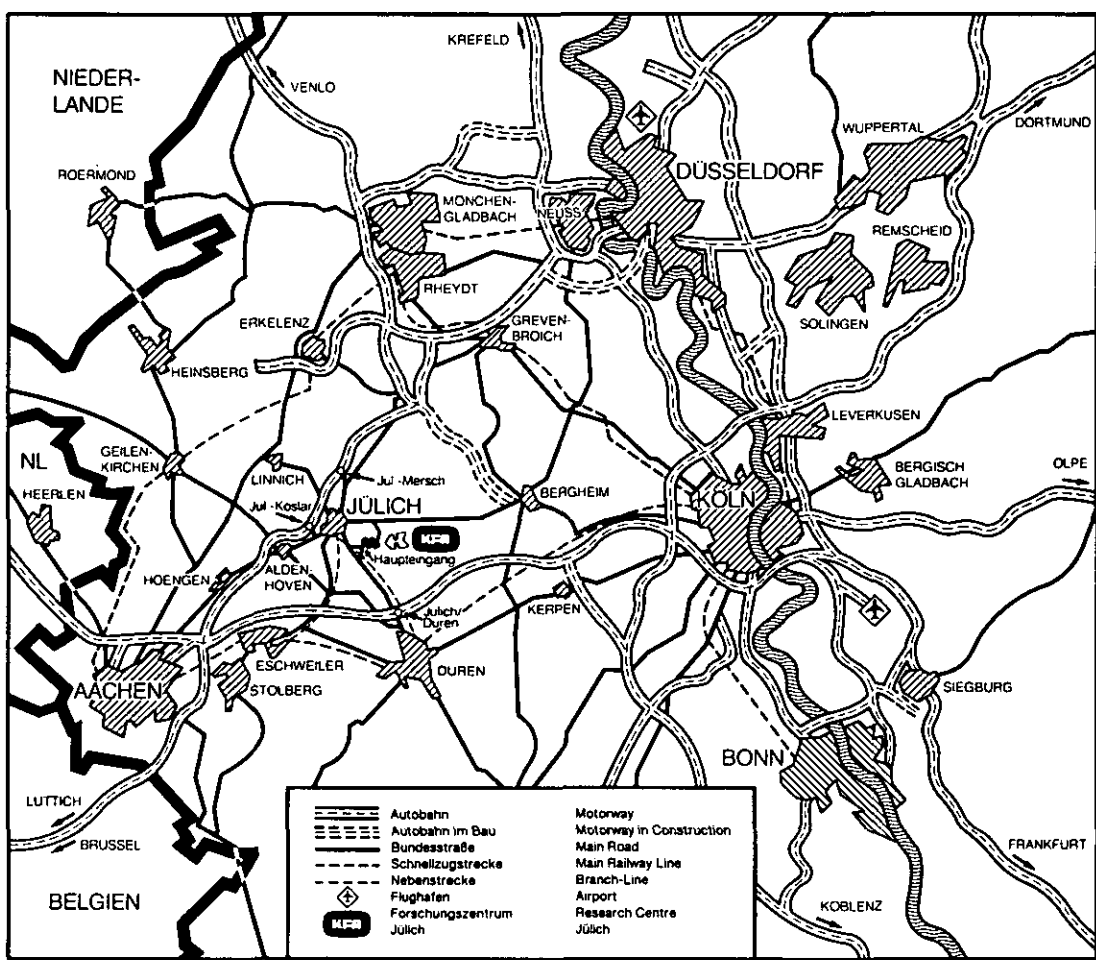
W. Katscher

K.-J. Loenißen

Jül-Spez-578

July 1990

ISSN 0343-7639



Als Manuskript gedruckt

Forschungszentrum Jülich: Spezielle Berichte Nr. 578

Institut für Sicherheitsforschung und Reaktortechnik Jül-Spez-578

Zu beziehen durch: ZENTRALBIBLIOTHEK · Forschungszentrum Jülich GmbH

Postfach 1913 · D-5170 Jülich (Bundesrepublik Deutschland)

Telefon: 02461/61-0 · Telefax: 02461/61-6103 · Telex: 833556-70 kfa d

**EXPERIMENTAL INVESTIGATION OF
CORROSION OF IG-110 GRAPHITE
BY STEAM**

H.-K. Hinssen

W. Katscher

K.-J. Loenißen

ABSTRACT

In the framework of a cooperation between the Japan Atomic Energy Research Institute (JAERI) and the Research Centre of Jülich (KFA) experiments on the corrosion of the Japanese graphite IG-110 by water vapour were carried out. The temperature of the graphite samples and the water vapour partial pressure were kept constant at 1000°C/474 mbar. The total pressure in the test loop using helium as carrier gas was varied between 3 and 55 bar. Burn-off and pressure dependent reaction rates and density profiles in corroded samples were measured.

As expected, the burn-off dependence of the reaction rate decreased with increasing pressure, while only a comparably low pressure dependence of the reaction rate was found. The latter indicates that the influence of the Knudsen diffusion is given even for the highest pressure.

This finding is in fair agreement with the results of density profile measurements carried out at a couple of corroded samples, which also revealed a relatively small pressure dependence of the "penetration depth". Correlations for the caculation of reaction rates and the penetration depth are given.

C O N T E N T S

1. INTRODUCTION	1
2. THE GRAPHITE SPECIMENS	1
2.1 Material properties	1
2.2 Sample manufacturing	1
3. EXPERIMENTAL AND RESULTS	3
3.1 The test facility HOVA	3
3.2 Selected experimental parameters	6
3.3 Experimental procedure	6
3.4 Evaluation of the reaction kinetic experiments	7
3.4.1 Temperature correction	7
3.4.2 Burn-off dependence of reaction rates	14
3.4.3 Pressure dependence of reaction rates	18
3.5 Density Profiles	20
3.5.1 Selection of samples, profiling method	21
3.5.2 The evaluation method	23
3.5.3 Results	25
4. CONCLUSION	31
5. LIST OF SYMBOLS	32
6. REFERENCES	33
7. APPENDIX	34

1. INTRODUCTION

In the framework of a cooperation between the Japan Atomic Energy Research Institute (JAERI) and the KFA Jülich corrosion experiments on the Japanese IG-110 graphite were carried out in the high pressure corrosion test facility HOVA of the Institute for Safety Research and Reactor Technique (ISR).

The aim of these experiments was the provision of data on the dependence of reaction rates of the water gas reaction on total gas pressure in the in-pore diffusion controlled regime.

Starting with a short description of the IG-110 material and the origin and production of the samples, the kinetic experiments and the results presented in the form of burn-off and pressure dependent reaction rates are described. Results from measurements of density profiles in the corroded material are added.

In the appendix data are compiled which may be useful for a more detailed evaluation.

2. THE GRAPHITE SPECIMENS

2.1 Material properties

IG-110 is a fine grain graphite manufactured by Toyo Tanso Co Ltd. as candidate structural material for the core components of high temperature gas-cooled nuclear reactors (HTR's). It consists of a petroleum coke filler with an average grain size of 10 µm, a coal tar pitch binder and is formed by isostatic moulding. The temperature of final heat treatment is 2800°C, the bulk density 1.75 g/cm³ and the ash content <80 ppm.

2.2 Sample manufacturing

For the corrosion experiments tubular graphite samples as shown in fig. 1 were manufactured by JAERI, the material being taken from a graphite block as shown in fig. 2.

As described in chapter 3, for each corrosion experiment always 7 graphite samples are stacked in the test section to form a tube through which the corrosive gas is pumped. Table 1 gives the sample plan for the different experiments. The outer samples, designated by T, were taken from German graphites in order to

smoothen the axial temperature profile (see below), while the central 5 samples consisted of IG-110.

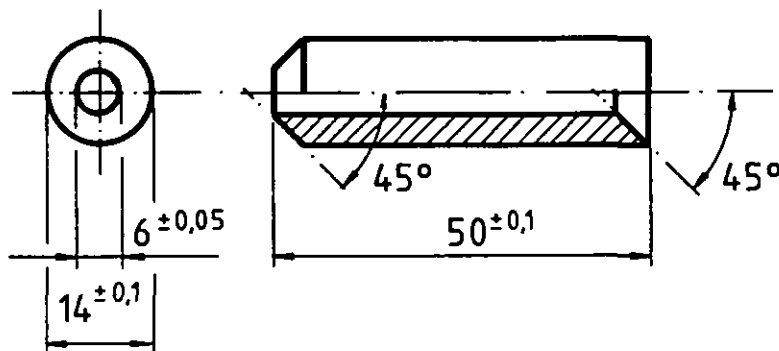


Fig. 1: Graphite sample for corrosion experiments

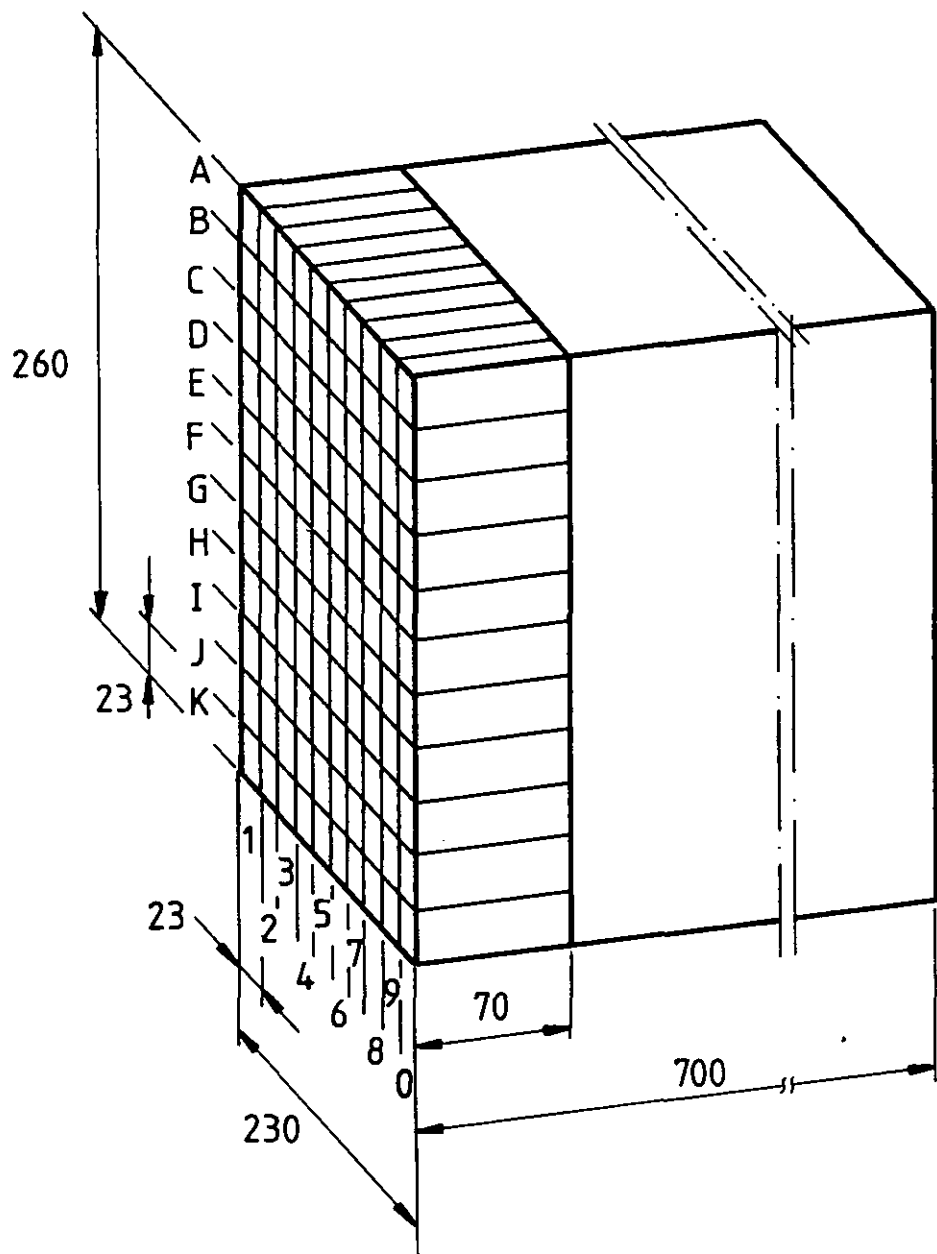


Fig. 2: Graphite block and sampling plan

Gaspressure	3 bar		7 bar			15 bar		55 bar	
Sample column	1	2	1	2	3	1	2	1	2
Sample No	T	T	T	T	T	T	T	T	T
	B1	B2	B3	B4	B0	B5	B6	B7	B8
	C2	E6	C3	E7	D2	I2	E5	I3	F7
	G7	F5	G4	F6	D5	F4	G5	E4	G6
	H4	C9	H5	C8	D7	H6	I8	H7	I9
	C1	D1	E1	F1	C0	G1	H1	I1	J1
	T	T	T	T	T	T	T	T	T

Table 1: Sample arrangement in the different experiments

3. EXPERIMENTAL AND RESULTS

3.1 The test facility HOVA

The experiments were carried out in the high pressure graphite corrosion test facility HOVA. This as well as the experimental procedure and the evaluation method for the reaction kinetic experiments is described in detail in /1/ and shall only be outlined here as far as is regarded necessary for basic understanding.

HOVA is a closed loop, in the test section of which graphite samples as shown in fig. 1 are stacked to form a tube of approx. 320 mm length. This tube is arranged between electrodes and heated to a desired temperature by using the self-resistance of the graphite. A mixture of helium and steam is pumped through the tube, which is placed inside a pressure vessel as shown in fig. 3; in fig. 4 a scheme of the entire HOVA facility is presented.

The temperature of the graphite tube is controlled and kept constant within ± 2 K at a fixed center position by an optical pyrometer, which is connected to the energy supply. Additionally the temperature of each sample is measured individually by a set of glass fibre optics which are connected to silicon detectors outside the pressure vessel. The optics can be moved in axial direction alongside the graphite tube to give a complete axial temperature scan. At a temperature of 1000°C the maximum deviation between indicated and true temperature is given as ± 5.2 K. The de-

viation between the inner and outer surface temperature of the samples was found to be <5 K.

Further basic data of the loop are:

max. total pressure:	60 bar
max. water vapor partial pressure:	4 bar
max. test section temperature:	1400°C
max. flow rate:	400 l/min

For further details see /1/.

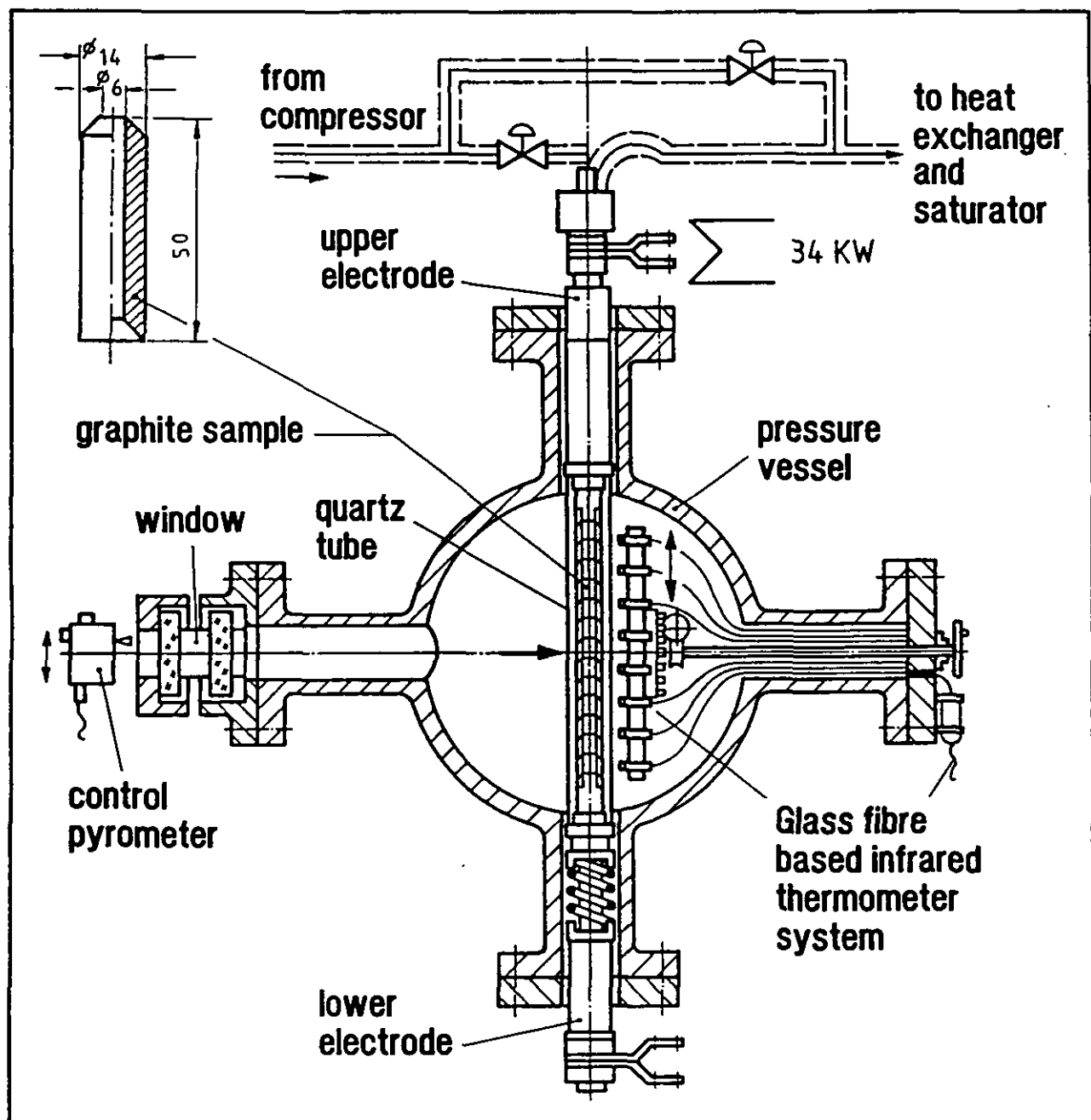
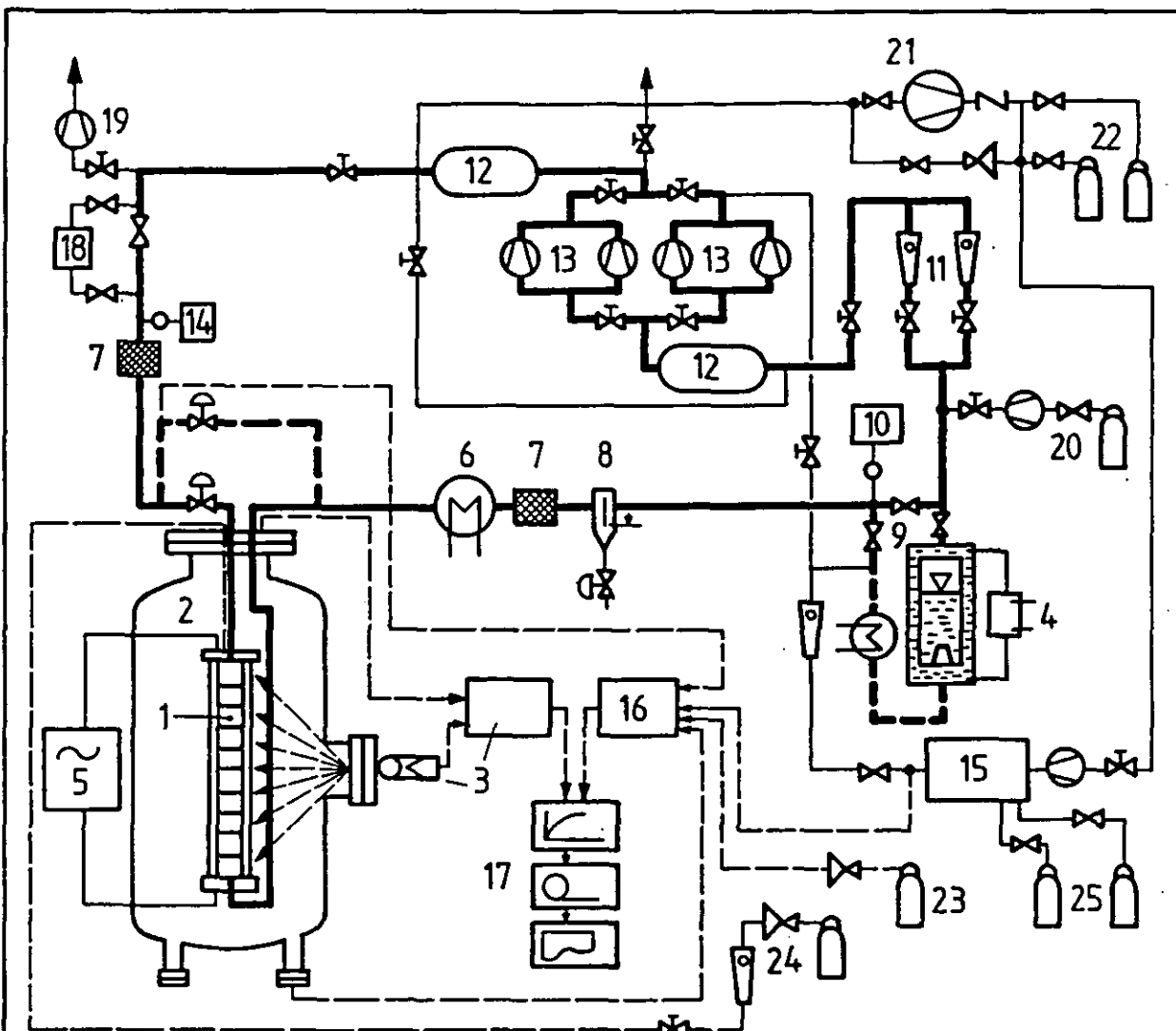


Fig. 3: HOVA test-section



- | | |
|---|-----------------------------------|
| 1 test section | 13 membrane compressors |
| 2 pressure vessel | 14 hygrometer 2 |
| 3 control pyrometer and
temperature measurement device | 15 gas clean-up plant |
| 4 thermostat | 16 gas chromatograph |
| 5 electricity supply for test section | 17 data processing system |
| 6 heat exchanger | 18 low temperature filter |
| 7 filter | 19 vacuum pump |
| 8 condensate discharge | 20 hydrogen pump |
| 9 saturator | 21 auxiliary compressor |
| 10 hygrometer 1 | 22 helium storage pressure vessel |
| 11 flow meters | 23 calibration gases |
| 12 pressure pulse dampers | 24 purge helium |
| | 25 bottles for regeneration gases |

Fig. 4: Scheme of HOVA

3.2 Selected experimental parameters

In order to limit the experimental parameters, the graphite temperature, the water vapor partial pressure and the flow rate were kept constant for all test runs at 1000°C, 474 mbar (80°C dew point) and 100 l/min (standard conditions) respectively. The total pressure was varied, the pressures selected being 3, 7, 15 and 55 bar.

3.3 Experimental procedure

The following procedure was selected: Prior to corrosion, the graphite samples are cleaned from graphite dust in acetone in an ultrasonic cleaning device, dried at 200°C, weighed (accuracy better 0.1 mg) and installed in the test section. After closing the pressure vessel, the loop is evacuated and purged by helium for a couple of times, until the oxygen content remains below 5 vpm. The loop is then pressurized by helium to the desired pressure. By-passing the test section, the helium is saturated with water vapour (max. temperature fluctuations in saturator ± 0.1 K), while the test section is heated up. After having reached the desired values, the bypass is closed and simultaneously the He/H₂O-mixture is pumped through the test section. Special care is taken to restrict corrosion to the inner surface of the graphite samples. This is accomplished by injecting pure helium into the gap between the graphite sample stack and the surrounding quartz tube, keeping a slight over-pressure. Temperature scans are taken over the entire length of the test section in time steps of 10 to 15 minutes (see appendix). As it is not possible to use the gas clean-up plant during the test runs, the concentration of the reaction products is frequently measured via the gas chromatograph to prove that the proportion of H₂/H₂O remains below 1/20. This is done to keep inhibition effects of hydrogen on the water gas reaction kinetics negligible.

After a given time, which is dependent on the burn-off of the samples and the gas pressure (at low burn-off typically between 0.3 and 1 hour), the test is terminated by isolating the test section from the loop, purging it by clean helium and cooling it down. The helium in the loop is cleaned in the clean-up plant and pumped

into the storage vessels. Then the samples are removed from the test section, weighed and re-installed for the next test run. Thus burn-off dependent reaction rates are established. Finally the test series is terminated when reaction rates have reached a stable value.

It should be mentioned here that the latter in several cases could not be achieved as corrosion induced changes in the electrical resistivity provided changes in the temperature distribution, which forced termination of the experiment, or that the decreasing mechanical strength caused a collapse of the test section. This makes an extrapolation to reaction rates at "infinite burn-off" necessary to produce comparable data (see chapter 3.4.2 and 3.4.3).

3.4 Evaluation of the reaction kinetic experiments

3.4.1 Temperature correction

A key value for the evaluation of the kinetic experiments is the graphite temperature. As was mentioned in chapter 3.3, the experimental method had to allow for certain local and also time dependent temperature deviations from the desired value, which only can be kept constant at that spot which is the reference for the control pyrometer. To limit the experimental uncertainties, in the following only such samples were evaluated, which were corroded at a temperature differing not more than ± 20 K from the nominal value (1000°C).

During temperature measurement the axial temperature distribution over the sample length was registered in steps of 5 mm distance. All temperature plots are compiled in the appendix. From these values a mean temperature T_s of the individual sample was calculated by using formula [1] which allows for the stronger influence of increasing temperatures on the reaction kinetics. For the activation energy E_A a value of 166 KJ/mol was taken referring to measurements at the DRAGON Project /2/. The real activation energy should not differ more than $\pm 25\%$ from this value. Such a deviation would cause deviations in the reaction rate at 1000°C of $\pm 7\%$.

$$T_S = \frac{\sum_{j=1}^{j=l} T_j \exp \left[\frac{-E_A}{R T_j} \right]}{\sum_{j=l}^{j=n} \exp \left[\frac{-E_A}{R T_j} \right]} \quad [1]^1$$

The time dependent changes of T_S are corrected to a mean temperature T_R valid for the whole corrosion time between two weight measurements using formula [2], where Δt_S was defined as shown in the example in fig. 5.

$$T_R = \frac{\sum_{S=1}^{S=n} T_S \exp \left[\frac{-E_A}{R T_S} \right] \frac{\Delta t_S}{t_R}}{\sum_{S=1}^{S=n} \exp \left[\frac{-E_A}{R T_S} \right] \frac{\Delta t_S}{t_R}} \quad [2]$$

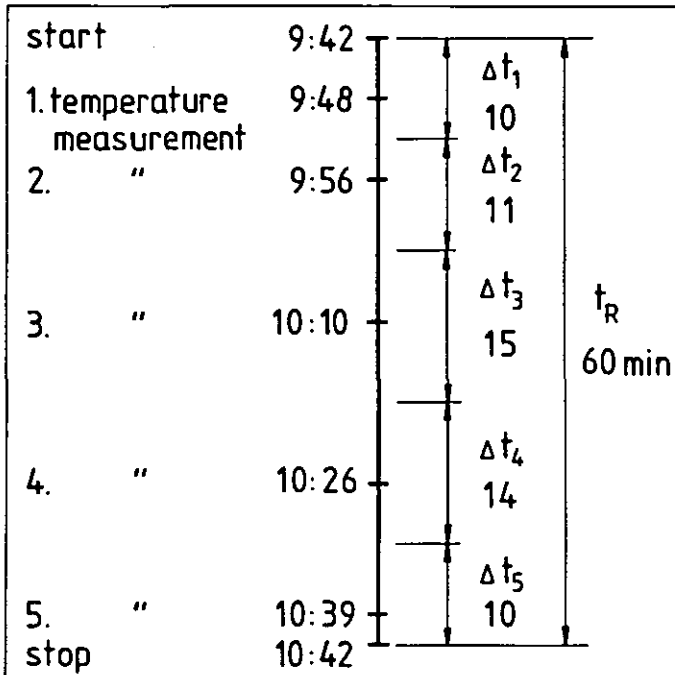


Fig. 5: Example for determination of T_R

The "true" mean reaction rate between two weight measurements is established by dividing the weight loss of the sample by the cor-

¹see list of symbols

rosion time and the original geometrical surface of the bore. For comparison, these values are corrected to a mean temperature of 1000°C using formula [3].

$$RG_{(1273K)} = RG_{T_R} \exp \left[\frac{-E_A}{R_m} \left(\frac{1}{1273} - \frac{1}{T_R} \right) \right] \quad [3]$$

Table 2 gives the results for all corrosion test runs. It has to be mentioned here that for sample column 3 in the 7 bar experiment and column 2 in the 55 bar case the values for run No. 1 are missing. In these cases at the first (short) run reaction rates were found which were at the level of those of the 3rd respective 4th run. Part of an explanation for this abnormal behaviour could be due to some instability in the saturator operation. In these two cases the state at the end of the first run was taken as the starting point for the evaluation.

3 bar

Sample No	Run No	Mean Temperature T_R [°C]	Burn-off [mg cm ⁻²]	Reaction Rate RG_{T_R} [mg cm ⁻² sec ⁻¹]	Reaction Rate [1000 °C] $RG_{(1273K)}$ [mg cm ⁻² sec ⁻¹]
B1	1	995.	0.8194E+00	0.9104E-03	0.9746E-03
	2	986.	0.2597E+01	0.1064E-02	0.1265E-02
	3	991.	0.5963E+01	0.1784E-02	0.1989E-02
C2	1	992.	0.6781E+00	0.7535E-03	0.8325E-03
	2	989.	0.2186E+01	0.9220E-03	0.1054E-02
	3	1007.	0.5598E+01	0.1913E-02	0.1762E-02
	4	1007.	0.1309E+02	0.2725E-02	0.2501E-02
	5	1004.	0.2785E+02	0.3650E-02	0.3474E-02
	6	995.	0.4822E+02	0.3895E-02	0.4127E-02
G7	1	997.	0.7716E+00	0.8573E-03	0.8930E-03
	2	995.	0.2669E+01	0.1251E-02	0.1327E-02
	3	998.	0.6388E+01	0.1921E-02	0.1972E-02
	4	999.	0.1374E+02	0.2646E-02	0.2669E-02
	5	999.	0.2835E+02	0.3646E-02	0.3698E-02
	6	994.	0.4940E+02	0.4151E-02	0.4461E-02

Sample No	Run No	Mean Temperature T_R [°C]	Burn-off [mg cm ⁻²]	Reaction Rate RG_{T_R} [mg cm ⁻² sec ⁻¹]	Reaction Rate [1000 °C] $RG_{(1273K)}$ [mg cm ⁻² sec ⁻¹]
H4	1	1008.	0.9716E+00	0.1080E-02	0.9767E-03
	2	1009.	0.3535E+01	0.1768E-02	0.1585E-02
	3	1006.	0.8664E+01	0.2620E-02	0.2429E-02
	4	1009.	0.1902E+02	0.3789E-02	0.3404E-02
	5	1012.	0.4075E+02	0.5522E-02	0.4778E-02
C1	1	1009.	0.7606E+00	0.8451E-03	0.7596E-03
	2	1012.	0.2684E+01	0.1292E-02	0.1119E-02
	3	1005.	0.6204E+01	0.1746E-02	0.1650E-02
	4	1007.	0.1289E+02	0.2407E-02	0.2216E-02
	5	1008.	0.2620E+02	0.3323E-02	0.3030E-02
E6	1	1000.	0.1051E+01	0.1167E-02	0.1171E-02
	2	1015.	0.3672E+01	0.1745E-02	0.1459E-02
	3	1006.	0.8315E+01	0.2276E-02	0.2120E-02
	4	1011.	0.1718E+02	0.3216E-02	0.2798E-02
F5	1	1001.	0.9699E+00	0.1078E-02	0.1060E-02
	2	1002.	0.3063E+01	0.1248E-02	0.1217E-02
	3	1002.	0.6997E+01	0.2082E-02	0.2022E-02
	4	1001.	0.1409E+02	0.2379E-02	0.2343E-02
	5	1003.	0.2732E+02	0.3313E-02	0.3175E-02
	6	1005.	0.4800E+02	0.4346E-02	0.4098E-02
C9	1	1008.	0.1037E+01	0.1153E-02	0.1051E-02
	2	1004.	0.3255E+01	0.1312E-02	0.1252E-02
	3	1008.	0.7566E+01	0.2319E-02	0.2093E-02
	4	1002.	0.1533E+02	0.2576E-02	0.2520E-02
	5	1001.	0.2926E+02	0.3440E-02	0.3406E-02
	6	1003.	0.5058E+02	0.4459E-02	0.4287E-02

7 bar

Sample No	Run No	Mean Temperature T_R [°C]	Burn-off [mg cm ⁻²]	Reaction Rate RG_{T_R} [mg cm ⁻² sec ⁻¹]	Reaction Rate [1000 °C] $RG_{(1273K)}$ [mg cm ⁻² sec ⁻¹]
B3	1	998.	0.6603E+00	0.7336E-03	0.7527E-03
	2	996.	0.3219E+01	0.1407E-02	0.1487E-02
	3	998.	0.8448E+01	0.1850E-02	0.1885E-02
C3	1	1002.	0.6060E+00	0.6734E-03	0.6561E-03
	2	991.	0.2903E+01	0.1252E-02	0.1404E-02
	3	992.	0.7496E+01	0.1612E-02	0.1780E-02
G4	1	996.	0.6579E+00	0.7310E-03	0.7639E-03

Sample No	Run No	Mean Temperature T_R [°C]	Burn-off [mg cm ⁻²]	Reaction Rate RG_{T_R} [mg cm ⁻² sec ⁻¹]	Reaction Rate [1000 °C] $RG_{(1273K)}$ [mg cm ⁻² sec ⁻¹]
	2	996.	0.3343E+01	0.1501E-02	0.1571E-02
	3	997.	0.9248E+01	0.2154E-02	0.2244E-02
H5	1	1008.	0.7277E+00	0.8086E-03	0.7327E-03
	2	1013.	0.4147E+01	0.1993E-02	0.1693E-02
	3	1017.	0.1268E+02	0.3246E-02	0.2635E-02
E1	1	998.	0.5311E+00	0.5901E-03	0.6027E-03
	2	1006.	0.2947E+01	0.1396E-02	0.1296E-02
	3	1011.	0.8903E+01	0.2262E-02	0.1975E-02
E7	1	1017.	0.1210E+01	0.1345E-02	0.1087E-02
	2	1000.	0.5280E+01	0.2118E-02	0.2126E-02
	3	997.	0.1187E+02	0.2074E-02	0.2154E-02
	4	1007.	0.2306E+02	0.2762E-02	0.2531E-02
F6	1	1002.	0.8604E+00	0.9560E-03	0.9353E-03
	2	1000.	0.4349E+01	0.1947E-02	0.1935E-02
	3	1003.	0.1122E+02	0.2357E-02	0.2277E-02
	4	1000.	0.2269E+02	0.2676E-02	0.2663E-02
C8	1	994.	0.6660E+00	0.7400E-03	0.7982E-03
	2	1004.	0.3668E+01	0.1730E-02	0.1647E-02
	3	1007.	0.9967E+01	0.2202E-02	0.2020E-02
	4	1001.	0.2101E+02	0.2624E-02	0.2592E-02
F1	1	981.	0.5207E+00	0.5785E-03	0.7308E-03
	2	997.	0.3002E+01	0.1452E-02	0.1509E-02
	3	998.	0.7936E+01	0.1652E-02	0.1694E-02
	4	992.	0.1584E+02	0.1827E-02	0.2009E-02
B0	2	1008.	0.6562E+01	0.1488E-02	0.1348E-02
	3	1012.	0.1284E+02	0.2374E-02	0.2045E-02
	4	1012.	0.2582E+02	0.3222E-02	0.2791E-02
	5	1006.	0.4905E+02	0.4039E-02	0.3729E-02
D2	2	1001.	0.5073E+01	0.1171E-02	0.1156E-02
	3	1005.	0.9875E+01	0.1789E-02	0.1689E-02
	4	1005.	0.1948E+02	0.2364E-02	0.2213E-02
D5	2	994.	0.4615E+01	0.1124E-02	0.1215E-02
	3	994.	0.9172E+01	0.1689E-02	0.1829E-02
	4	992.	0.1791E+02	0.2110E-02	0.2334E-02
	5	990.	0.3312E+02	0.2641E-02	0.2993E-02
	6	987.	0.5286E+02	0.2843E-02	0.3360E-02
D7	2	1008.	0.5513E+01	0.1551E-02	0.1399E-02
	3	1011.	0.1223E+02	0.2567E-02	0.2234E-02
	4	1012.	0.2641E+02	0.3543E-02	0.3058E-02

Sample No	Run No	Mean Temperature T_R [°C]	Burn-off [mg cm ⁻²]	Reaction Rate RG_{T_R} [mg cm ⁻² sec ⁻¹]	Reaction Rate [1000 °C] $RG_{(1273K)}$ [mg cm ⁻² sec ⁻¹]
	5	1015.	0.5410E + 02	0.5033E-02	0.4198E-02
C0	2	1008.	0.4576E + 01	0.1213E-02	0.1104E-02
	3	1011.	0.1013E + 02	0.2174E-02	0.1894E-02
	4	1011.	0.2190E + 02	0.2912E-02	0.2535E-02
	5	1015.	0.4424E + 02	0.4021E-02	0.3339E-02

15 bar

Sample No	Run No	Mean Temperature T_R [°C]	Burn-off [mg cm ⁻²]	Reaction Rate RG_{T_R} [mg cm ⁻² sec ⁻¹]	Reaction Rate [1000 °C] $RG_{(1273K)}$ [mg cm ⁻² sec ⁻¹]
B5	1	992.	0.1737E + 01	0.1287E-02	0.1420E-02
	2	989.	0.5418E + 01	0.1080E-02	0.1232E-02
	3	995.	0.1137E + 02	0.1485E-02	0.1584E-02
I2	1	996.	0.1722E + 01	0.1275E-02	0.1333E-02
	2	994.	0.5814E + 01	0.1317E-02	0.1411E-02
	3	998.	0.1319E + 02	0.1855E-02	0.1898E-02
	4	993.	0.2726E + 02	0.2517E-02	0.2739E-02
F4	1	1003.	0.1761E + 01	0.1305E-02	0.1263E-02
	2	1002.	0.6274E + 01	0.1529E-02	0.1498E-02
	3	1004.	0.1469E + 02	0.2098E-02	0.2006E-02
	4	1001.	0.3064E + 02	0.2855E-02	0.2831E-02
	5	1004.	0.6077E + 02	0.3677E-02	0.3498E-02
	6	999.	0.1039E + 03	0.3237E-02	0.3275E-02
	7	998.	0.1417E + 03	0.4004E-02	0.4109E-02
H6	1	1007.	0.1861E + 01	0.1378E-02	0.1272E-02
	2	1004.	0.6912E + 01	0.1772E-02	0.1678E-02
	3	1007.	0.1681E + 02	0.2485E-02	0.2267E-02
	4	1006.	0.3628E + 02	0.3543E-02	0.3292E-02
	5	1011.	0.7511E + 02	0.4829E-02	0.4213E-02
	6	1015.	0.1357E + 03	0.4791E-02	0.4005E-02
B6	1	995.	0.1202E + 01	0.8906E-03	0.9518E-03
	2	990.	0.4005E + 01	0.8893E-03	0.1003E-02
E5	1	993.	0.1182E + 01	0.8753E-03	0.9507E-03
	2	996.	0.4196E + 01	0.1018E-02	0.1068E-02
	3	995.	0.1098E + 02	0.1833E-02	0.1947E-02
	4	993.	0.2358E + 02	0.2126E-02	0.2327E-02
G5	1	999.	0.1293E + 01	0.9577E-03	0.9754E-03
	2	1002.	0.4810E + 01	0.1236E-02	0.1213E-02

Sample No	Run No	Mean Temperature T_R [°C]	Burn-off [mg cm ⁻²]	Reaction Rate RG_{T_R} [mg cm ⁻² sec ⁻¹]	Reaction Rate [1000 °C] $RG_{(1273K)}$ [mg cm ⁻² sec ⁻¹]
	3	1002.	0.1314E+02	0.2261E-02	0.2219E-02
	4	1000.	0.2946E+02	0.2837E-02	0.2823E-02
	5	998.	0.6243E+02	0.4214E-02	0.4339E-02
	6	1002.	0.1157E+03	0.3333E-02	0.3267E-02
I8	1	1002.	0.1338E+01	0.9910E-03	0.9637E-03
	2	1003.	0.5028E+01	0.1307E-02	0.1254E-02
	3	1004.	0.1356E+02	0.2288E-02	0.2186E-02
	4	1003.	0.2996E+02	0.2838E-02	0.2721E-02
	5	1007.	0.6391E+02	0.4395E-02	0.4018E-02
H1	1	993.	0.1137E+01	0.8419E-03	0.9157E-03

55 bar

Sample No	Run No	Mean Temperature T_R [°C]	Burn-off [mg cm ⁻²]	Reaction Rate RG_{T_R} [mg cm ⁻² sec ⁻¹]	Reaction Rate [1000 °C] $RG_{(1273K)}$ [mg cm ⁻² sec ⁻¹]
J3	1	1011.	0.1101E+01	0.6116E-03	0.5314E-03
	2	1003.	0.5310E+01	0.1151E-02	0.1110E-02
	3	1002.	0.1382E+02	0.1502E-02	0.1470E-02
	4	1001.	0.2926E+02	0.1857E-02	0.1838E-02
E4	1	1000.	0.9693E+00	0.5385E-03	0.5386E-03
	2	997.	0.4825E+01	0.1069E-02	0.1114E-02
	3	998.	0.1274E+02	0.1396E-02	0.1429E-02
	4	996.	0.2762E+02	0.1825E-02	0.1908E-02
	5	996.	0.5071E+02	0.2299E-02	0.2411E-02
	6	1002.	0.8833E+02	0.2955E-02	0.2889E-02
H7	1	1005.	0.1056E+01	0.5866E-03	0.5535E-03
	2	1004.	0.5530E+01	0.1266E-02	0.1211E-02
	3	1010.	0.1567E+02	0.1867E-02	0.1646E-02
	4	1011.	0.3649E+02	0.2611E-02	0.2283E-02
F7	2	998.	0.3038E+01	0.9636E-03	0.9855E-03
	3	1000.	0.7849E+01	0.1140E-02	0.1134E-02
	4	999.	0.1617E+02	0.1457E-02	0.1481E-02
	5	993.	0.3142E+02	0.1843E-02	0.2008E-02
	6	996.	0.5223E+02	0.2400E-02	0.2525E-02
G6	2	1002.	0.3259E+01	0.1088E-02	0.1061E-02
	3	1005.	0.8673E+01	0.1280E-02	0.1196E-02
	4	1004.	0.1819E+02	0.1683E-02	0.1598E-02
	5	1004.	0.3722E+02	0.2390E-02	0.2278E-02

Sample No	Run No	Mean Temperature T_R [°C]	Burn-off [mg cm ⁻²]	Reaction Rate RG_{TR} [mg cm ⁻² sec ⁻¹]	Reaction Rate [1000 °C] $RG_{(1273K)}$ [mg cm ⁻² sec ⁻¹]
	6	1010.	0.6455E +02	0.3189E-02	0.2834E-02
19	2	999.	0.2834E +01	0.9255E-03	0.9333E-03
	3	1001.	0.7388E +01	0.1070E-02	0.1060E-02
	4	997.	0.1491E +02	0.1286E-02	0.1339E-02
	5	999.	0.2944E +02	0.1824E-02	0.1842E-02
	6	1000.	0.5010E +02	0.2388E-02	0.2385E-02
J1	2	989.	0.2922E +01	0.9518E-03	0.1088E-02
	3	991.	0.7605E +01	0.1100E-02	0.1228E-02

Table 2: Reaction rates for all corrosion test runs and pressures of 3, 7, 15 and 55 bar

3.4.2 Burn-off dependence of reaction rates

Changes of the material properties during corrosion cause changes of the chemical reactivity, the active surface area and the effective diffusion coefficient. For corrosion in the in-pore diffusion controlled regime which is valid for the experimental parameters given, the consequence of these changes is, that from an originally low value the reaction rates grow with increasing burn-off and finally reach a stable (maximum) value.

Fig. 6 gives a scheme for the arrangement of reaction rates as a function of burn-off as they were taken from table 2 for the following diagrams. Here Δb_i always denotes the burn-off calculated from the weight loss measurements and RG_i the related reaction rate corrected to 1000°C.

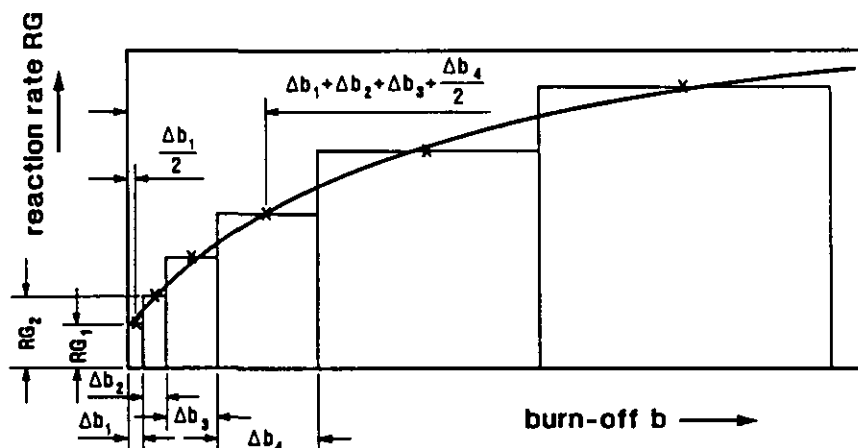


Fig. 6: Scheme of arrangement of values from table 2

Referring to /3/ and using the method of least squares, the resulting values are correlated by a function of the type given in equation [4] with the empirical constants A, B and C.

$$RG_{(burn-off)} = \frac{A + b}{1 + B * b} + C \quad [4]$$

This formula allows for an extrapolation to maximum reaction rates towards infinite burn-off where these maxima could not be achieved in the experiment, as mentioned in chapter 3.3. For accident analyses as well as for evaluation of the pressure dependence of the reaction rate, these maximum values are of special interest.

Fig. 7-10 show the burn-off dependence of the reaction rates for the total pressures of 3, 7, 15 and 55 bar for all test runs including the smoothed curve from formula [4]. At the upper right end of the diagram the reaction rate for infinite burn-off is indicated, giving a maximum value of up to a factor of approx. 1.4 higher than that measured during the last test run. Especially for the 55 bar case this is certainly a very conservative value (see also chapter 4).

In fig. 11 the results for all pressures are compiled.

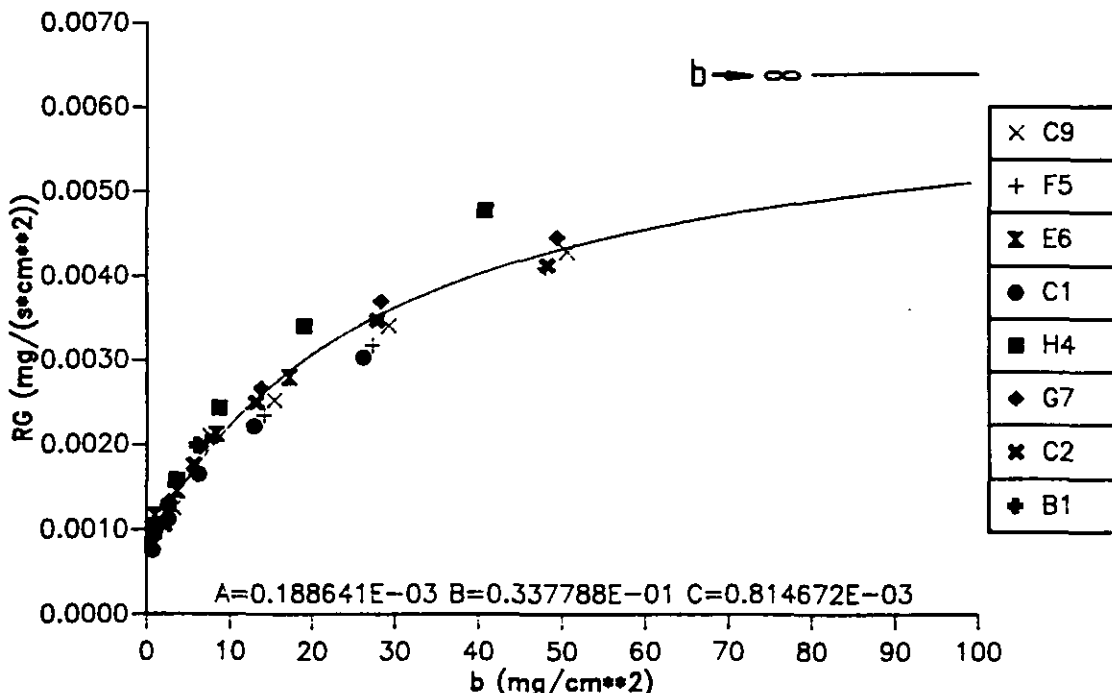


Fig. 7: Burn-off dependence of reaction rate at p = 3 bar

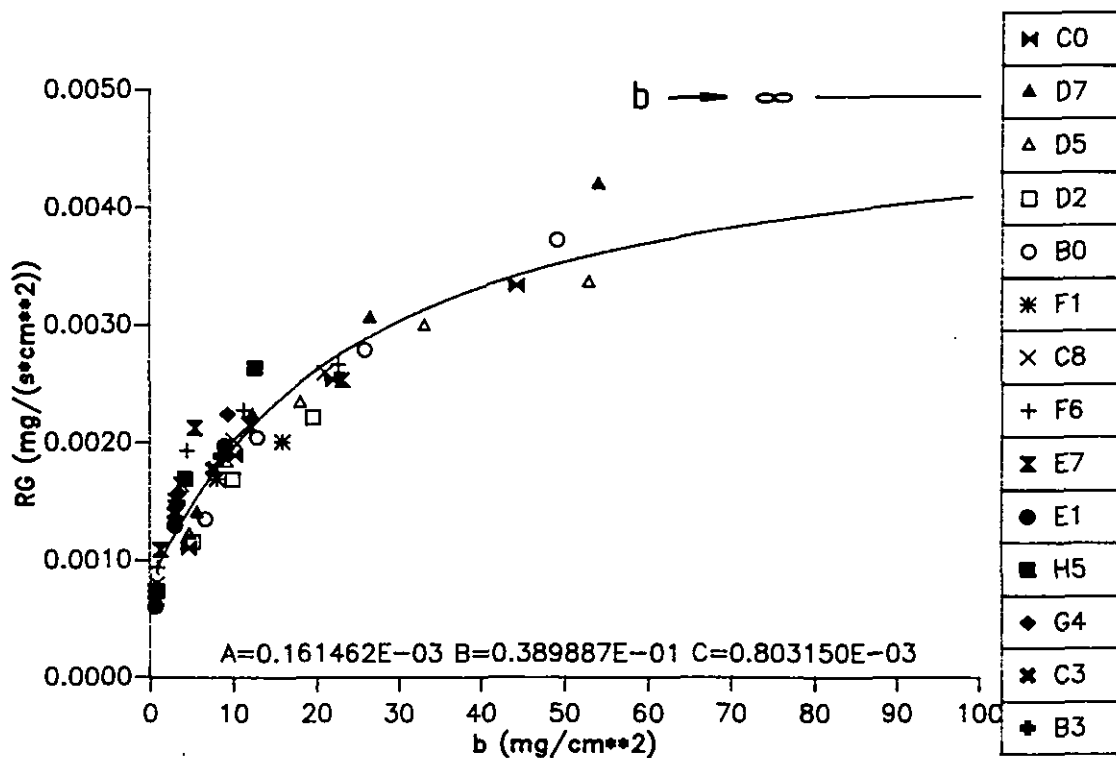


Fig. 8: Burn-off dependence of reaction rate at $p = 7$ bar

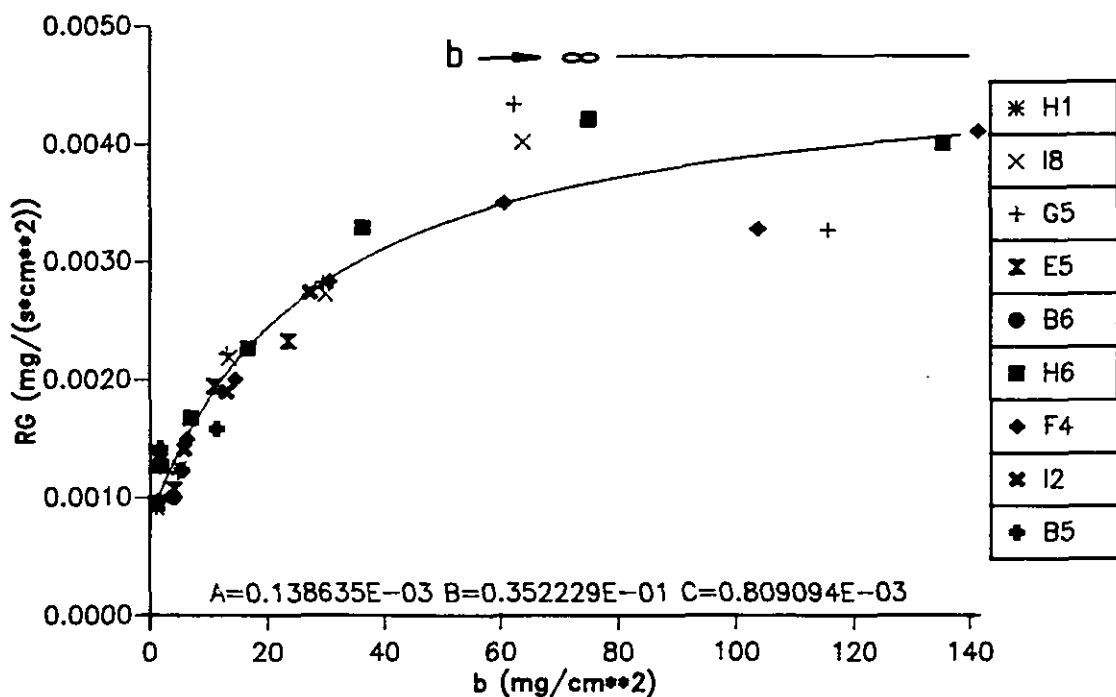


Fig. 9: Burn-off dependence of reaction rate at $p = 15$ bar

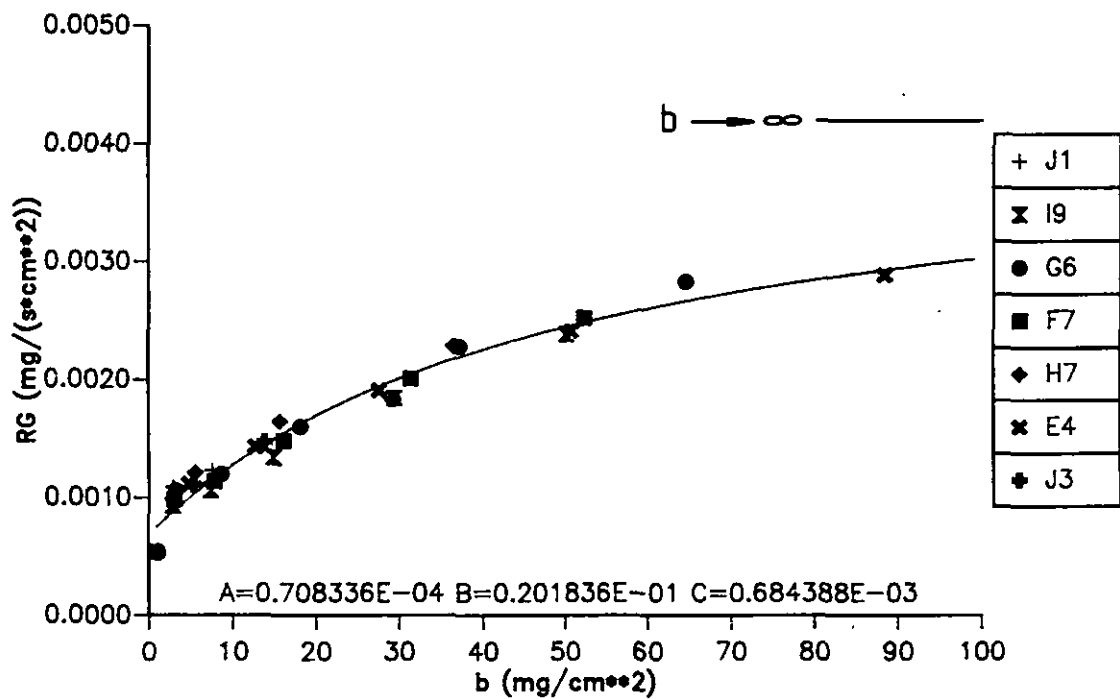


Fig. 10: Burn-off dependence of reaction rate at $p = 55$ bar

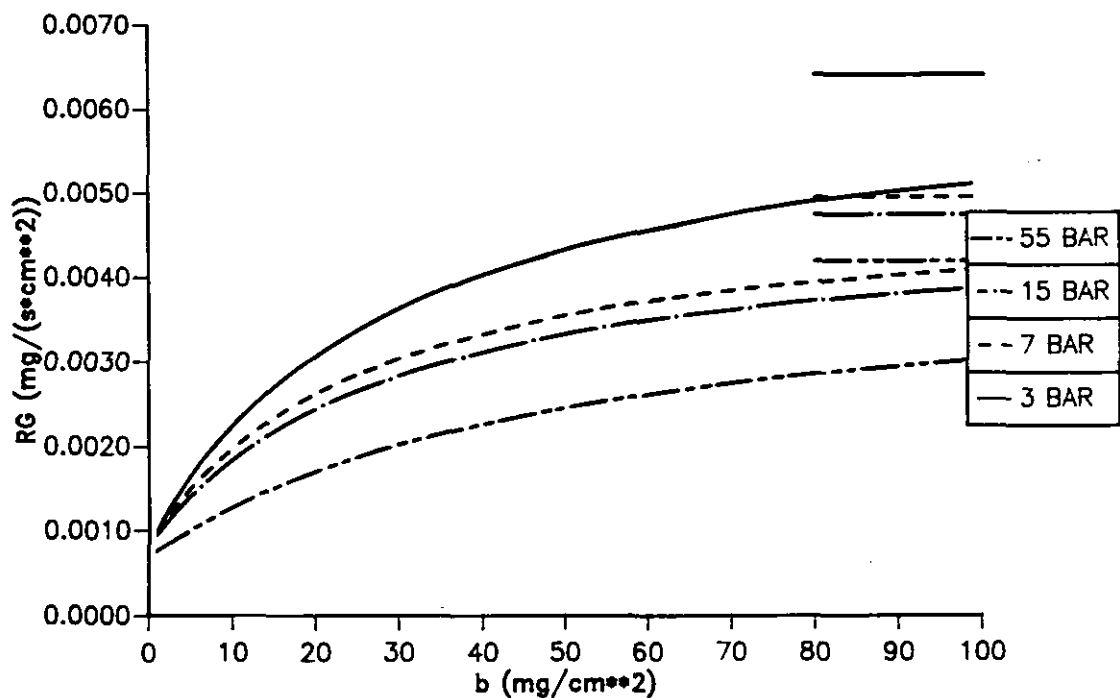


Fig. 11: Burn-off dependence of reaction rates for different pressures

3.4.3 Pressure dependence of reaction rates

As was discussed in /1/ and /3/, for certain suppositions a linear relation between reaction rate and the inverse square root of the total gas pressure can be predicted. This is only valid, where the effective diffusion coefficient not is influenced by Knudsen type diffusion. If the pore diameter in the graphite is in the order of the free path length, Knudsen type diffusion becomes effective, thus diminishing the pressure dependence.

Fig. 12 shows the pressure dependence of the reaction rate. The values connected by a solid line were taken from fig. 7-12 for infinite burn-off, following a relation between reaction rate and pressure as given in [5].

$$RG_{(p)} = 0.004853 \frac{1}{\sqrt{p}} + 0.003435 \quad [5]$$

For comparison results from corrosion experiments on German A3-3 fuel element matrix material which were carried out under the same conditions as outlined here /1/, are included in the diagram. In this case it can be seen that the values below approx. $p = 15$ bar are proportional to $1/\sqrt{p}$, indicating that here the Knudsen diffusion is rate determining, while the 55 bar value shows the expected decline. In contrast to that, for IG-110 even up to 55 bar a considerable Knudsen effect seems to exist.

As will be outlined in chapter 4, density profile measurements at samples corroded at 55 and also at 15 bar give a strong indication that the stable profile and hence the maximum reaction rates had already been reached for the last runs. Taking this into account, for the 15 bar case a mean value was calculated from all measuring points in fig. 9 above a burn-off of 60 mg/cm^2 , and for the 55 bar case the last value (fig. 10, at 90 mg/cm^2) was taken and also inserted in the diagram fig. 12. But also taking these values, for the whole pressure range the linear relation between reaction rate and $1/\sqrt{p}$ is evident [6].

While equation [5] at high pressures tends to give conservative reaction rate values, for more realistic calculations equation [6] is recommended.

$$RG_{(p)} = 0.007789 \frac{1}{\sqrt{p}} + 0.001920 \quad [6]$$

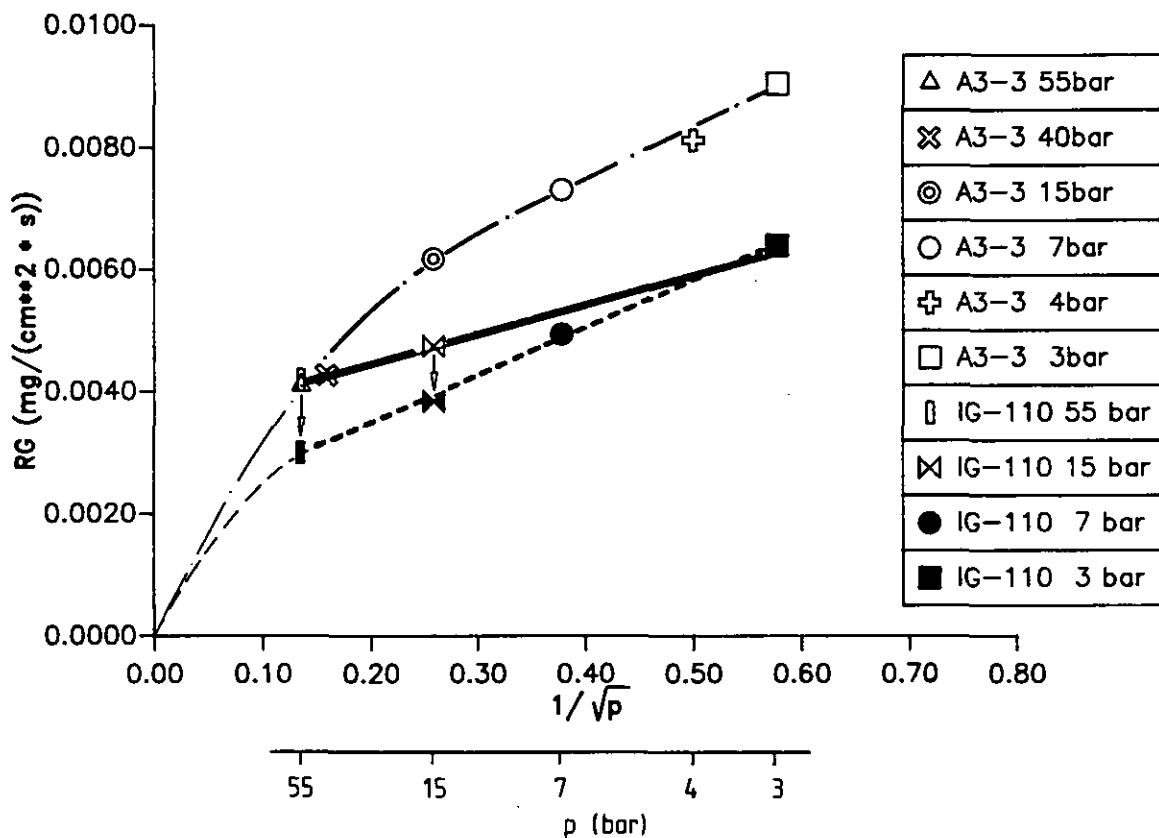


Fig. 12: Pressure dependence of reaction rate of IG-110 compared with A3-3 matrix material

3.5 Density Profiles

As an addition to the kinetic experiments, for selected corroded samples density profiles were taken as also described in /4/. They provide an indication on the depth of the material damage on the one and, on the other hand, the extent to which a stable profile and hence the maximum reaction rate had been reached.

3.5.1 Selection of samples, profiling method

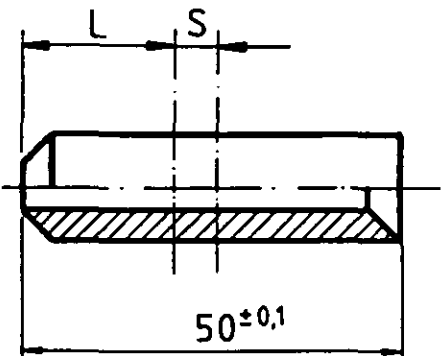
For profiling, samples were selected (see table 3), which had

- been corroded under isothermal conditions and
- reached a stable or nearly stable corrosion profile.

The first criterion was fulfilled at least in the part of that sample at which the temperature was kept constant via the control pyrometer even in those cases where the last corrosion test run had to be abandoned from the reaction kinetic evaluation because of too big changes of the axial temperature profile, as is the case for samples No G7, F6, G5 and G6.

The second criterion is obviously fulfilled, where the bore diameter of the sample has been widened. But also in cases where no widening is observed, the material density at the original bore surface and the shape of the profile give an indication for the achievement of the stable profile, as will be discussed in 3.5.3. A measured density at the surface smaller than the density value G (fig. 14 and formula 8) was taken as an appropriate criterion (see table 3).

From the samples selected, a disk was cut as indicated in fig. 13. This disk normally had a thickness of approx. 4.0 mm. For mechanical reasons, in some cases a thickness of up to 5 mm was chosen. The bore of this disc was turned on a lathe in radial steps of 0.1 mm and weighed. From the geometry and the weight losses the density for each step was calculated, the results giving a density profile as shown in fig. 13. The profiling was terminated when the remaining graphite ring lost its strength.



Pres- sure [bar] / Sam- ple No	Mean Tem- pera- ture [°C]	Burn- off [%]	Dis- tance L [mm]	Thick- ness S [mm]	Densi- ty sur- face [g/cm²]	Dénsi- ty value G [g/cm³]	Pe- ne- tra- tion depth δ [mm]	Diam- eter widен- ing ?	Stable corro- sion profile ?
3bar									
G7	999	11.49	19.32	3.96	0.75	0.71	-	no	(yes)
7bar									
F6	1001	9.68	19.32	3.82	0.80	0.75	3.0	no	(yes)
15bar									
F4	1001	13.03	21.52	4.14	0.55	0.75	3.4	yes	yes
G5	1000	17.09	20.92	3.93	0.38	0.78	3.6	yes	yes
55bar									
E4	999	9.41	18.38	4.04	0.46	0.74	2.2	yes	yes
G6	1005	12.57	17.64	4.38	0.51	0.76	2.5	yes	yes

Table 3: Data of samples for density profile measurement

In those cases where the bore due to uneven erosion of the very loose material near the original surface was not entirely cylindrical, a "first radius" had to be established by turning carefully until a cylindrical bore was achieved.

For a couple of samples (G7, F6, G5, E4) density profiles were taken from the outer surface. Note, that these measurements were carried out on a different disk adjacent to that taken for internal profiling.

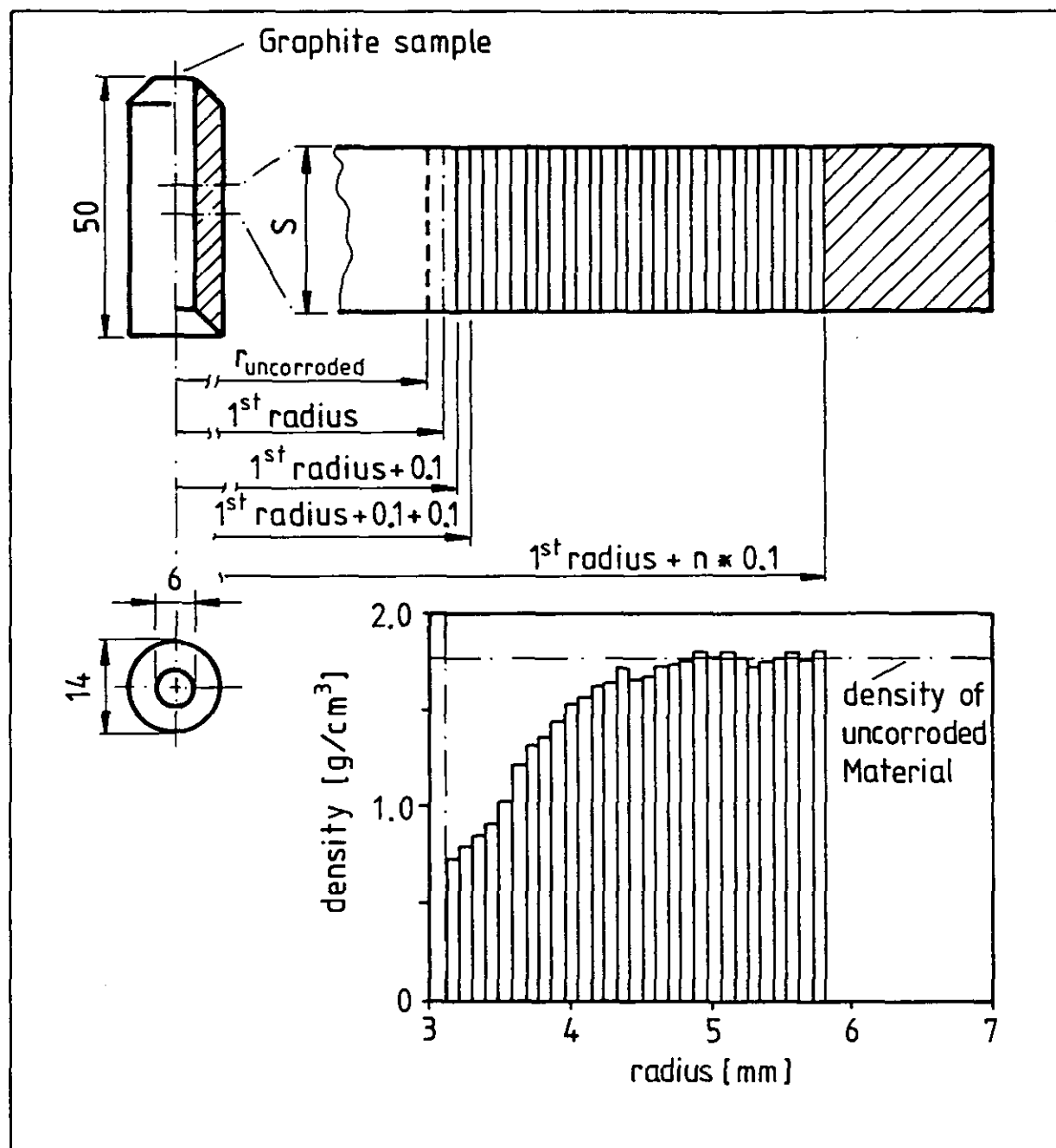


Fig. 13: Profiling method

3.5.2 The evaluation method

As is outlined in /5/, under in-pore diffusion controlled conditions, the corrosion profile - as well as the overall reaction rate - is influenced by the diffusion coefficient in the pore system of the graphite and the local chemical reactivity. Both are burn-off dependent. While the effective diffusion coefficient increases monotonically with burn-off, the active surface area (which is proportional to the chemical reactivity) goes through a maximum and finally reaches low values.

This results in the formation of a density profile which - constant corrosion conditions and sufficient sample thickness provided - reaches its final shape, when burn-off close to the geometrical surface of the graphite body has reached a value where the active surface area has decreased to an extent where this part of the material practically no longer contributes to the overall oxidation or where it is removed by erosion processes.

For comparison of the density profiles measured, an exponential function [7] was taken (see also fig. 14) with the radius dependent densities derived from this equation as given in [8]:

$$Y = 1 - e^{(-F X)} \quad [7]$$

$$\frac{\rho}{\rho_0} = [1 - e^{-F(R - 1^s R - H)}] + G \quad [8]$$

Using the least square method, the measured densities are correlated by this formula. Fig. 14 shows the definition for the "penetration depth" (δ) which was chosen. The most important detail is the point "0", where the exponential function originates. Above "0" the function describes the expected "s-formed" shape of the density profile quite exactly, which does not apply for the part below "0". The latter, however, is of minor practical importance, as the density measurement in this loose layer close to the original surface is quite uncertain and, on the other hand, for all samples examined the radius difference between "0" and the "1. radius" (H) remained below 0.4 mm. According to this, the radius

at point "0" was taken as the reference radius for the calculation of the penetration depth δ , which, divergent to /5/, was defined as the radius difference, where 98 % ($= 1.73 \text{ g/cm}^3$) of the mean density of the uncorroded material ($= 1.76 \text{ g/cm}^3$, see 3.5.3) is reached.

$$\delta = \frac{\ln (G + 1 - 1.73)}{-F} \quad [9]$$

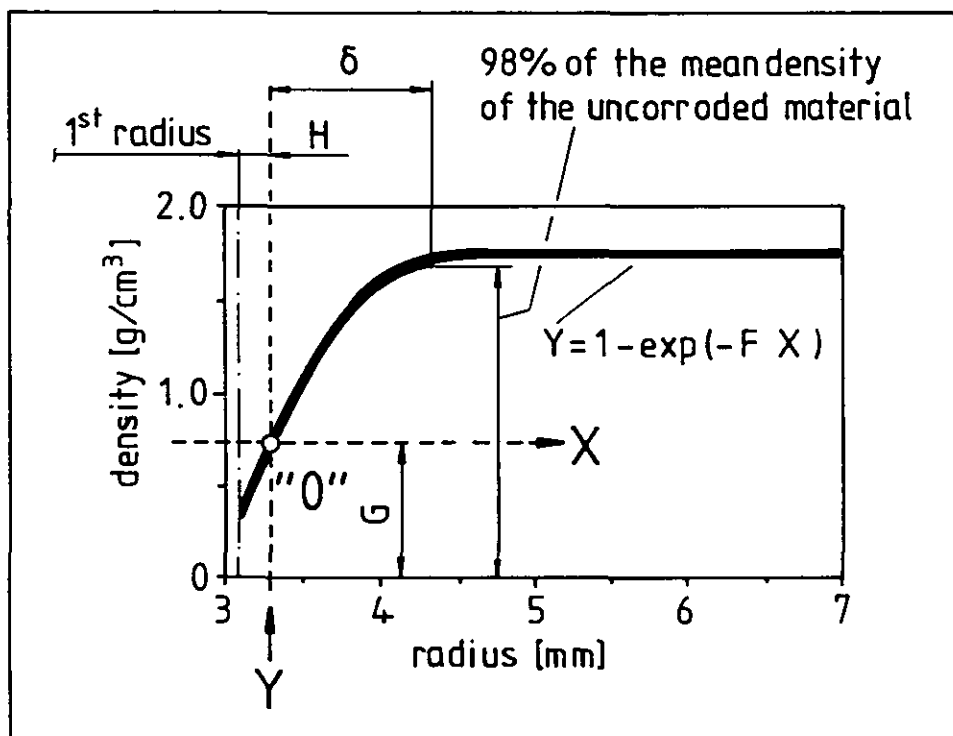


Fig. 14: Scheme for evaluation of density profiles

The results are included in table 3. Only for the 3 bar-case (sample G7) a penetration depth could not be calculated, as the density function remains below the limit value defined above.

3.5.3 Results

The results from the density profile measurements are presented below. Fig. 15 demonstrates how these diagrams read.

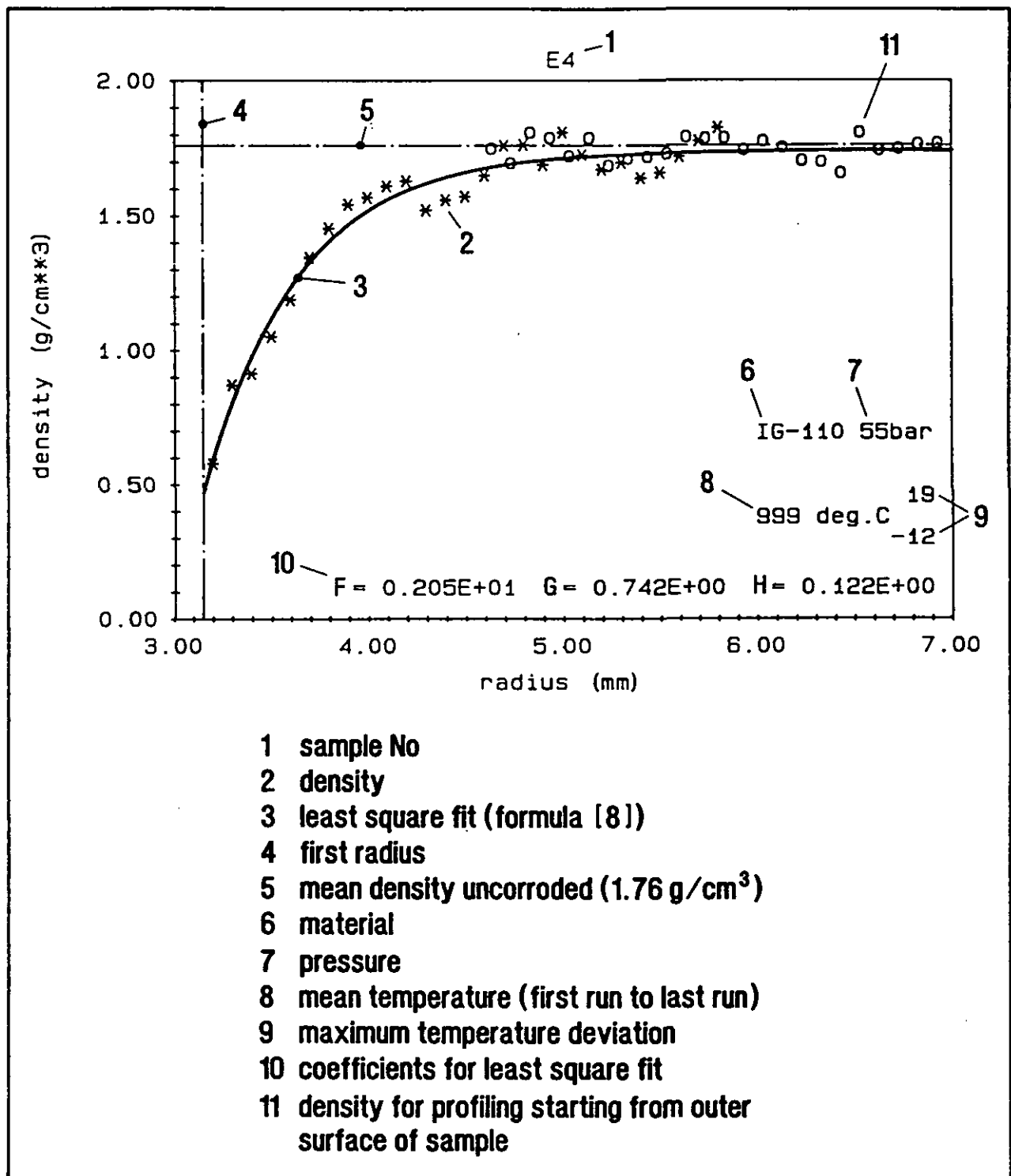


Fig. 15: Explanation for density profile diagrams

Density variations which have to be expected in the uncorroded material using the profiling method described are shown in fig. 16

by the example of sample J0. The measured mean density ρ_m of 1.76 g/cm³, which also was found in different samples, was very close to the nominal value of 1.75 g/cm³.

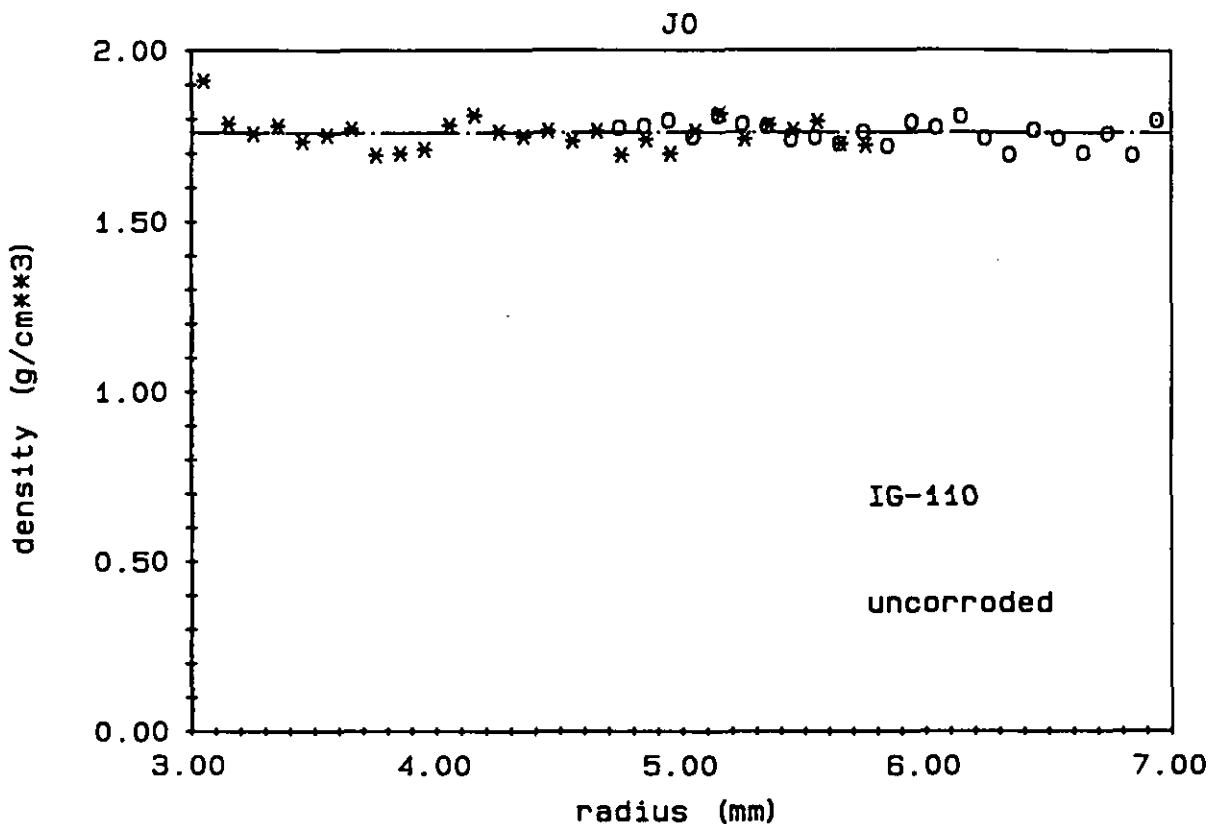


Fig. 16: Density in uncorroded sample

Fig. 17-22 present the density profiles measured at the corroded samples. As mentioned in 3.5.1, for some samples density profiles were taken from the outer surface. Where these values were available, they were included in the diagrams.

All density functions are plotted in fig. 23 and, for better comparison, in fig. 24, where the origin of the function is the density at point "0" (see fig. 14). As expected, the profiles with the steepest curvature are found for the 55 bar cases. For the other pressures no major differences can be realized, which is in fair agreement to the penetration depth calculations results in table 3 and the comparably small pressure dependence of the reaction rate shown in 3.4.3.

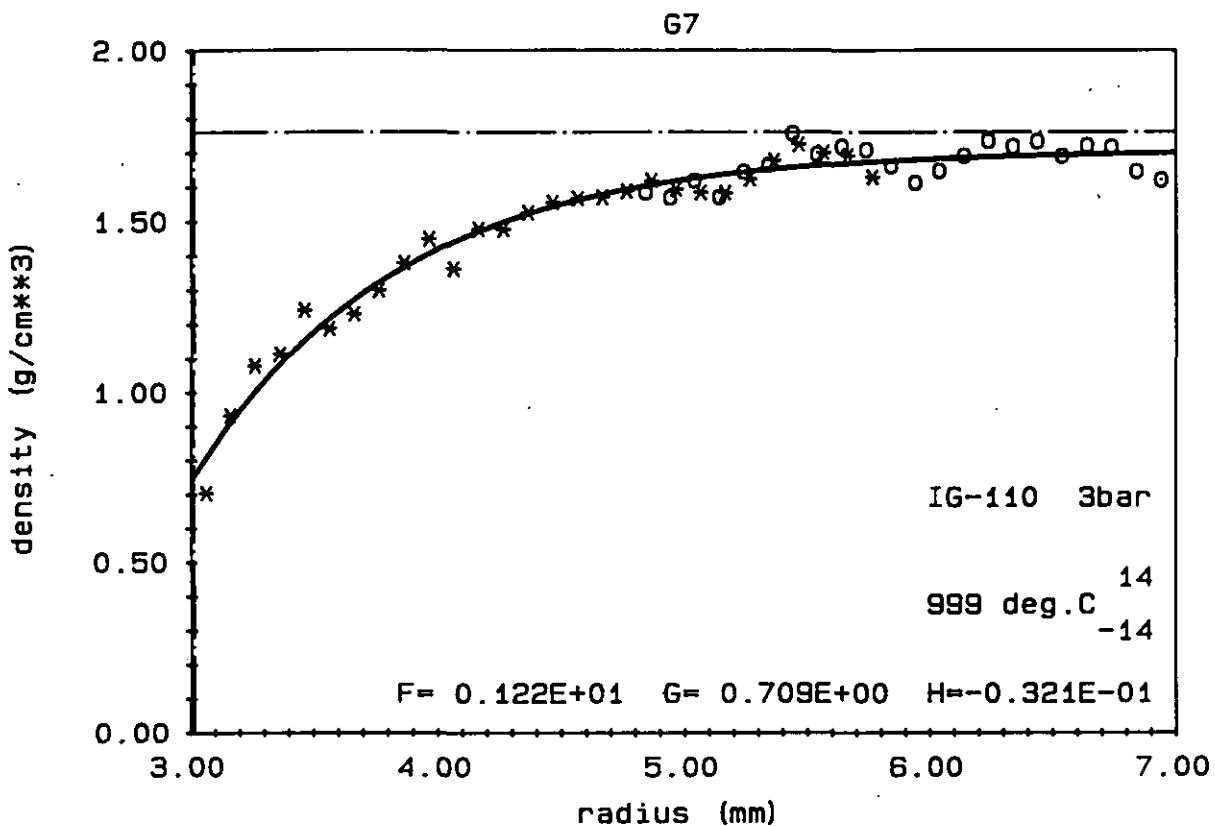


Fig. 17:

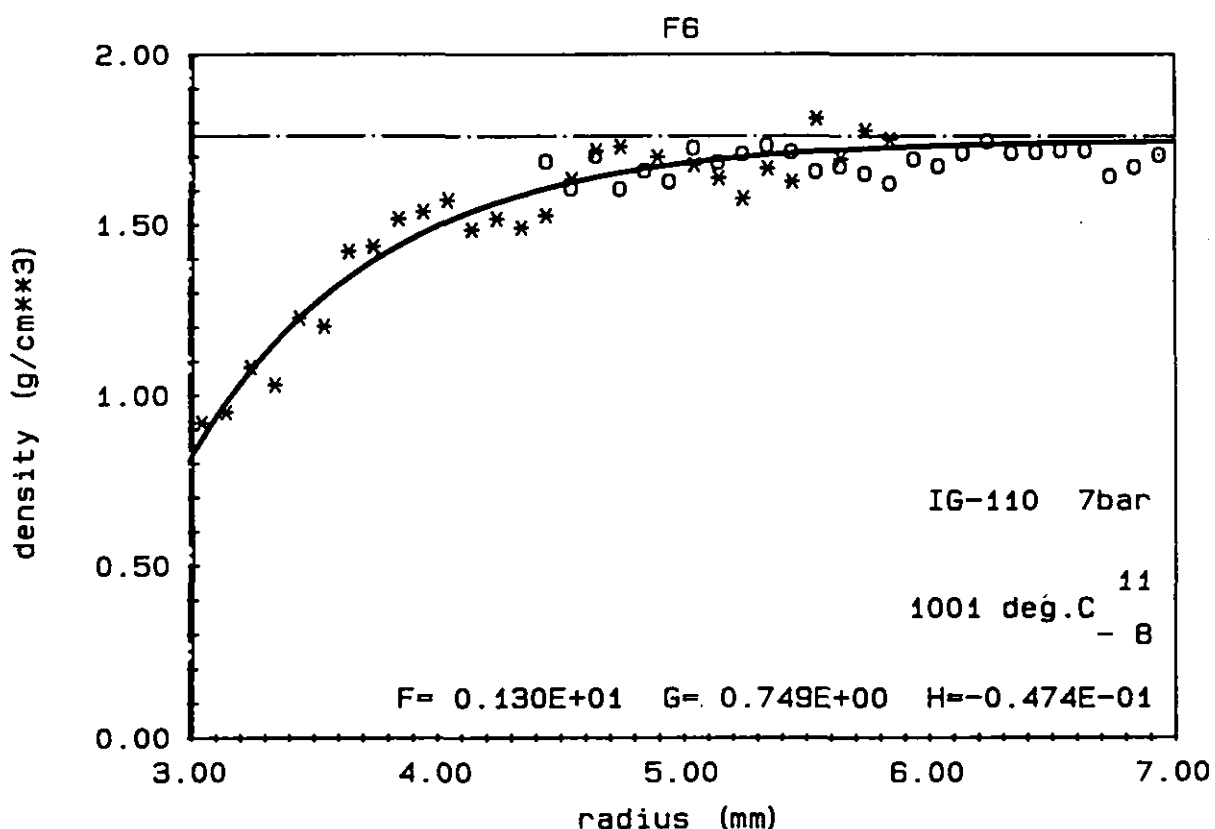


Fig. 18:

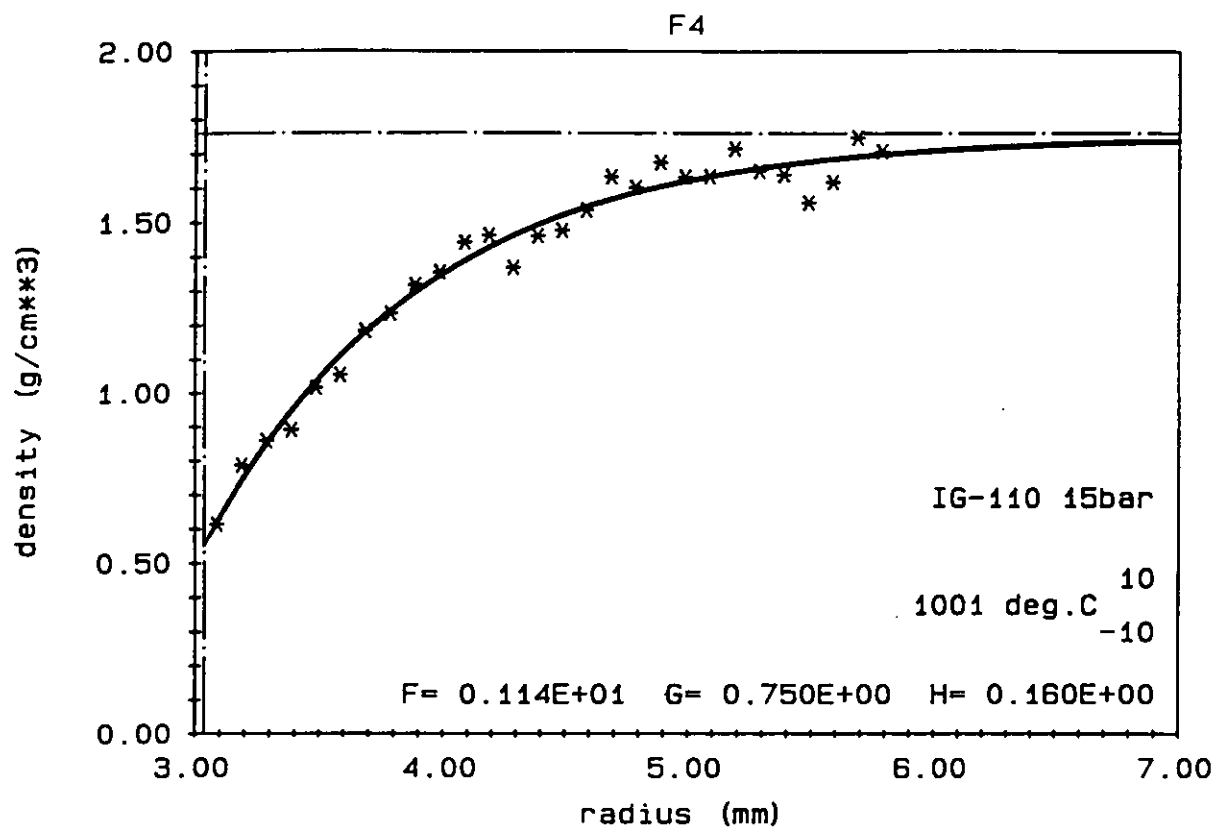


Fig. 19:

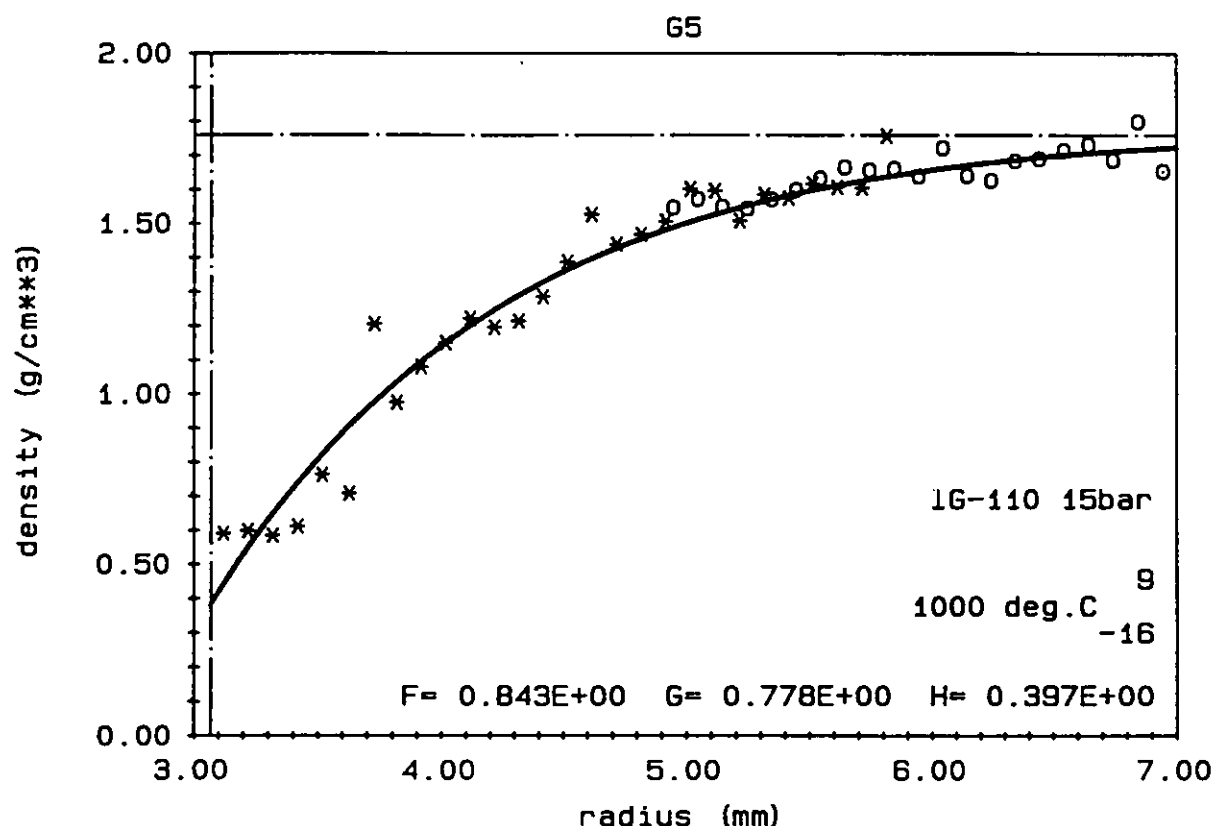


Fig. 20:

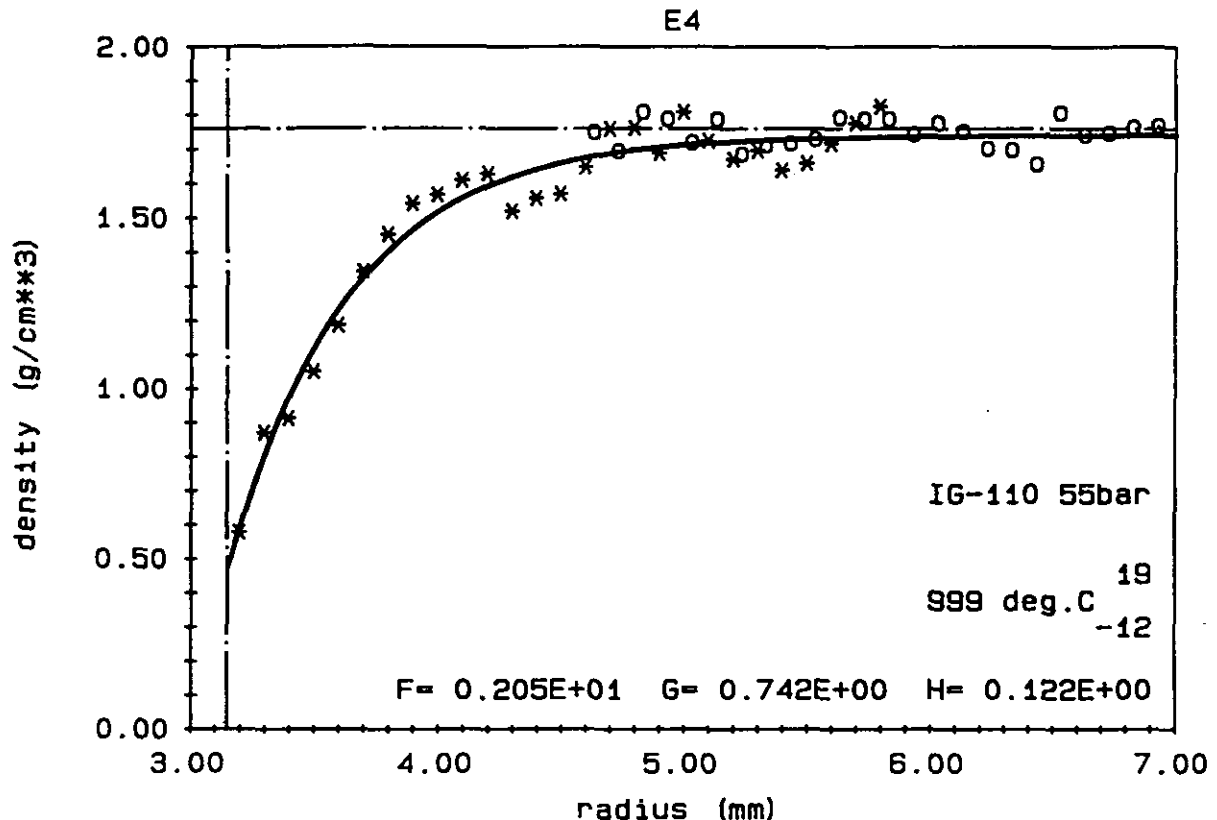


Fig. 21:

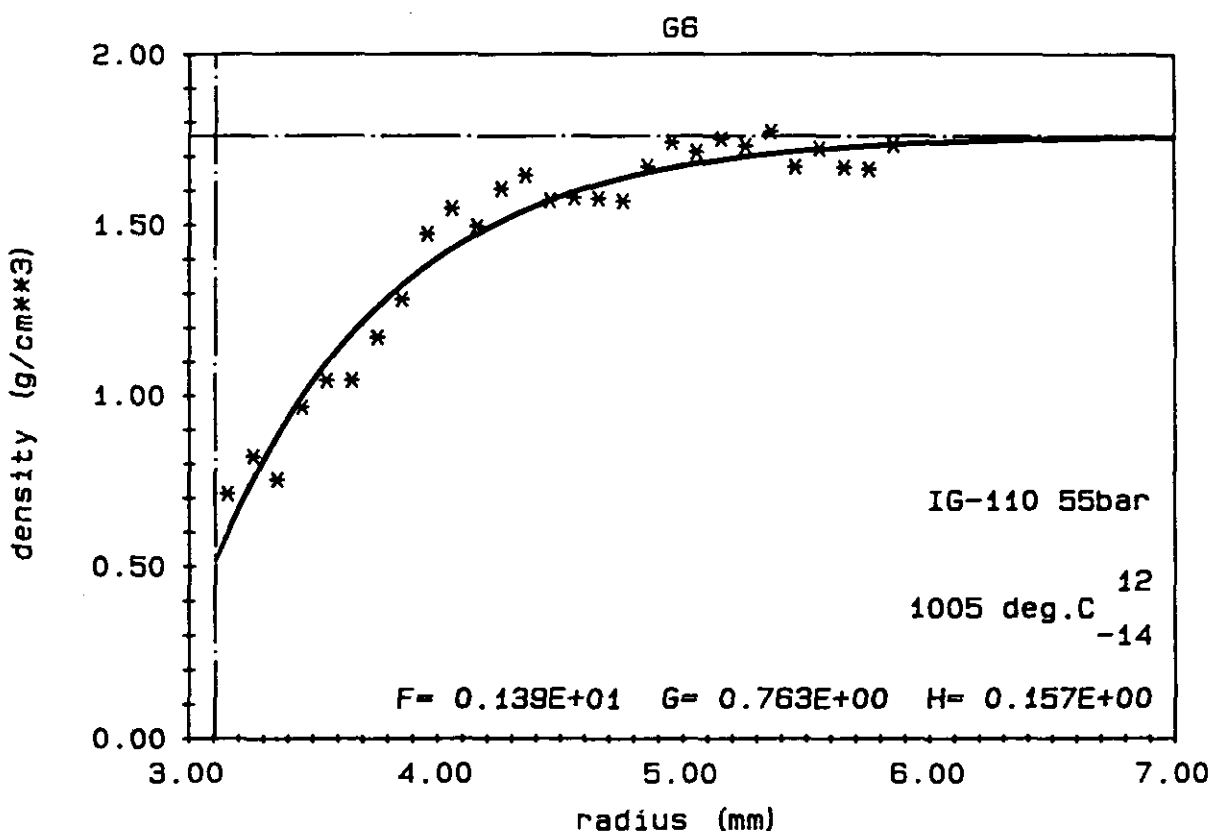


Fig. 22:

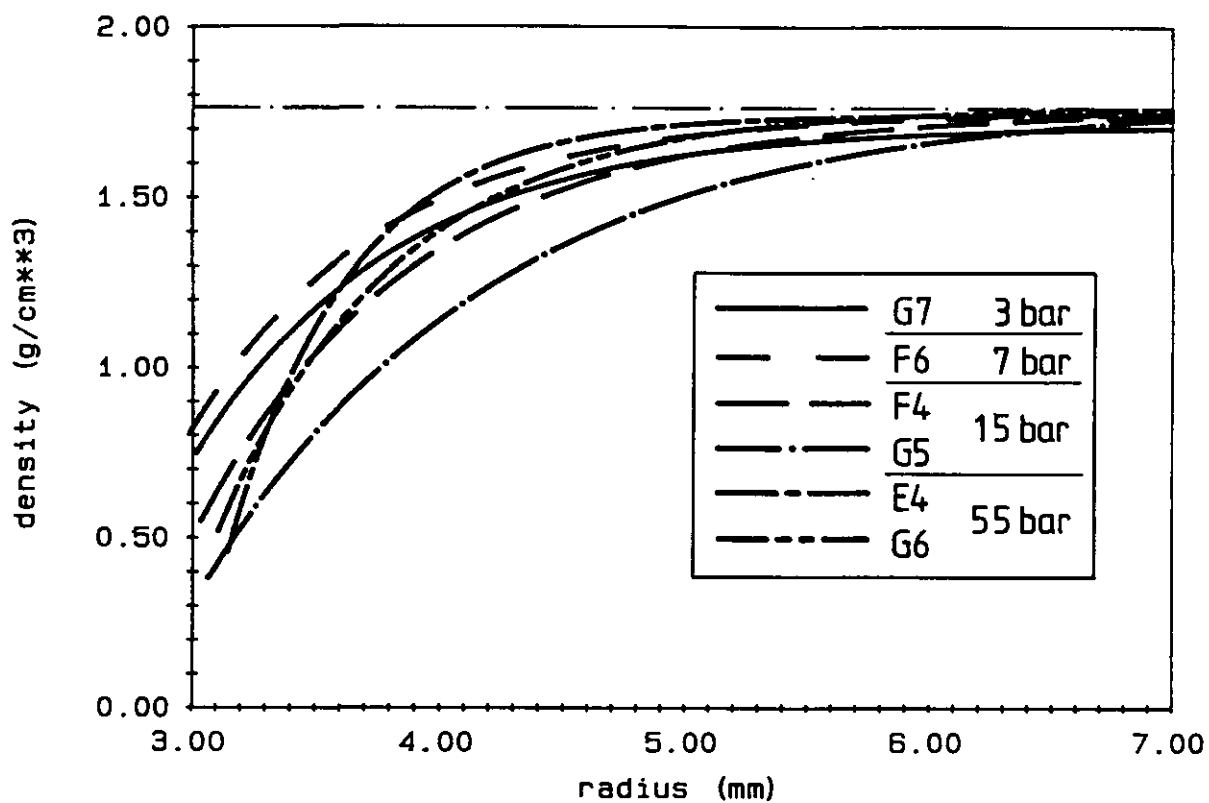


Fig. 23: Compilation of density functions

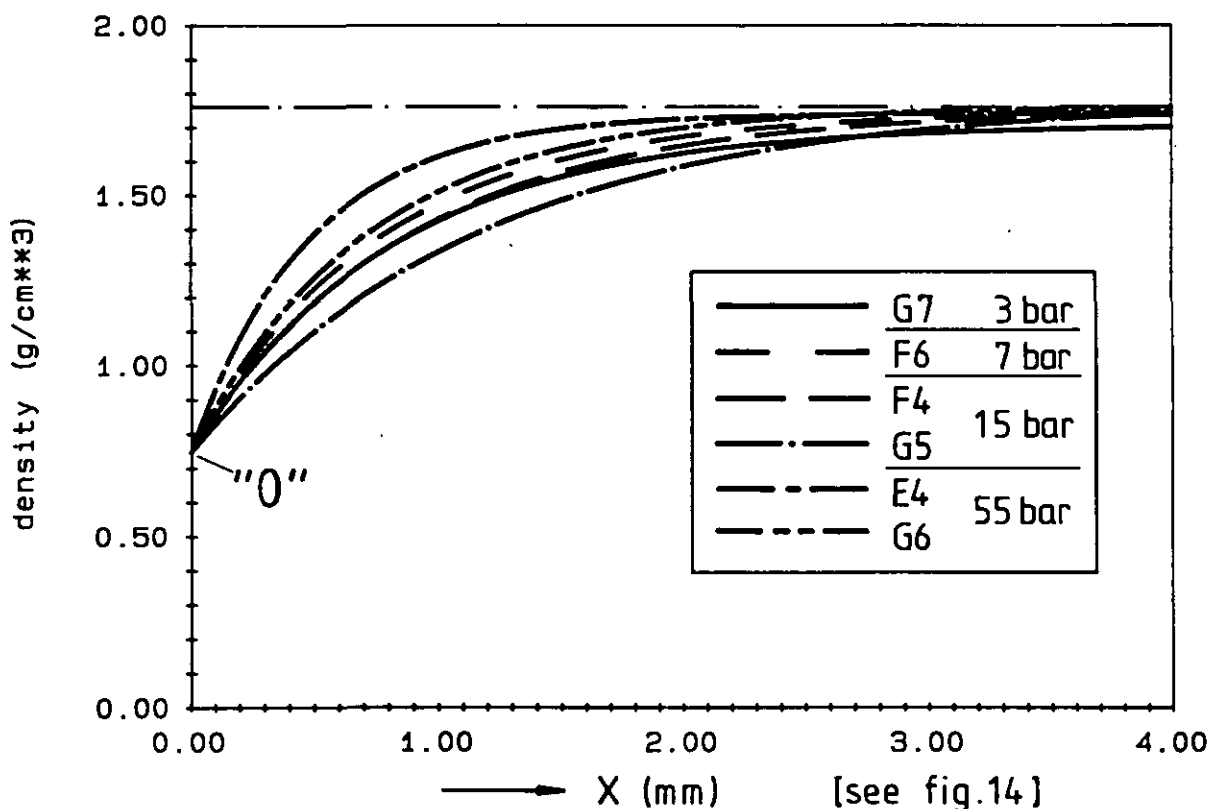


Fig. 24: Comparison of curvature of density functions originating at point "0" (see fig. 14)

4. CONCLUSION

Burn-off and pressure dependent reaction rates for the water gas reaction with the Japanese graphite IG-110 were measured in the parameter range: temperature 1000°C; water vapor partial pressure (in He as carrier gas) 474 mbar; total pressure 3-55 bar. As expected, the burn-off dependence of the reaction rate decreases with increasing pressure. In contrast to this the pressure dependence e.g. measured for German fuel element matrix graphite was found only partly: for IG-110 the influence of Knudsen-diffusion on the reaction rate apparently remains evident even for the highest pressure.

These findings are in fair agreement with the results of density profile measurements carried out at a couple of corroded samples. As expected, the profile with the steepest curvature and thus the smallest "penetration depth" was measured for the case with the highest pressure, but altogether the pressure dependence is rather small. A correlations for the calculations of penetration depths is given.

5. LIST OF SYMBOLS

A	= coefficient formula [4]
b	= burn-off [$mg\ cm^{-2}$]
B	= coefficient formula [4]
C	= coefficient formula [4]
E_A	= activation energy [$KJ\ mol^{-1}$]
F	= coefficient formula [8] [mm^{-1}]
G	= coefficient formula [8]
H	= coefficient formula [8] [mm]
f	= first location of temperature measurement at sample
l	= last location of temperature measurement at sample
p	= pressure [bar]
R	= radius [mm]
$1^{st}R$	= 1 st radius [mm]
R_m	= molar gas constant [$KJ\ mol^{-1}\ K^{-1}$]
RG	= reaction rate [$mg\ cm^{-2}\ sec^{-1}$]
RG_{1273K}	= reaction rate corrected to 1273 K
RG_{T_R}	= reaction rate at T_R
S = 1	= first temperature measurement
S = n	= last temperature measurement
T_s	= mean sample temperature [K]
T_R	= mean temperature of sample between two weight measurements [K]
δ	= penetration depth formula [9] [mm]
Δt_s	= time interval (s. fig. 5)
t_R	= corrosion time between two weight measurements
ρ	= density [$g\ cm^{-3}$]
ρ_0	= reference density = 1.0 g cm^{-3}
ρ_m	= mean density of uncorroded material = 1.76 g cm^{-3}

6. REFERENCES

/1/ K.-J. Loenißen

Untersuchungen zur Druckabhängigkeit der Graphit/Wasserdampf-Reaktion im Porendiffusionsbereich im Zusammenhang mit Wassereinbruchstörfallen in Hochtemperatur-Reaktoren

KFA-Bericht JüL-2159, September 1987

/2/ F.P.O. Ashworth, D.V. Kinsey, V.J. Wilkinson

A Review of HTR-Graphite-Corrosion

DPR 858/1972

/3/ H.-K. Hinssen, W. Katscher, R. Moormann

Kinetik der Graphit/Sauerstoff-Reaktion im Porendiffusionsbereich

Teil 1: Matrixmaterial A3-3 und A3-27

KFA-Bericht JüL. 1875, November 1983

/4/ H.-K. Hinssen

Dichteprofile in mit Sauerstoff korrodierten graphitischen Reaktormaterialien

Jahrestagung Kerntechnik 1989, Düsseldorf, Proc. S. 159-162

/5/ W. Katscher, W. Delle, H.-K. Hinssen, R. Moormann, E. Wallura

Changes in the macroporosity of nuclear reactor graphite under oxygen corrosion

High Temperature - High Pressure 13 (1981) S. 275-279

7. APPENDIX

This appendix gives a complete survey over the temperature distribution measured over the length of the test section for all corrosion experiments. Included is the distribution of the measured weight losses of the individual samples compared to the total weight loss of the sample stack. For the German expressions see glossary in Fig. A.0.

Table A.1 provides a link between samples, corrosion test runs and temperature diagrams. Fig. A.0 explains how the diagrams read.

Sample No	Pressure [bar]	Run No	Figure No
B1,C2,G7,H4,C1	3	1	A. 1
B1,C2,G7,H4,C1		2	A. 2
B1,C2,G7,H4,C1		3	A. 3
-,C2,G7,H4,C1		4	A. 4
-,C2,G7,H4,C1		5	A. 5
-,C2,G7, -, -		6	A. 6
E6,F5,C9	3	1	A. 7
E6,F5,C9		2	A. 8
E6,F5,C9		3	A. 9
E6,F5,C9		4	A.10
-,F5,C9		5	A.11
-,F5,C9		6	A.12
B3,C3,G4,H5,E1	7	1	A.13
B3,C3,G4,H5,E1		2	A.14
B3,C3,G4,H5,E1		3	A.15
E7,F6,C8,F1	7	1	A.16
E7,F6,C8,F1		2	A.17
E7,F6,C8,F1		3	A.18
E7,F6,C8,F1		4	A.19
B0,D2,D5,D7,C0	7	2	A.20
B0,D2,D5,D7,C0		3	A.21
B0,D2,D5,D7,C0		4	A.22
B0, -,D5,D7,C0		5	A.23
-, -,D5, -, -		6	A.24
B5,I2,F4,H6	15	1	A.25
B5,I2,F4,H6		2	A.26
B5,I2,F4,H6		3	A.27
-,I2,F4,H6		4	A.28
-, -,F4,H6		5	A.29
-, -,F4,H6		6	A.30
-, -,F4, -		7	A.31

Sample No	Pressure [bar]	Run No	Figure No
B6,E5,G5,I8,H1	15	1	A.32
B6,E5,G5,I8, -		2	A.33
-,E5,G5,I8, -		3	A.34
-,E5,G5,I8, -		4	A.35
-, -,G5,I8, -		5	A.36
-, -,G5, -, -		6	A.37
J3,E4,H7	55	1	A.38
J3,E4,H7		2	A.39
J3,E4,H7		3	A.40
J3,E4,H7		4	A.41
-,E4, -		5	A.42
-,E4, -		6	A.43
F7,G6,J9,J1	55	2	A.44
F7,G6,J9,J1		3	A.45
F7,G6,J9, -		4	A.46
F7,G6,J9, -		5	A.47
F7,G6,J9, -		6	A.48

Table A.1: List of temperature diagrams

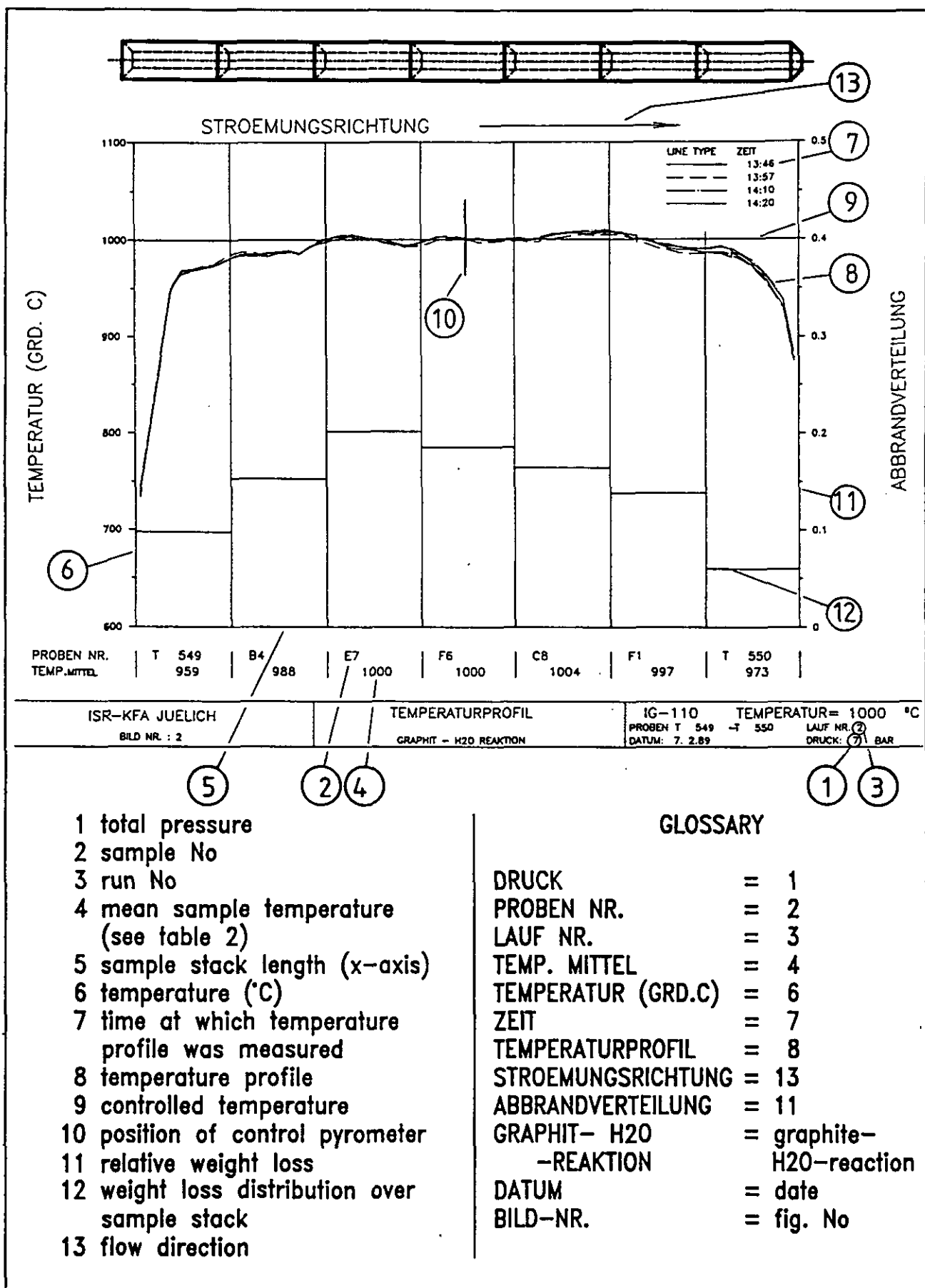


Fig. A.0: Explanation scheme for temperature diagrams

3 bar

B1, C2, G7, H4, C1
E6, F5, C9

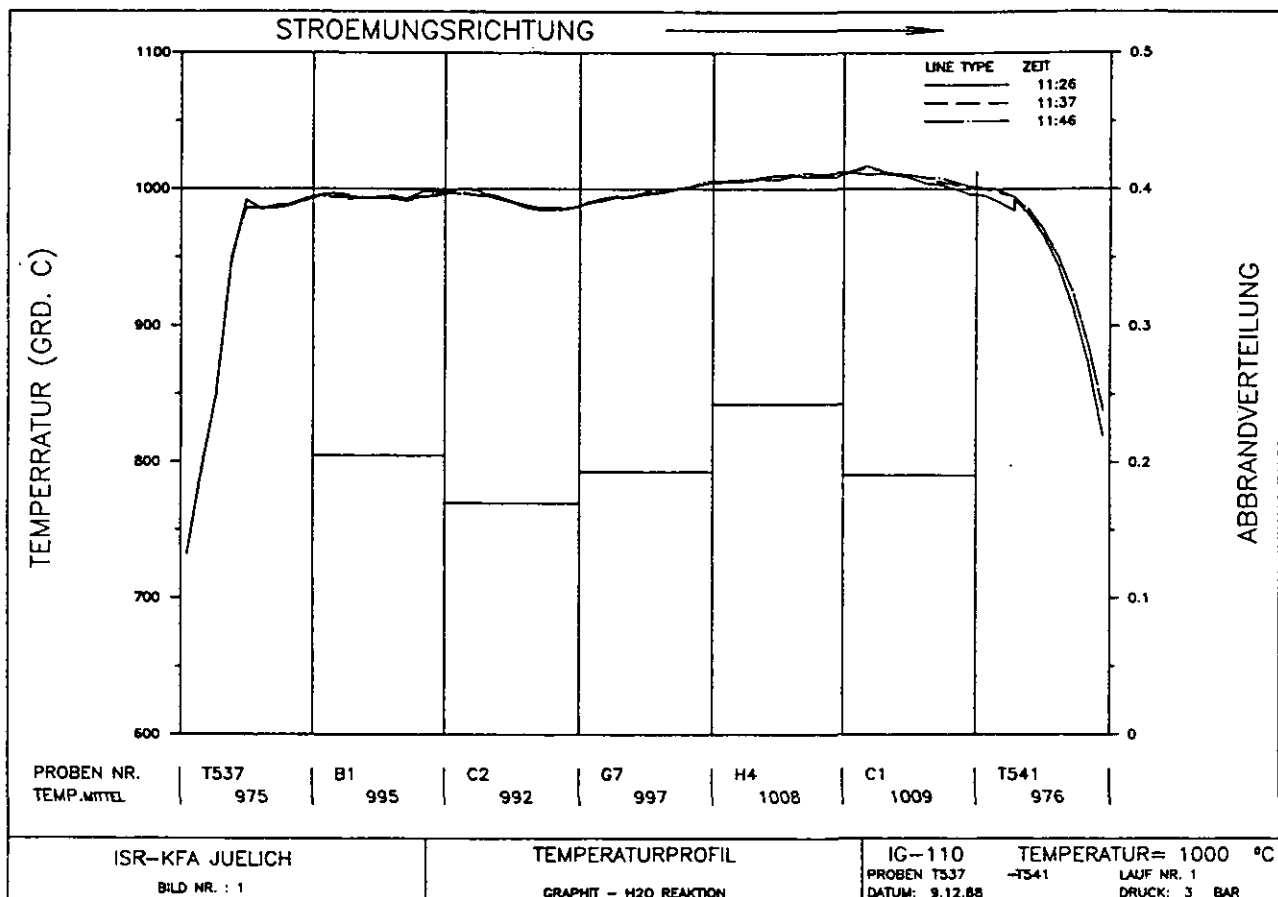


Fig. A.1:

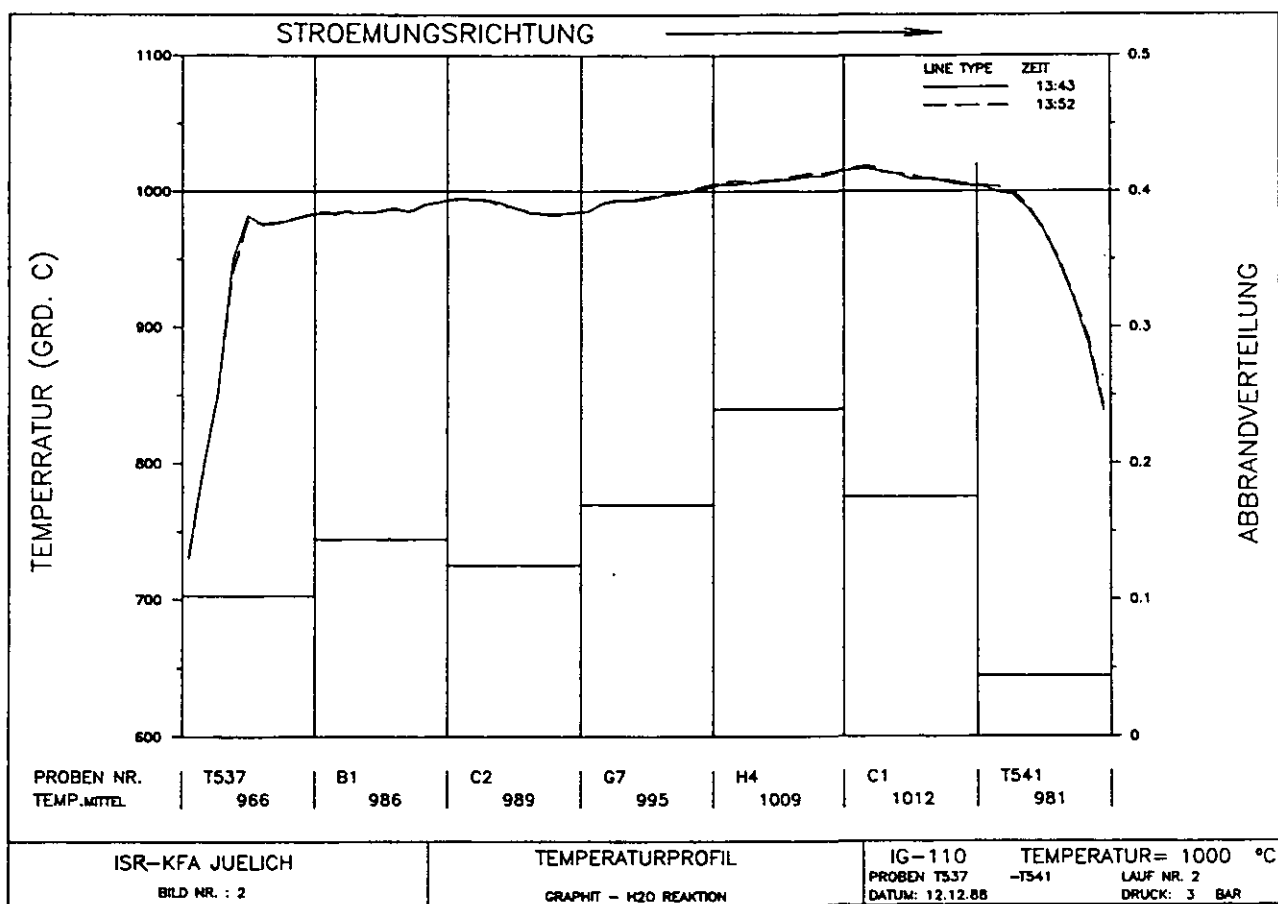


Fig. A.2:

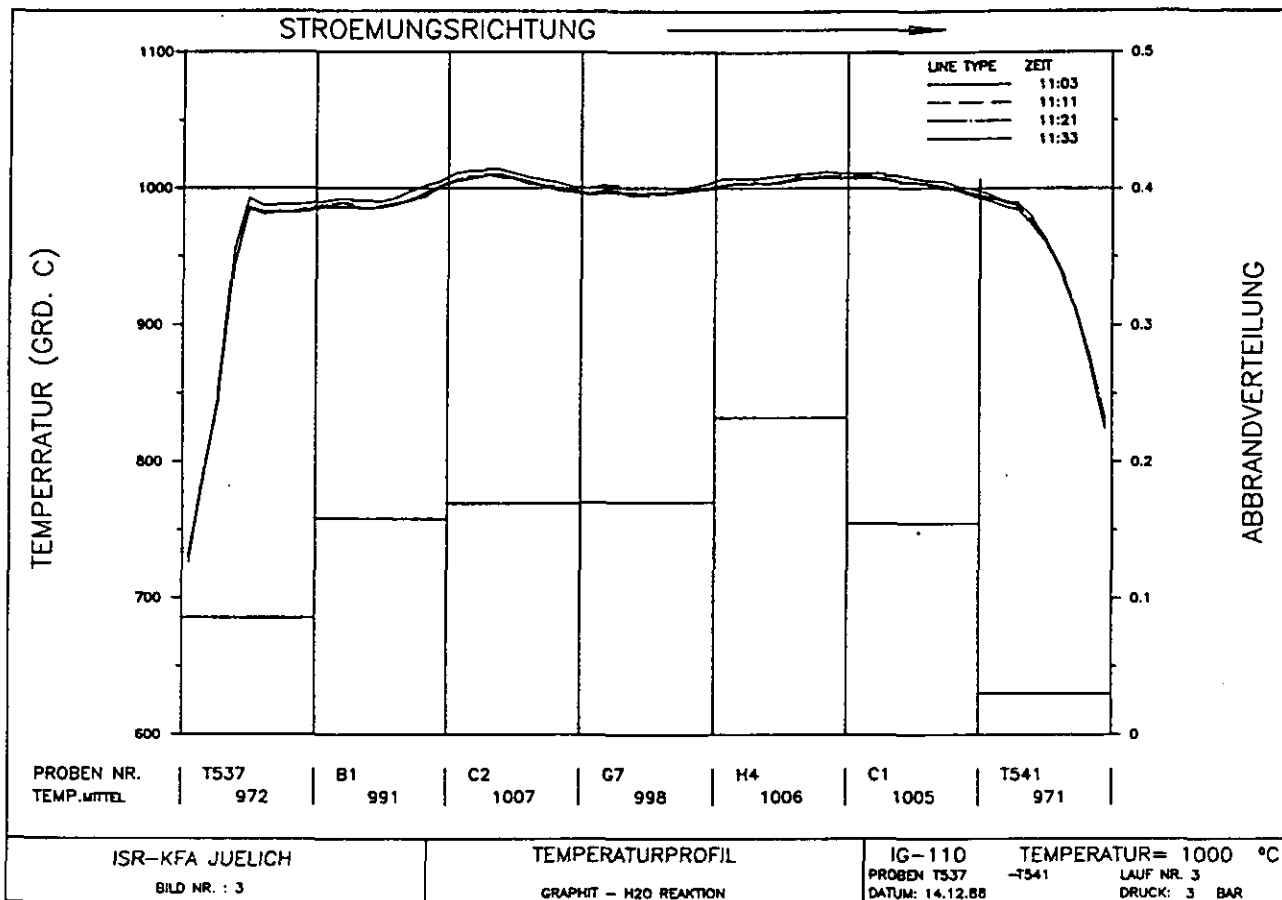


Fig. A.3:

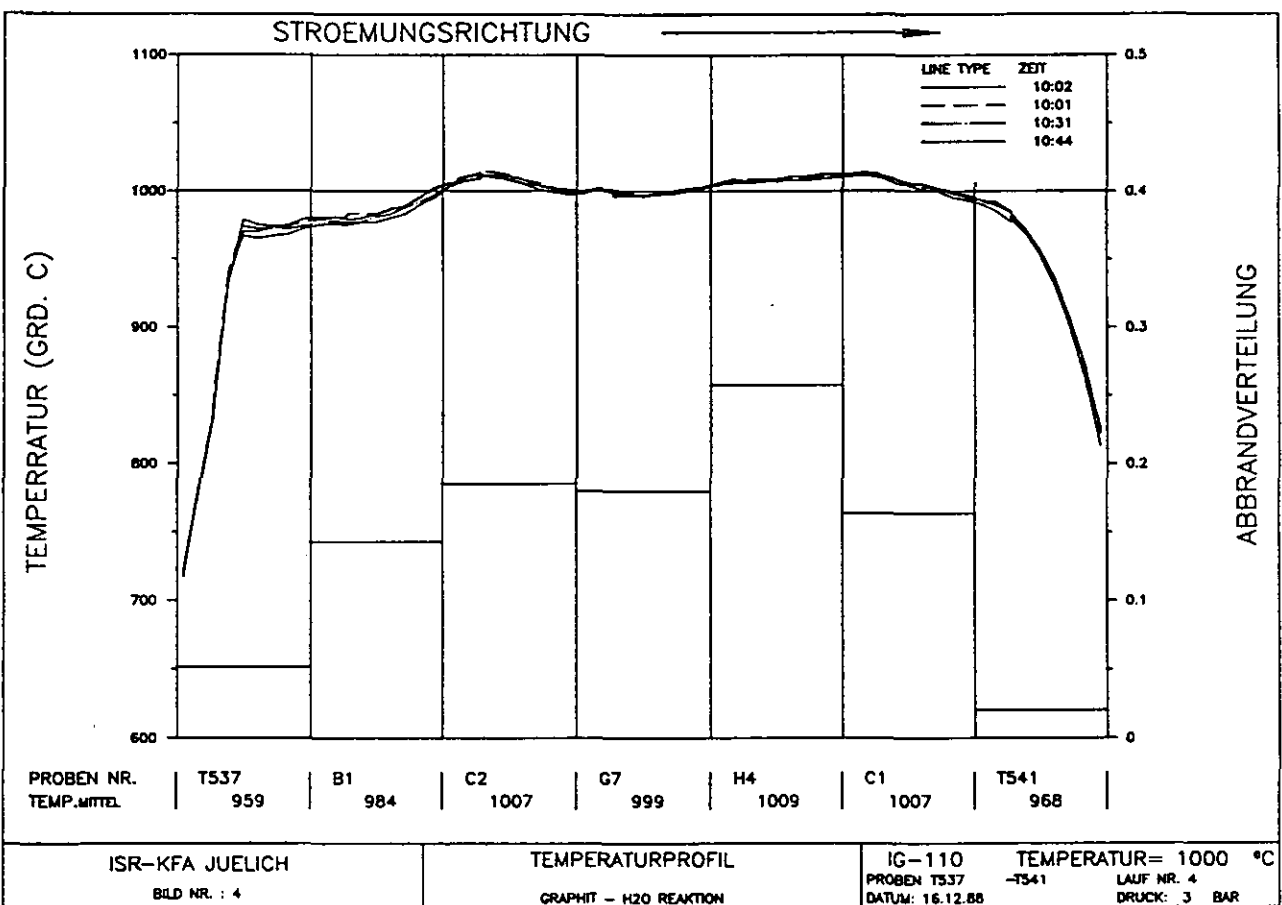


Fig. A.4:

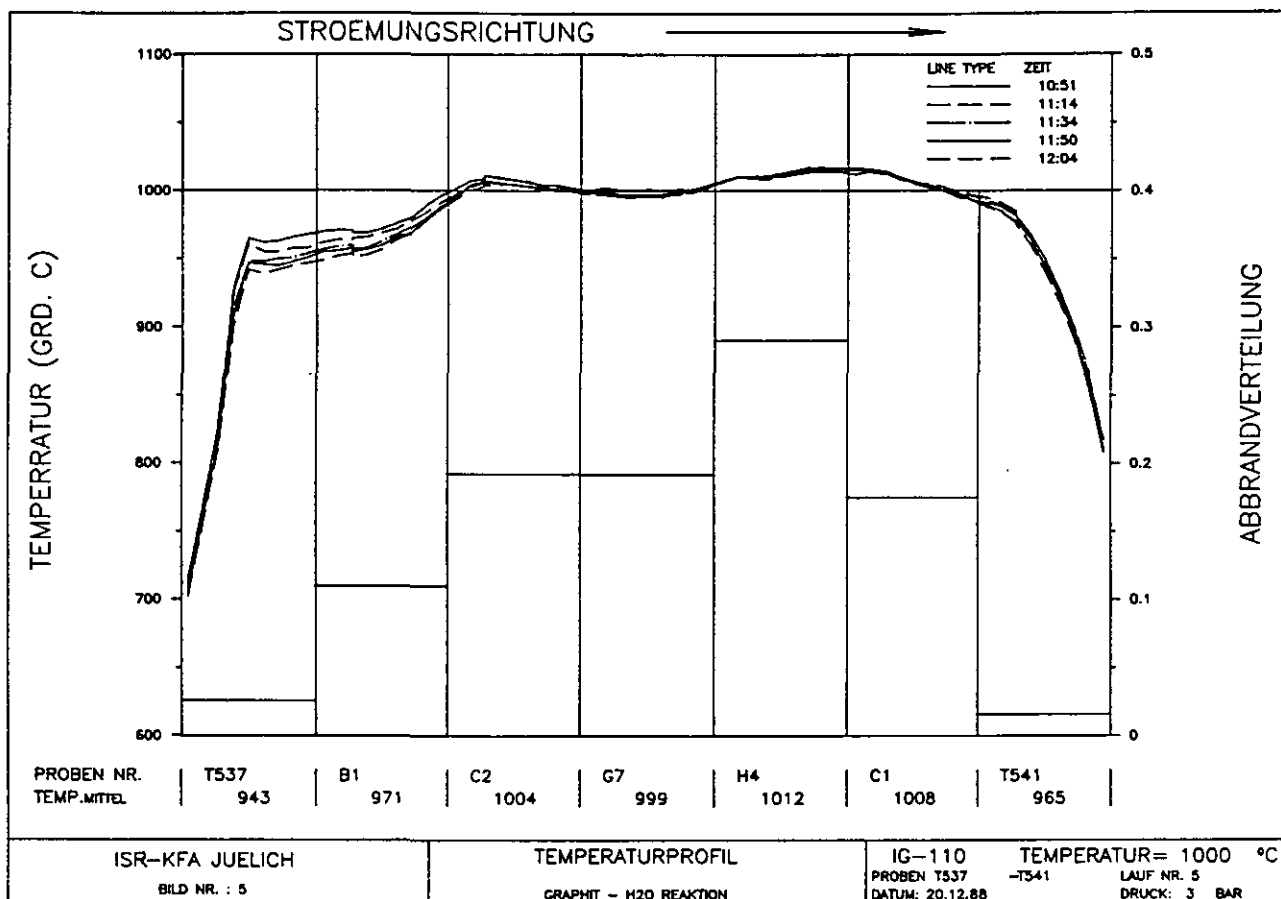


Fig. A.5:

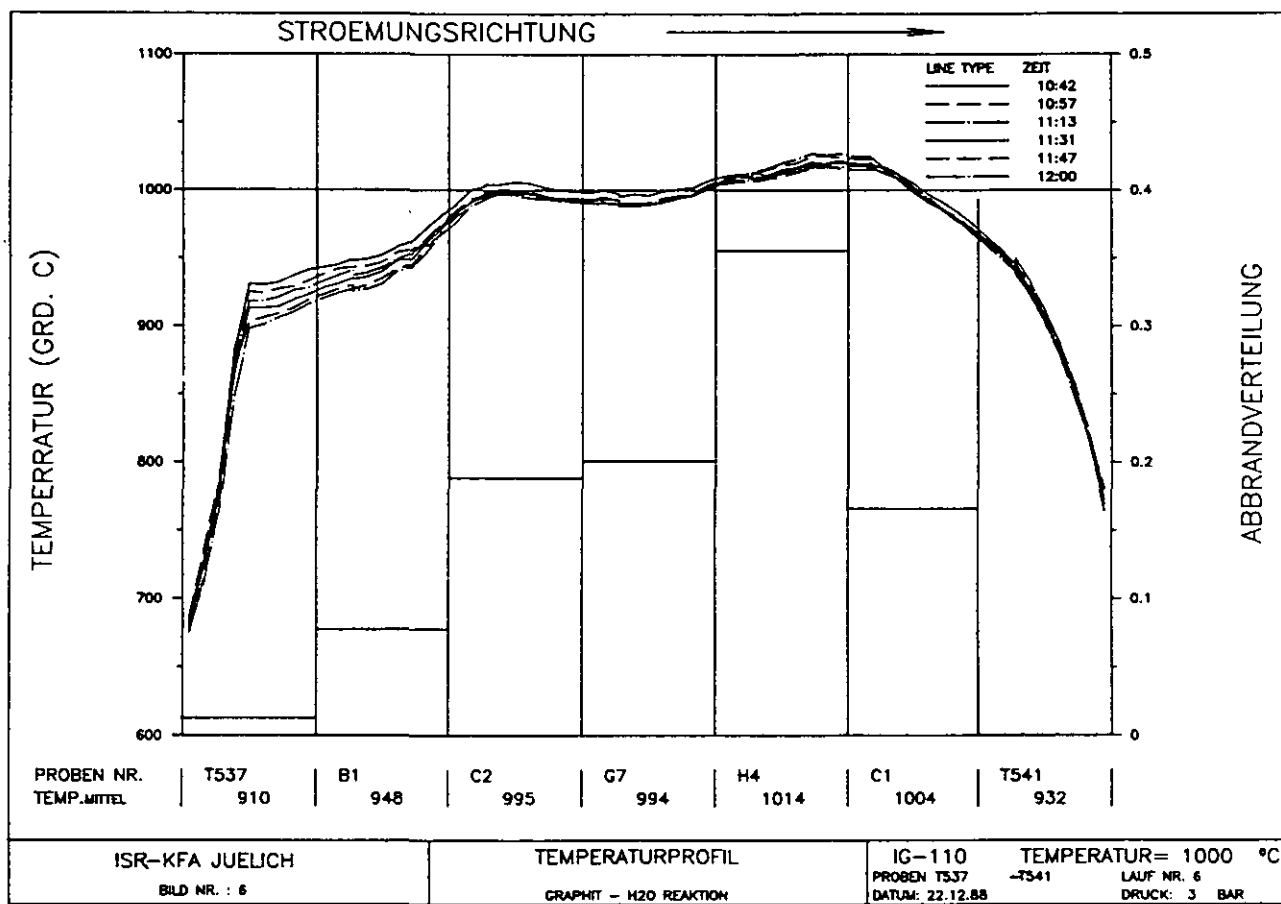


Fig. A.6:

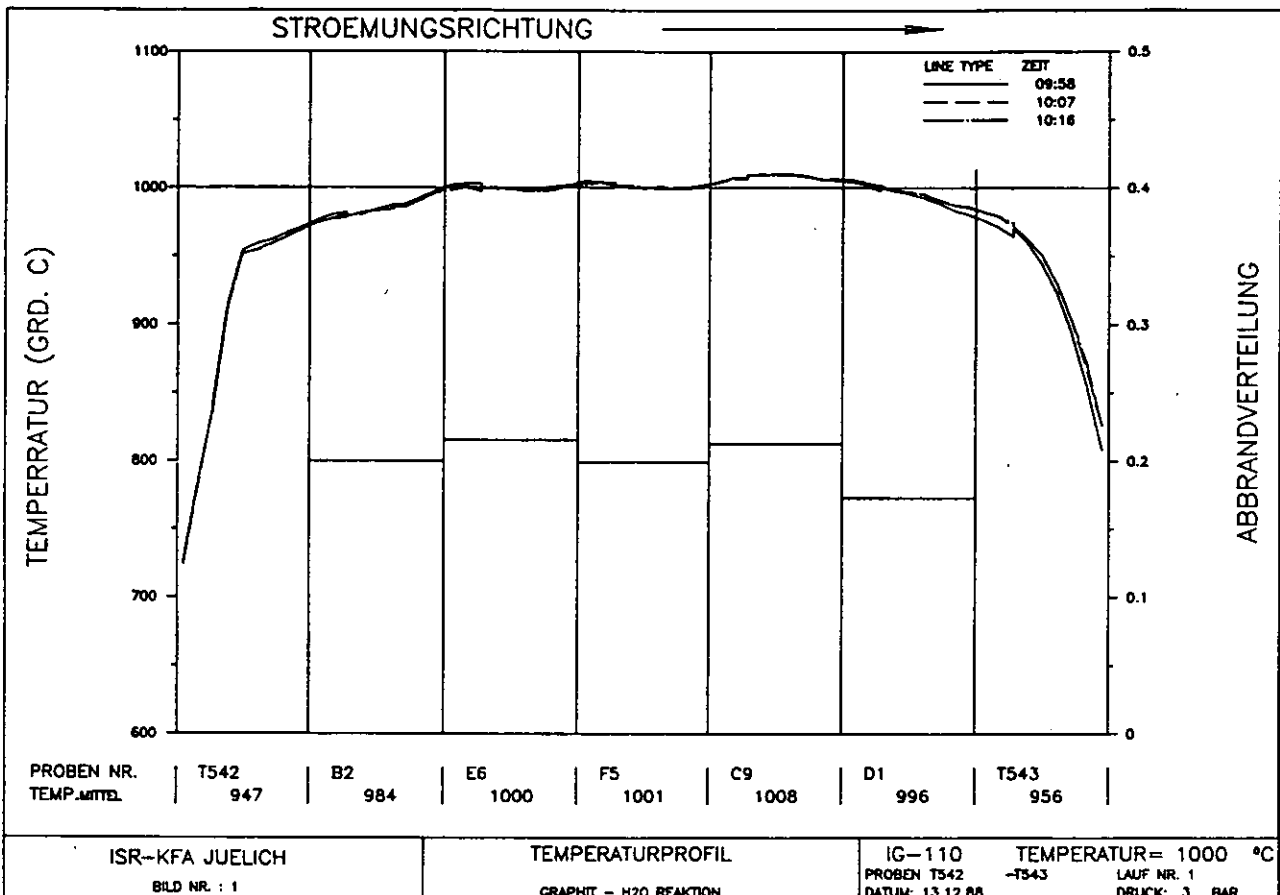


Fig. A.7:

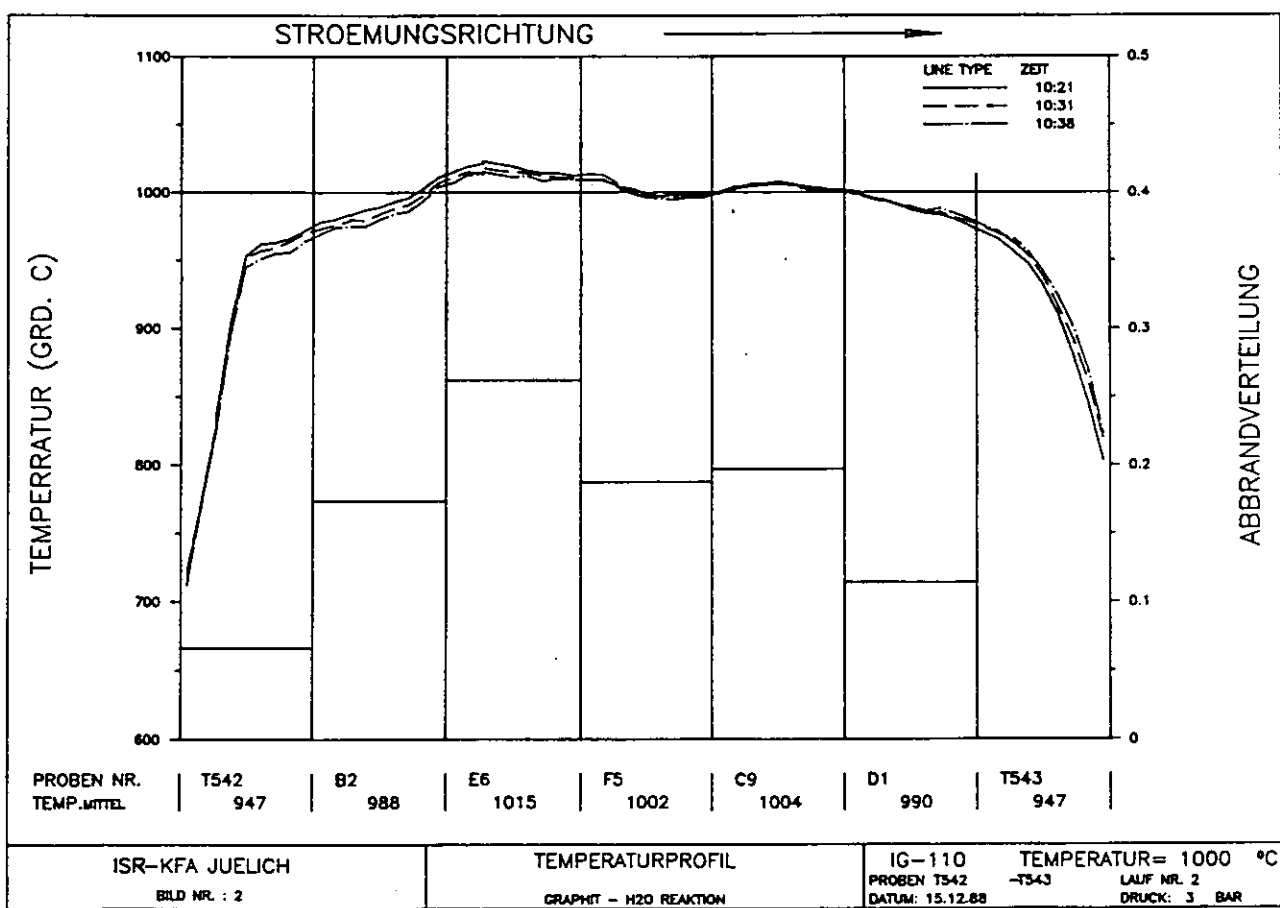


Fig. A.8:

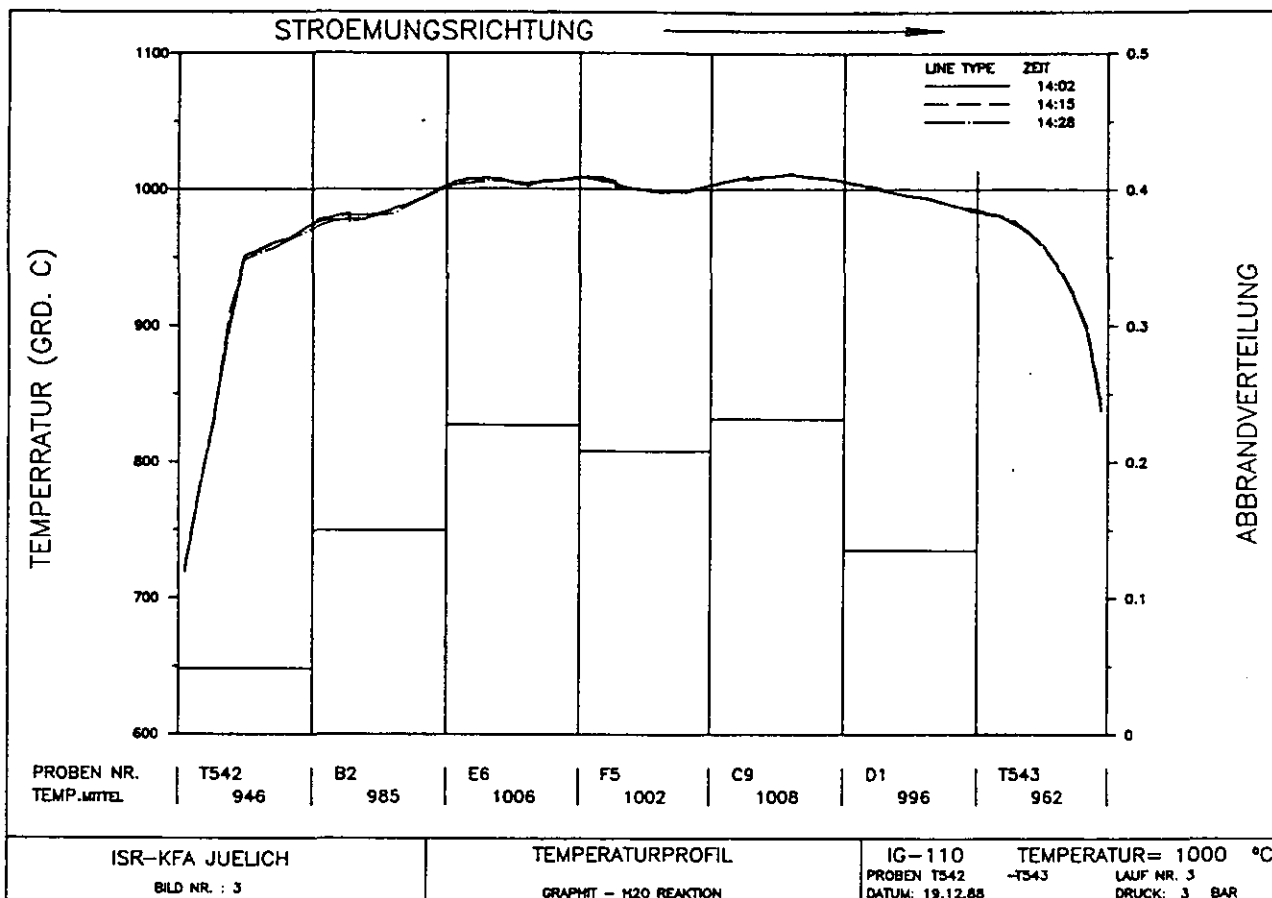


Fig. A.9:

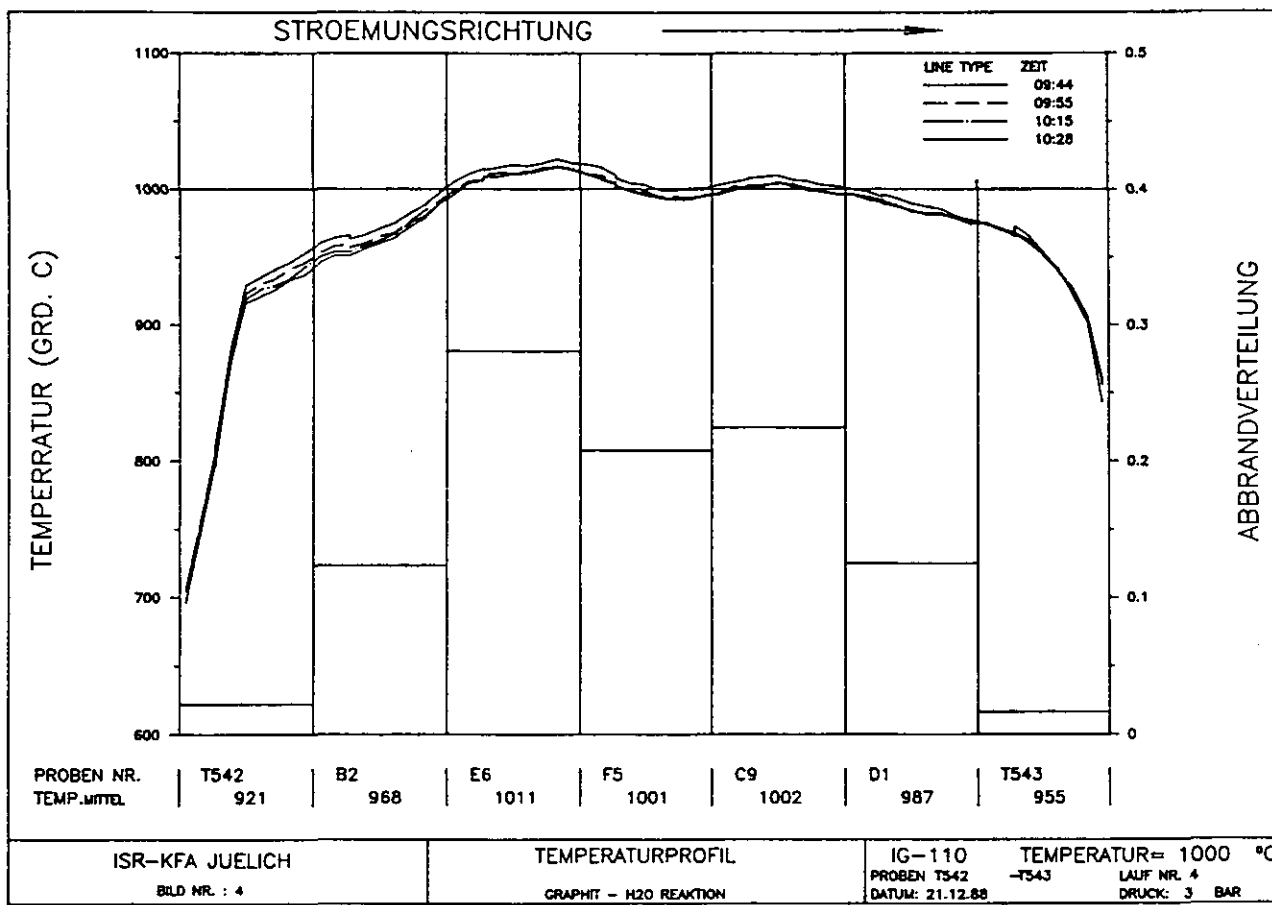


Fig. A.10:

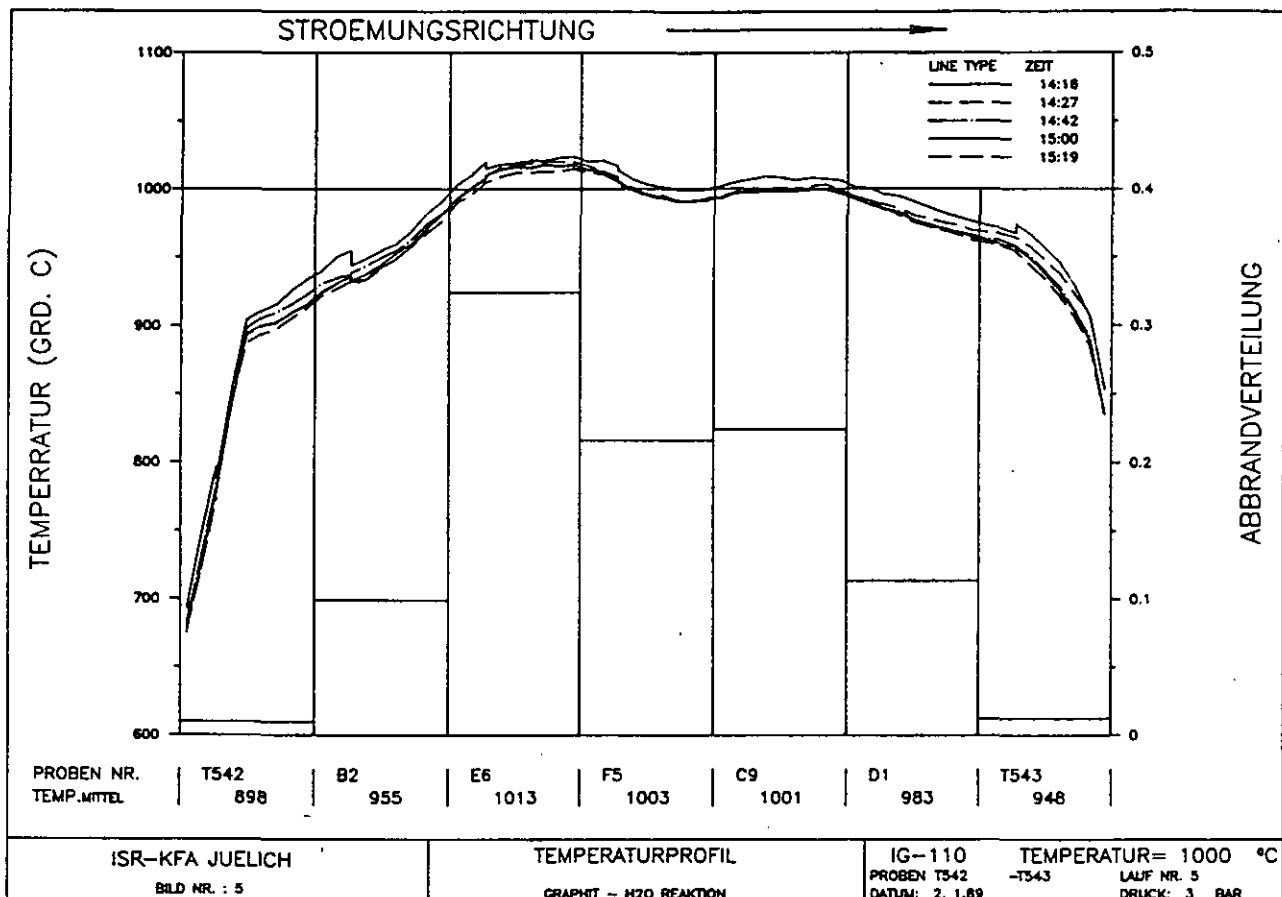


Fig. A.11:

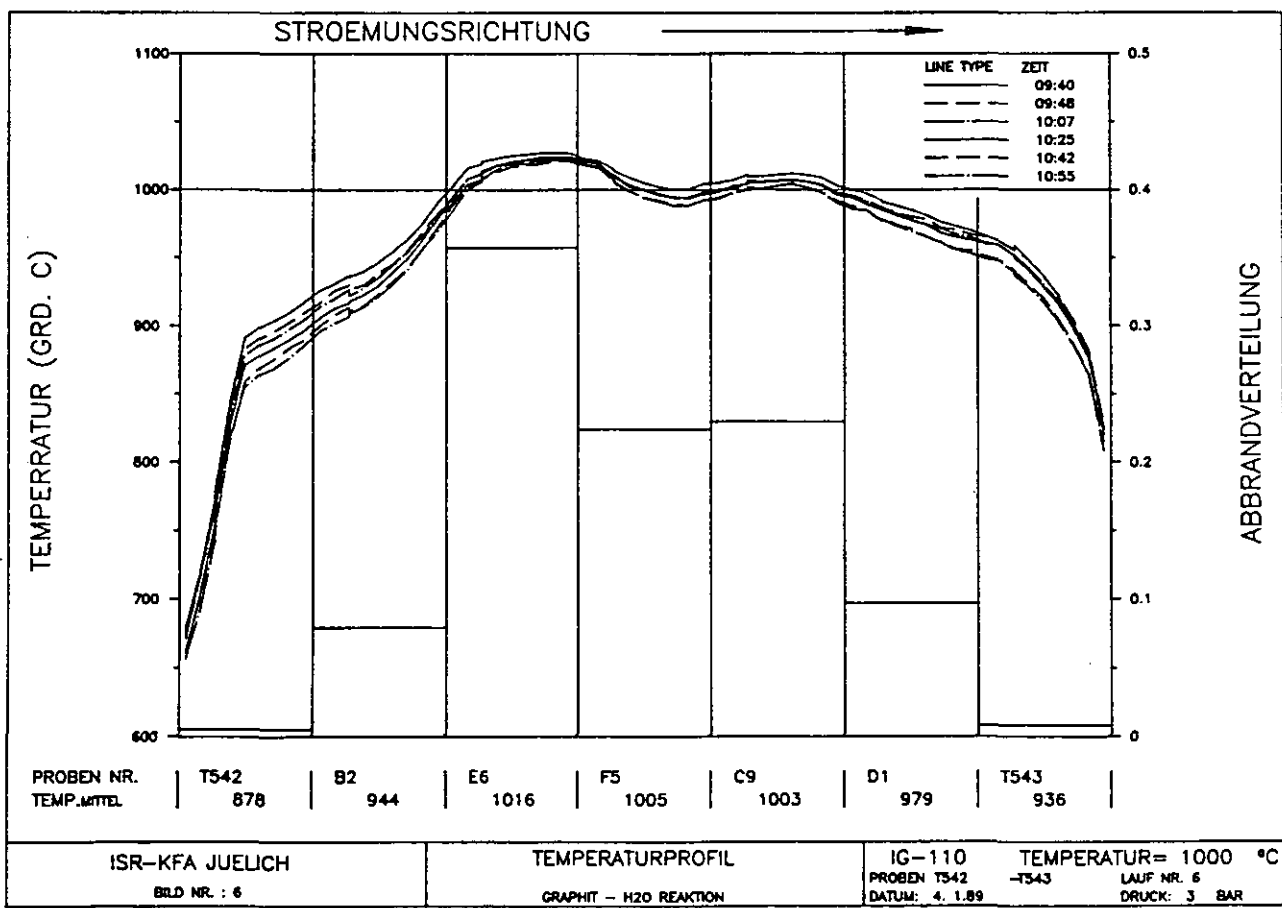


Fig. A.12:

7 bar

B3, C3, G4, H5, E1
E7, F6, C8, F1
B0, D2, D5, D7, C0

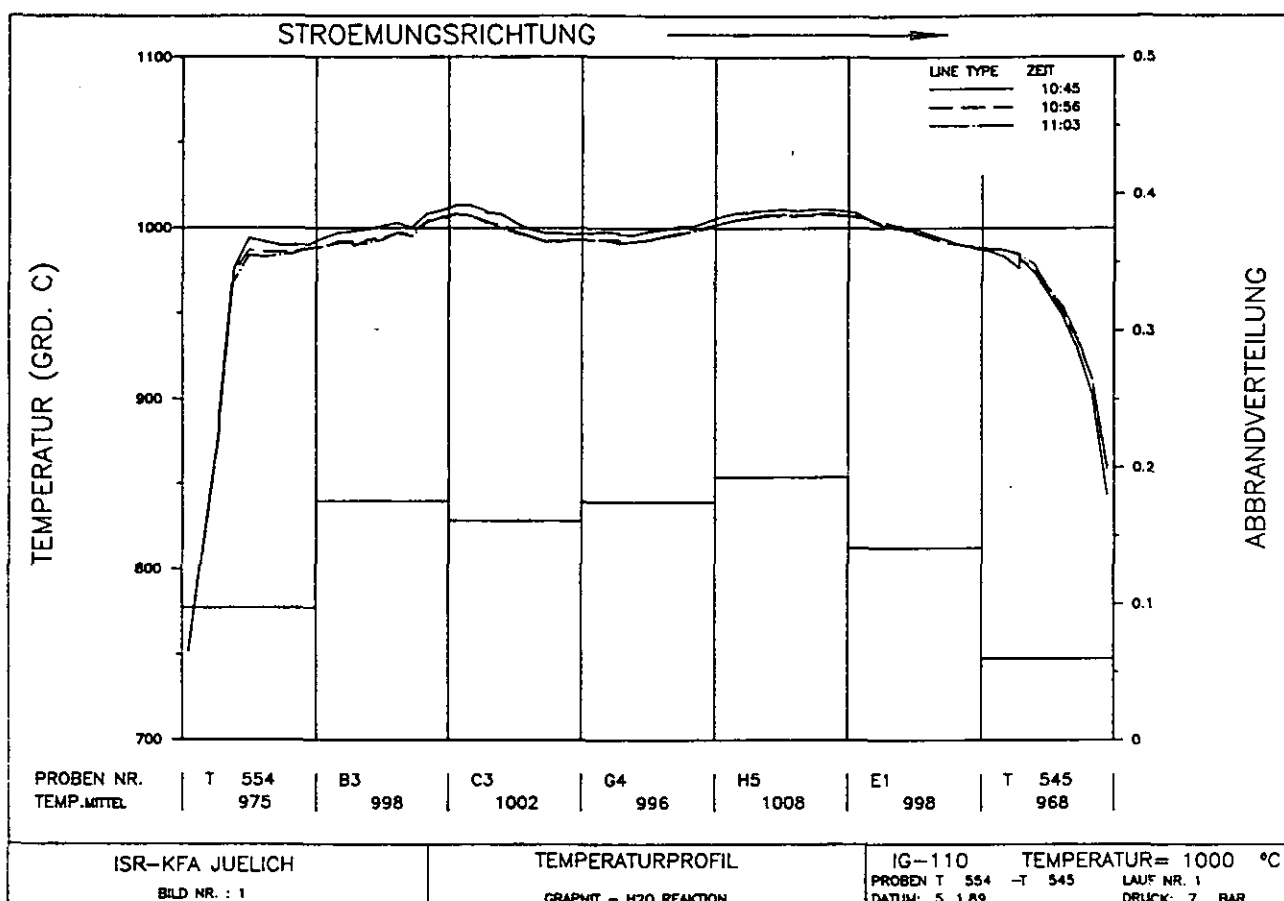


Fig. A.13:

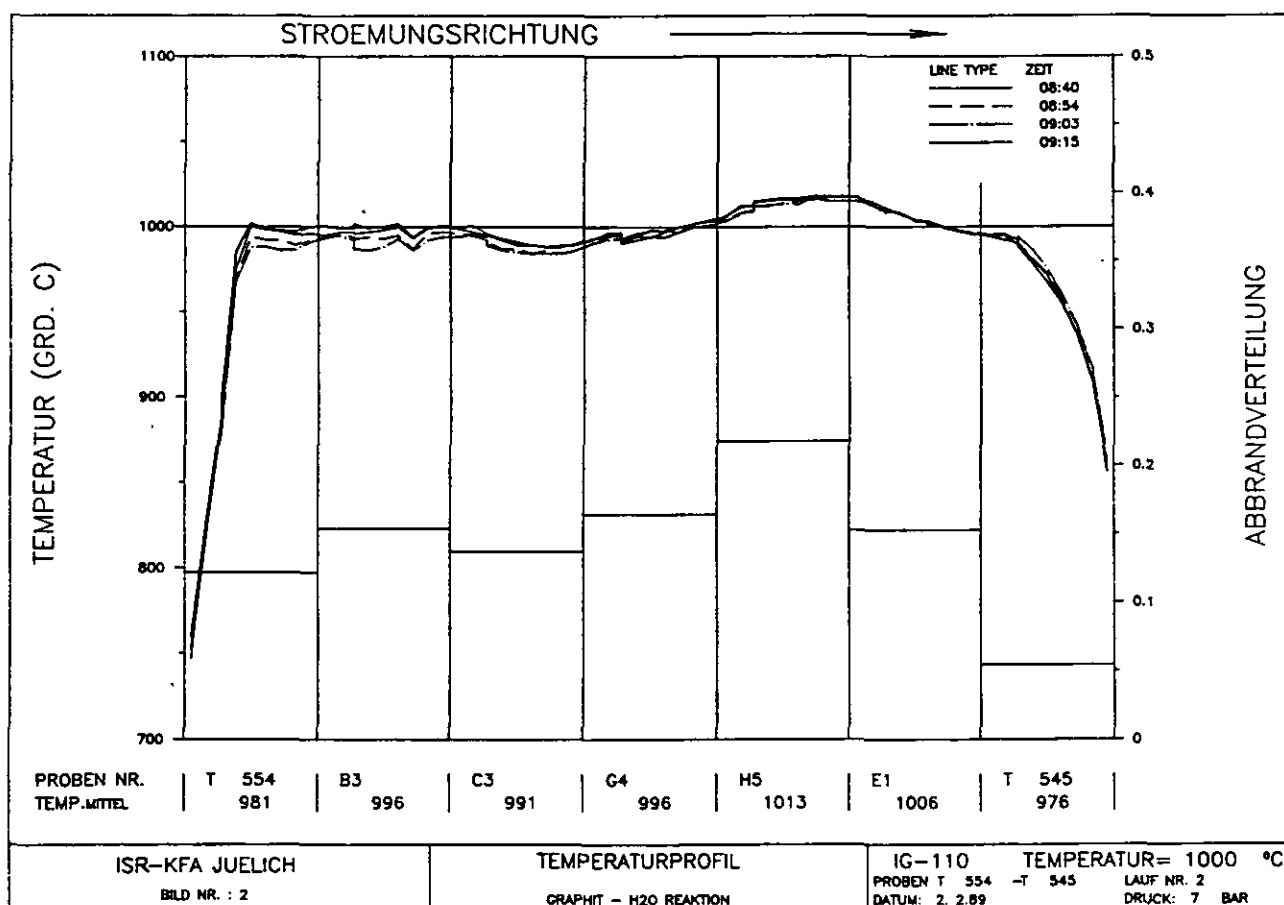


Fig. A.14:

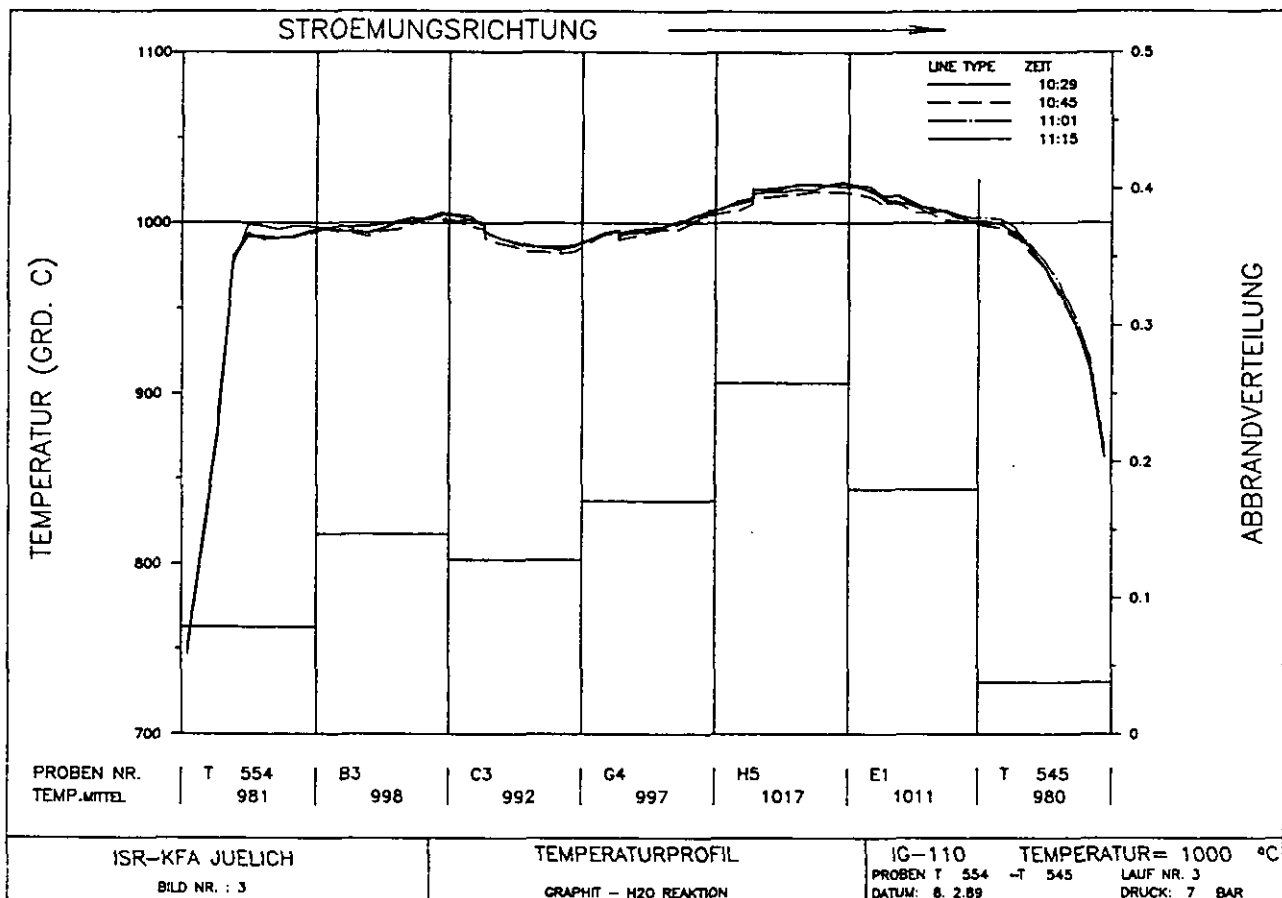


Fig. A.15:

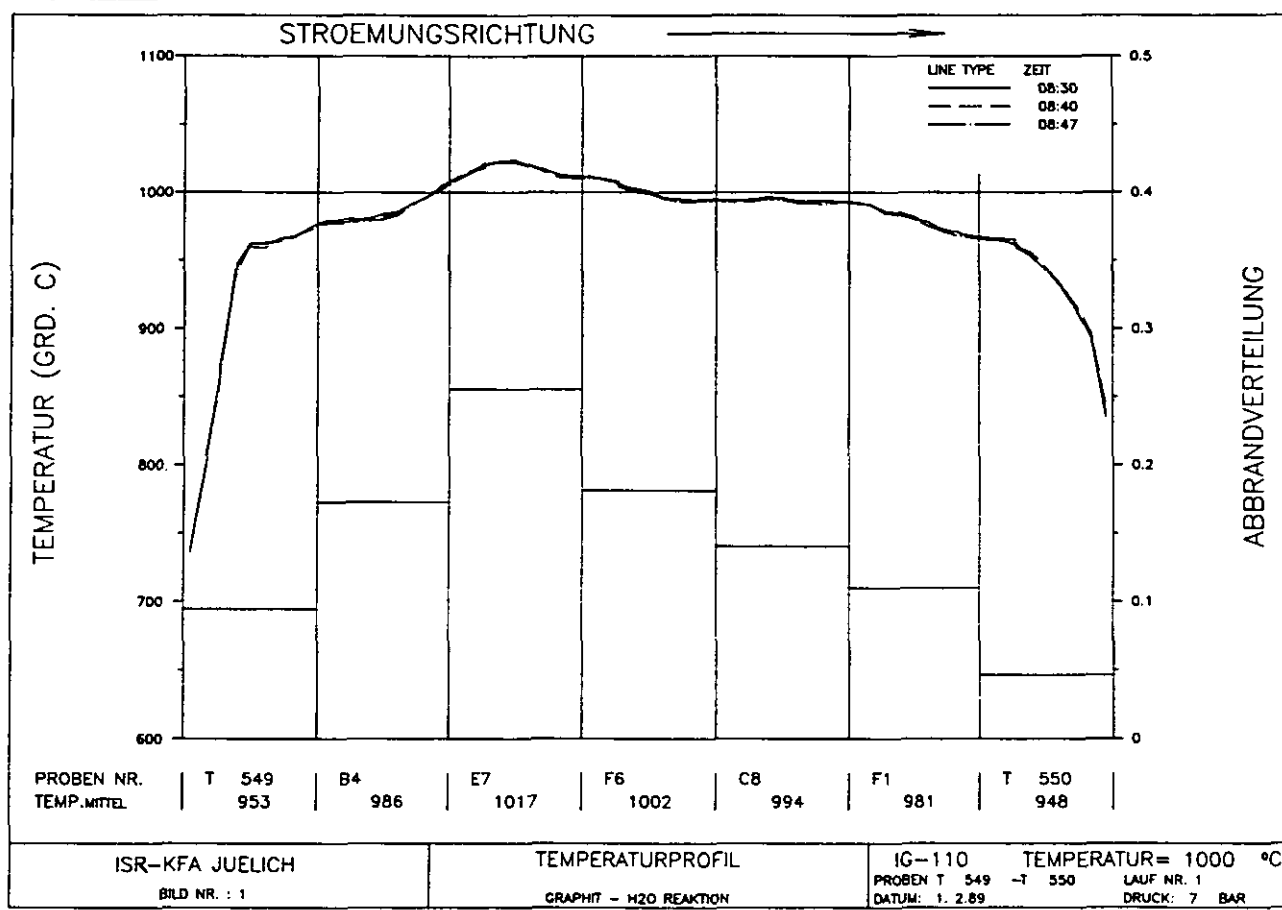


Fig. A.16:

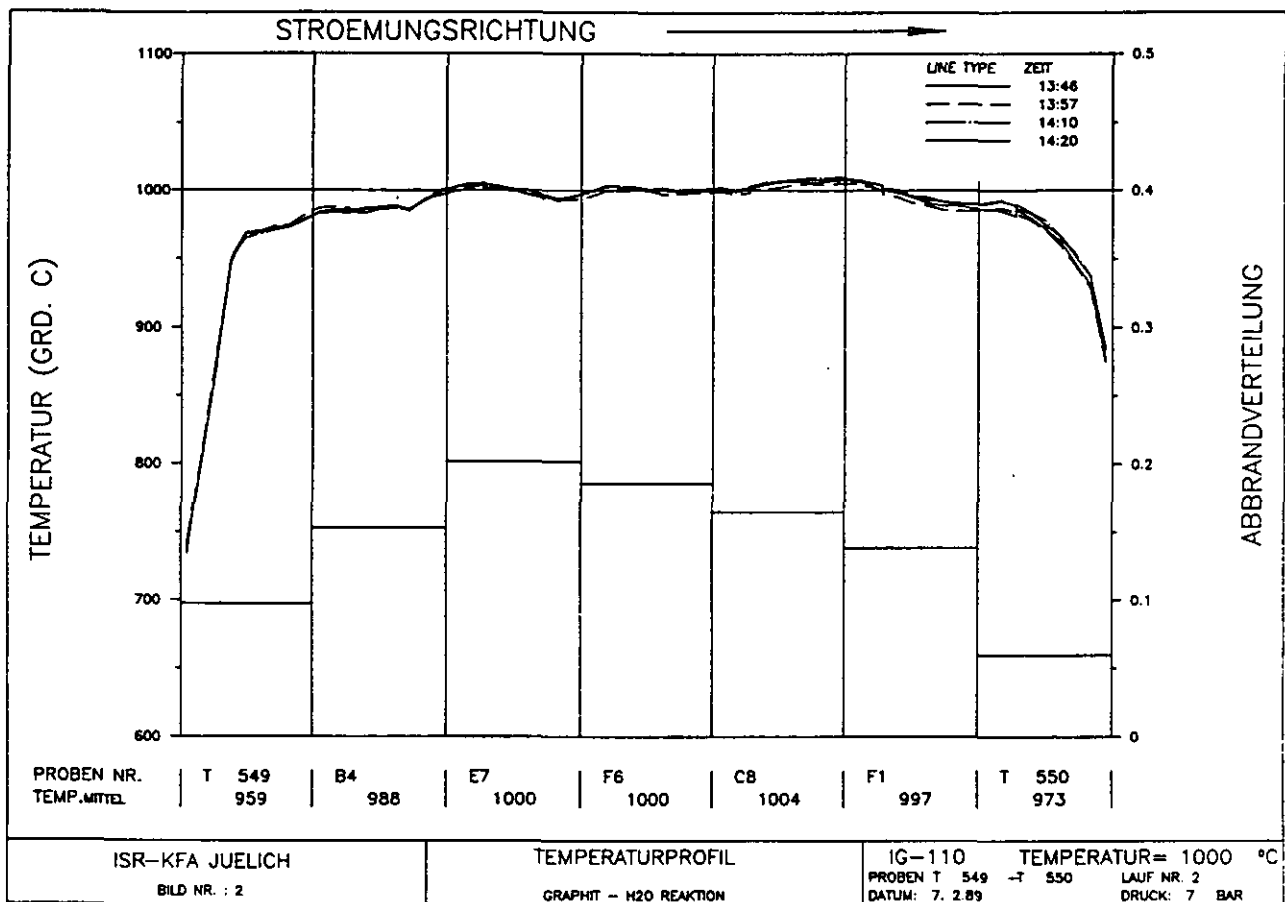


Fig. A.17:

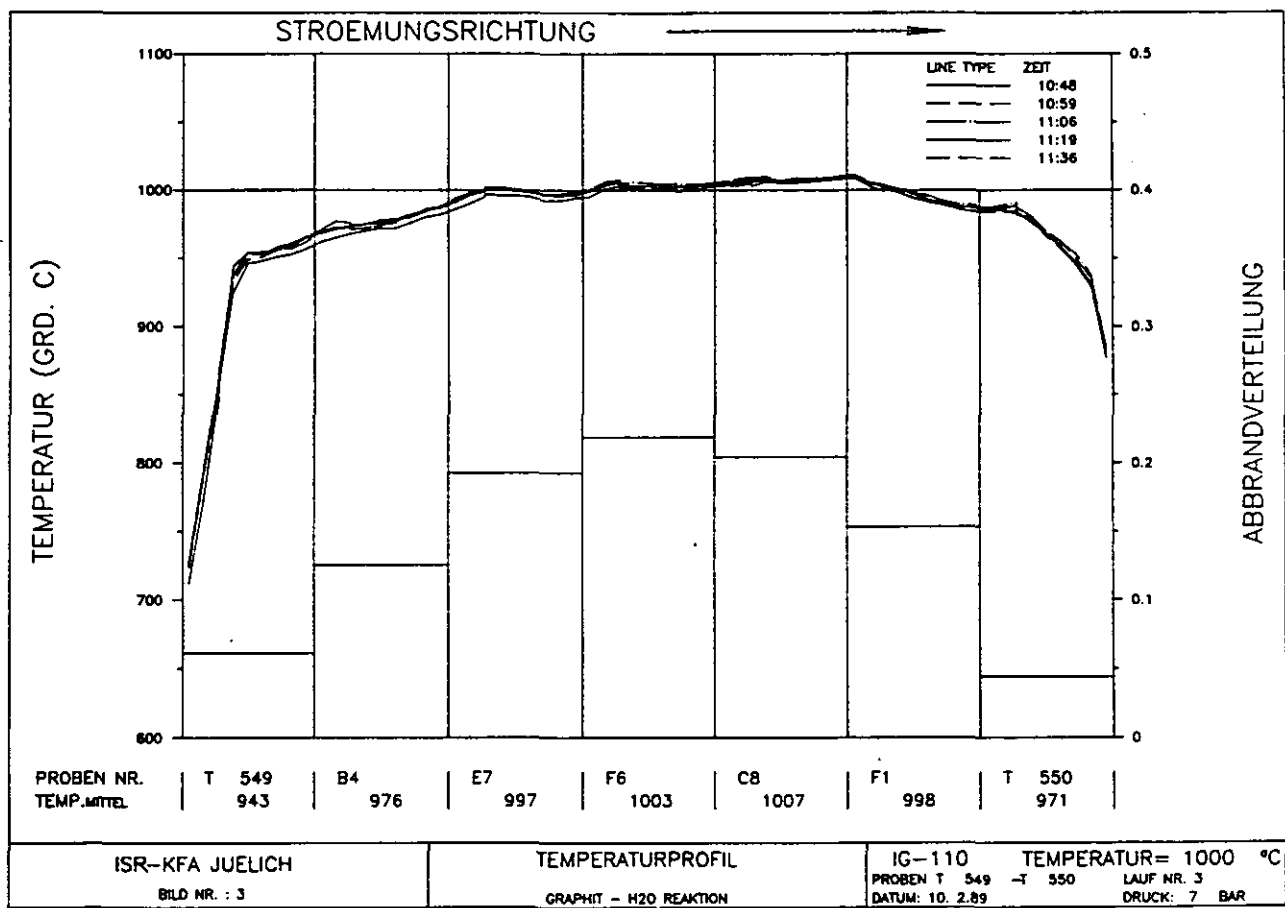


Fig. A.18:

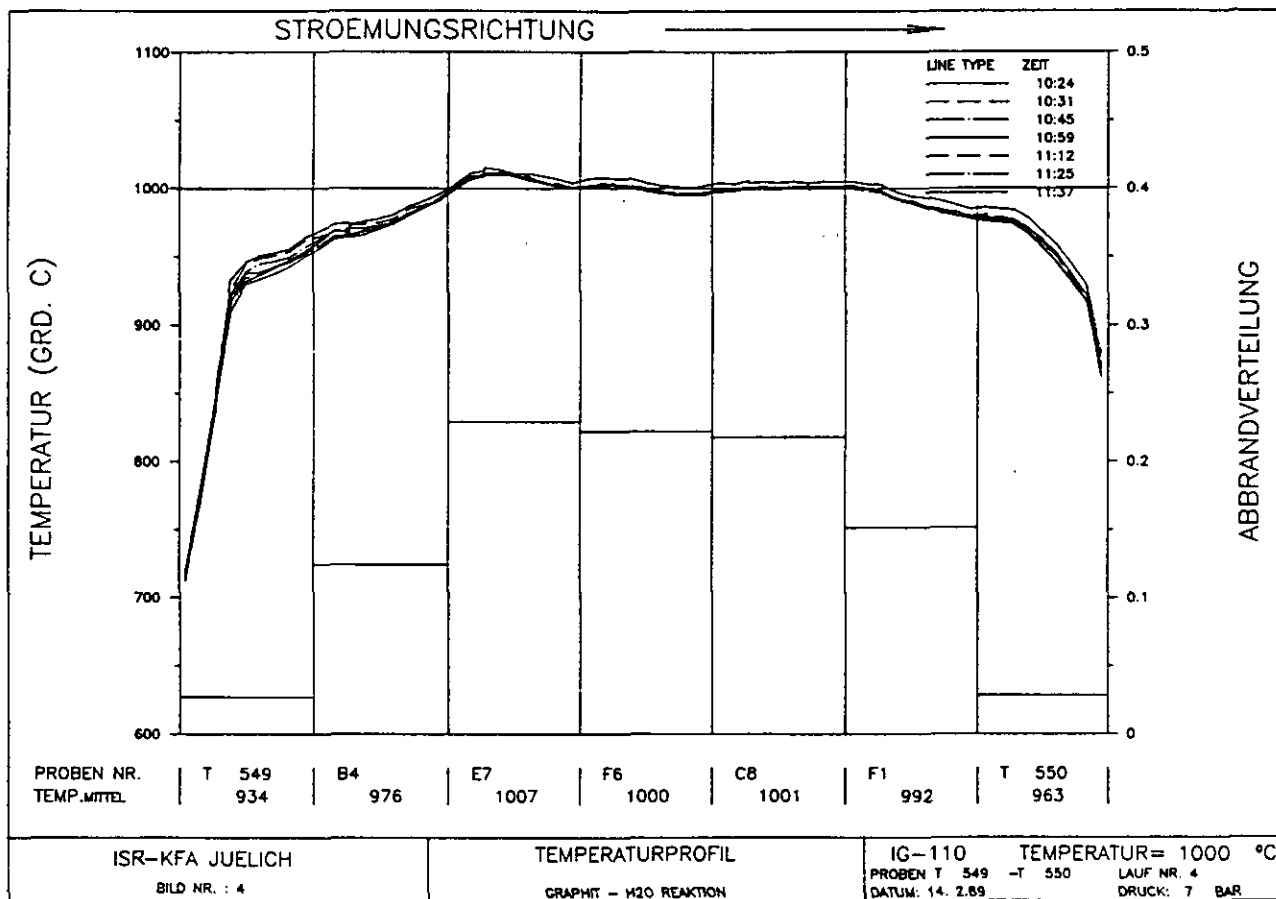


Fig. A.19:

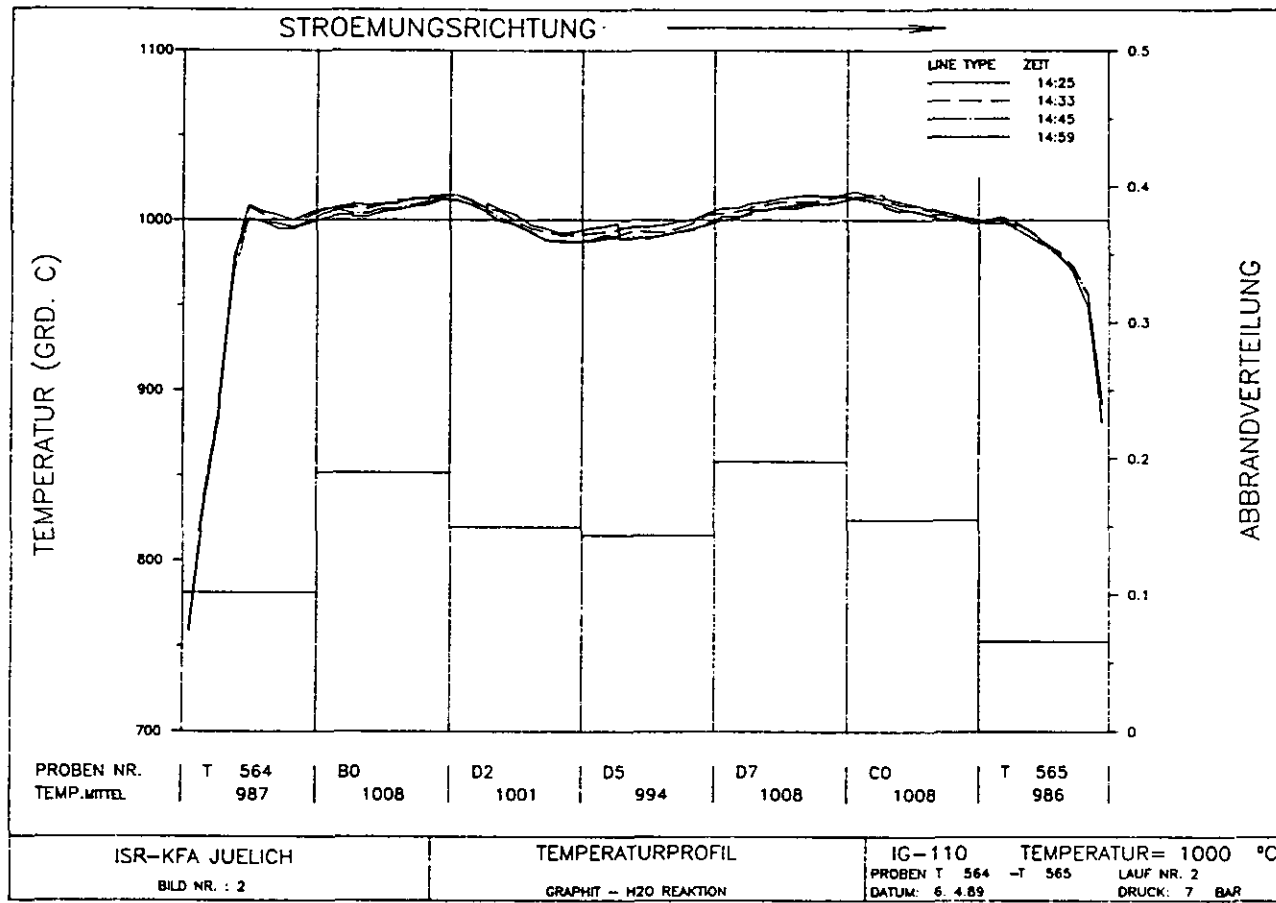


Fig. A.20:

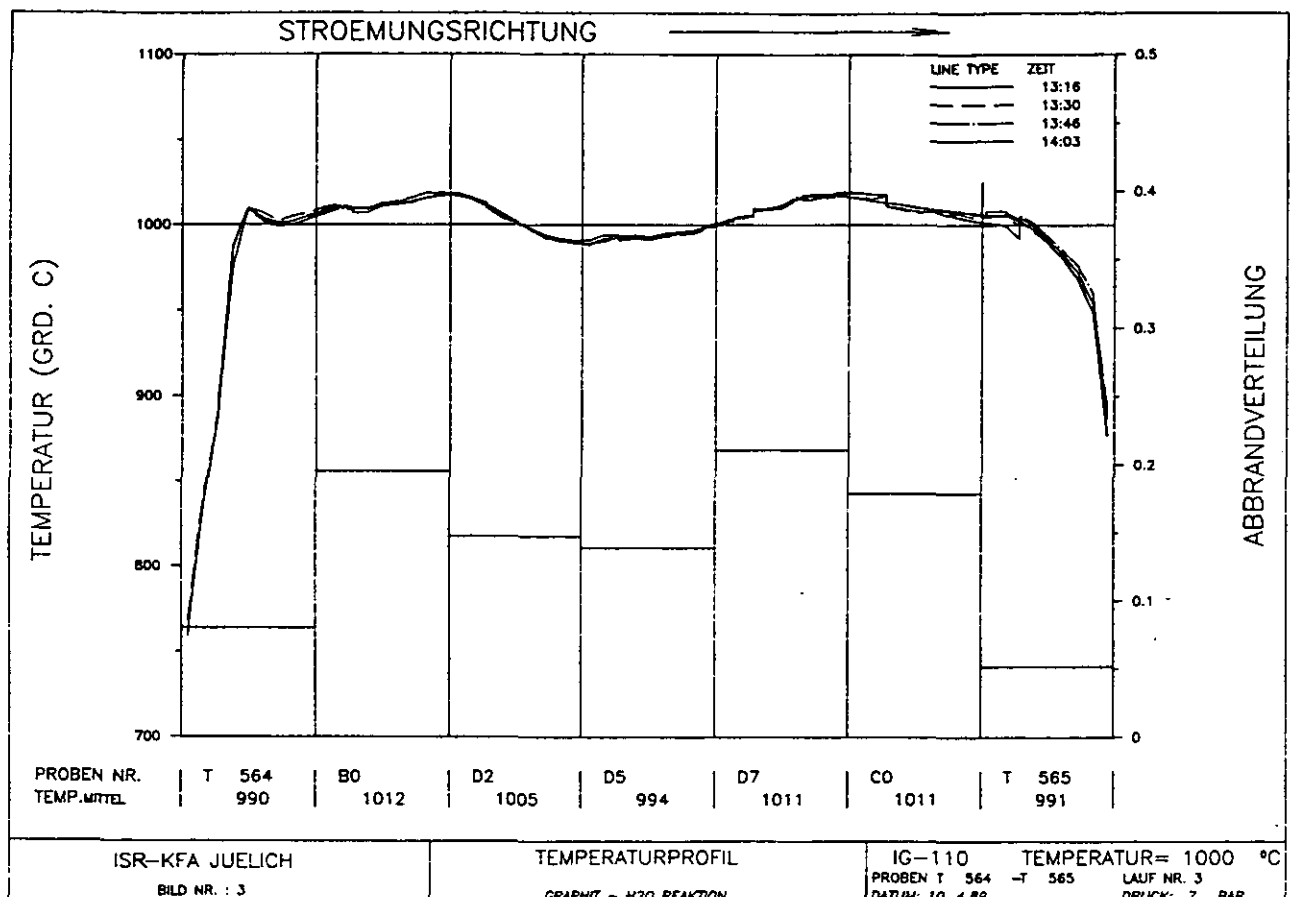


Fig. A.21:

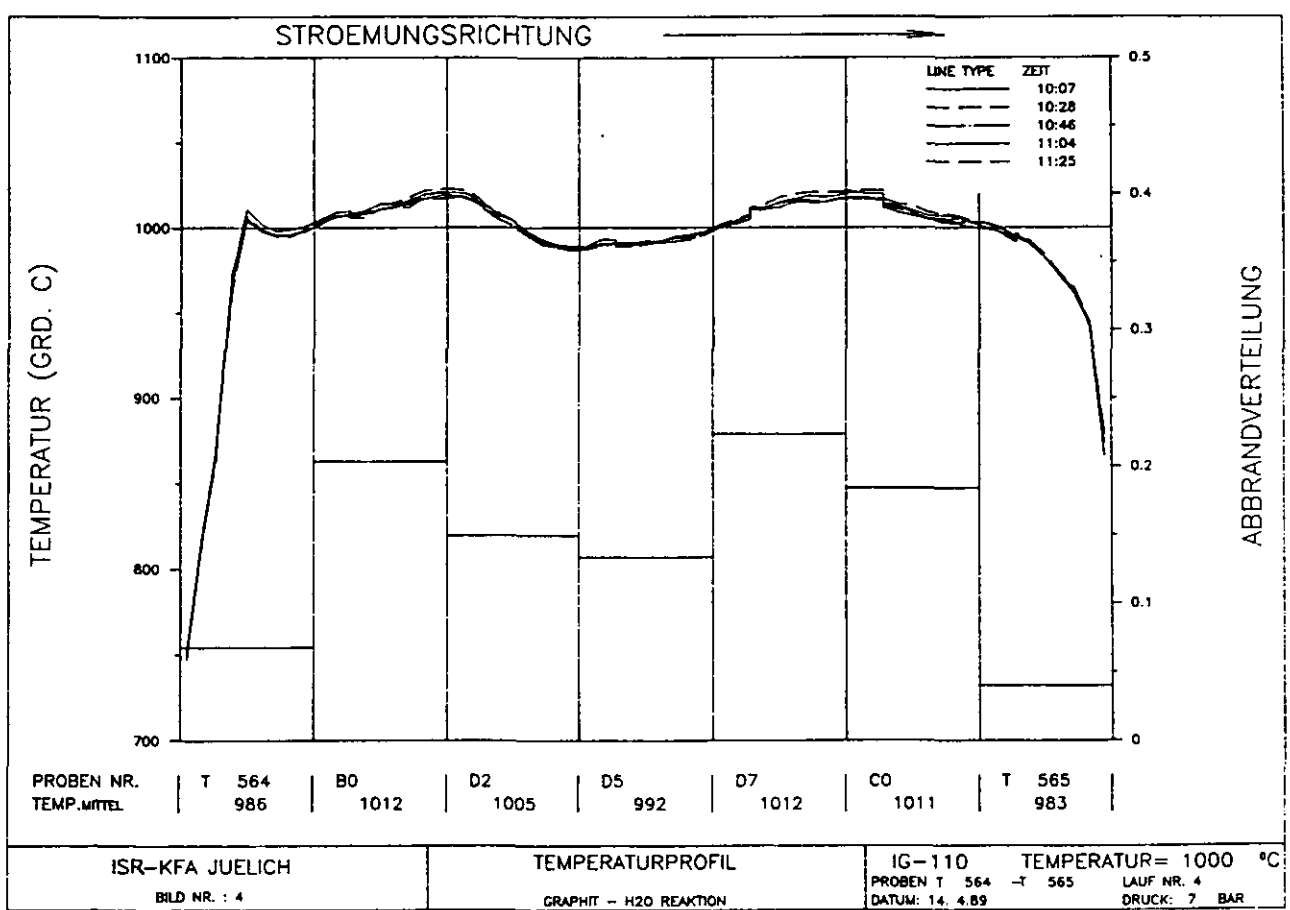


Fig. A.22:

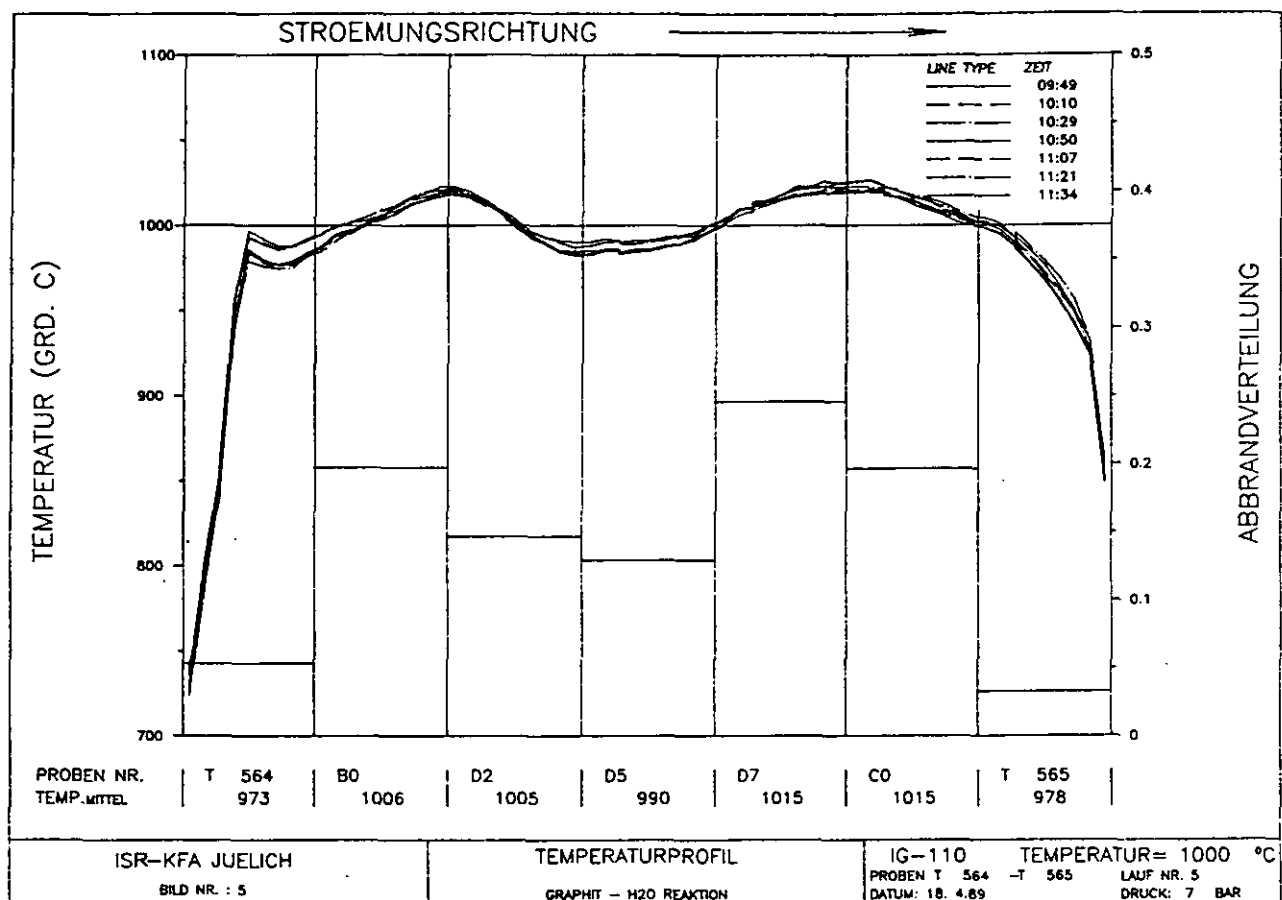


Fig. A.23:

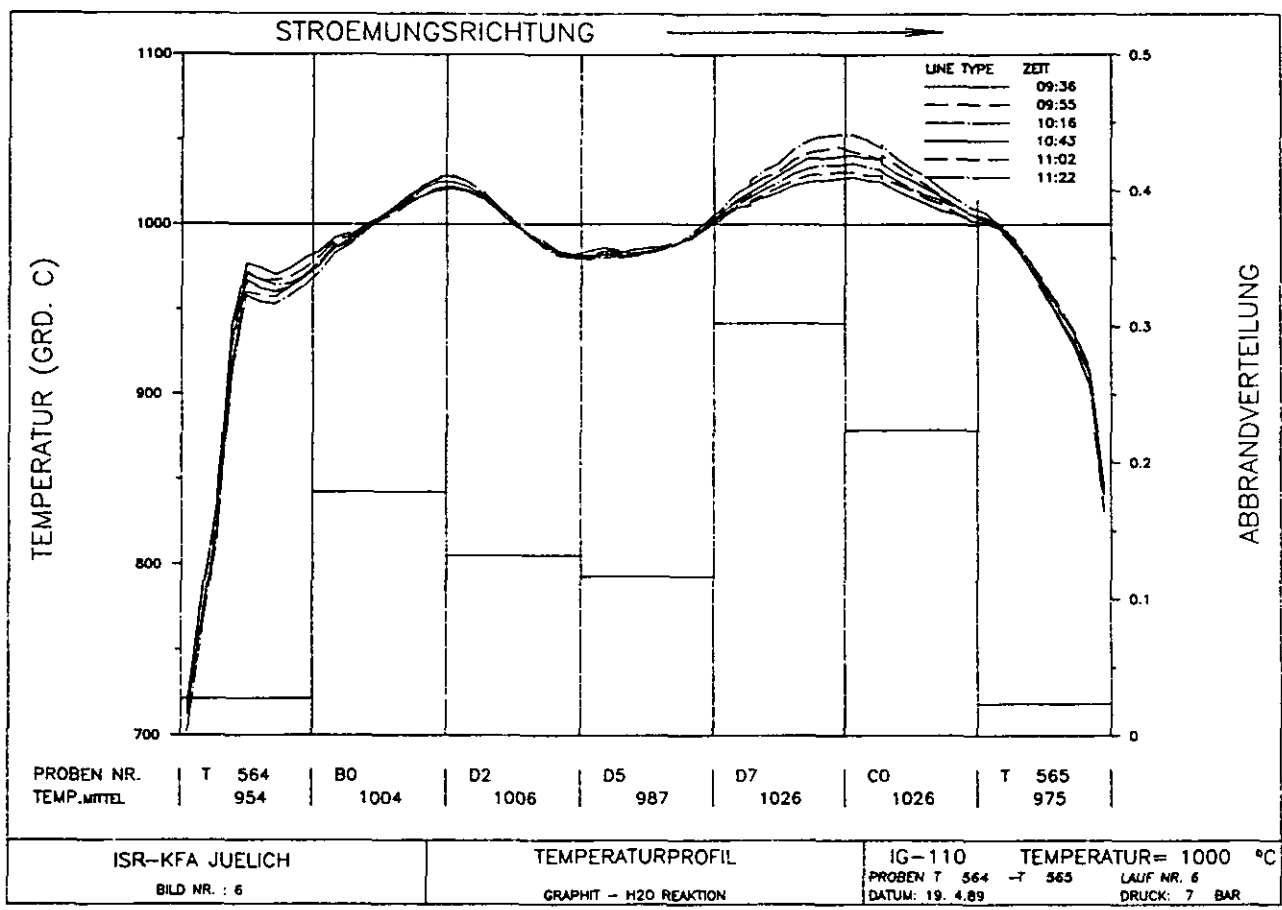


Fig. A.24:

15 bar

B5, I2, F4, H6
B6, E5, G5, I8, H1

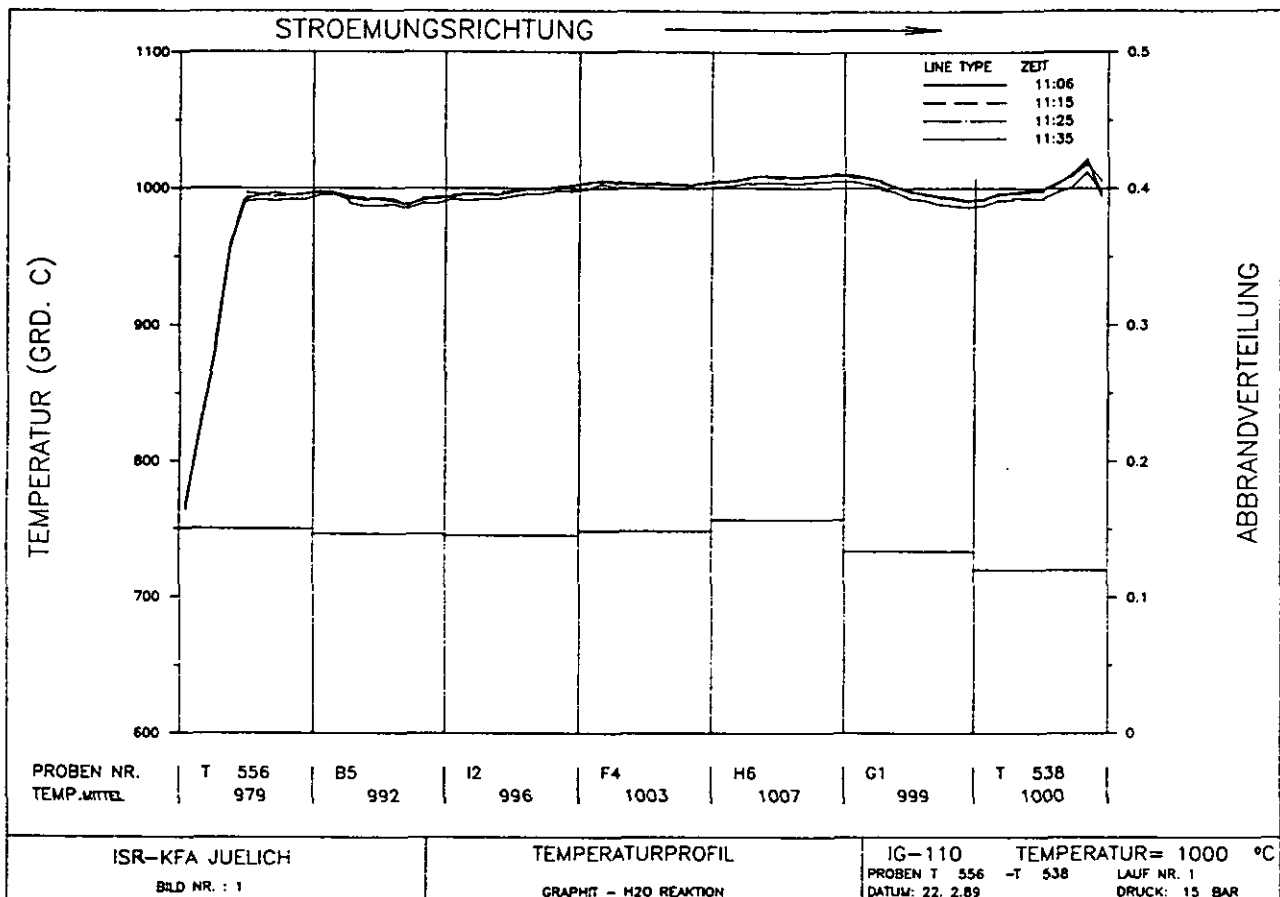


Fig. A.25:

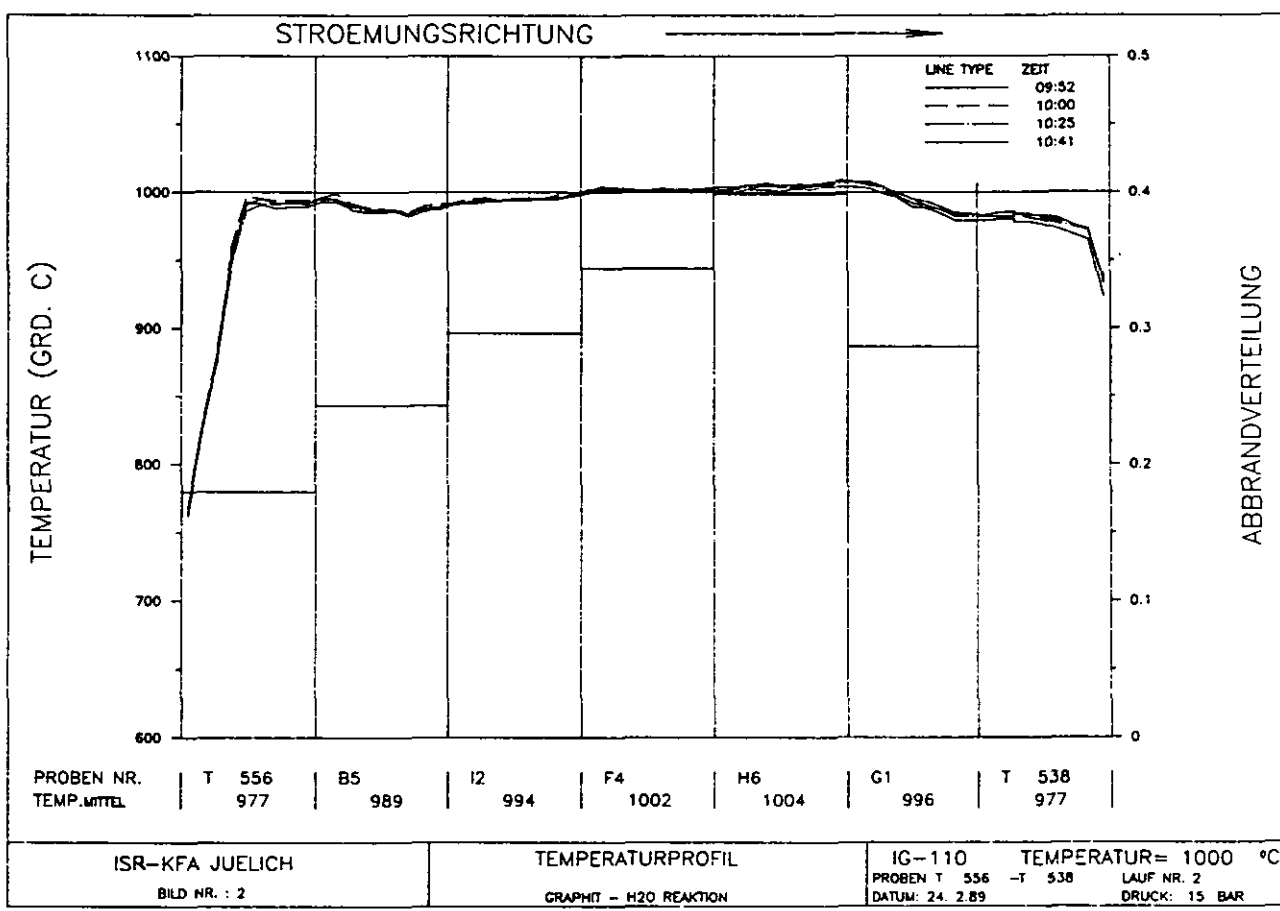


Fig. A.26:

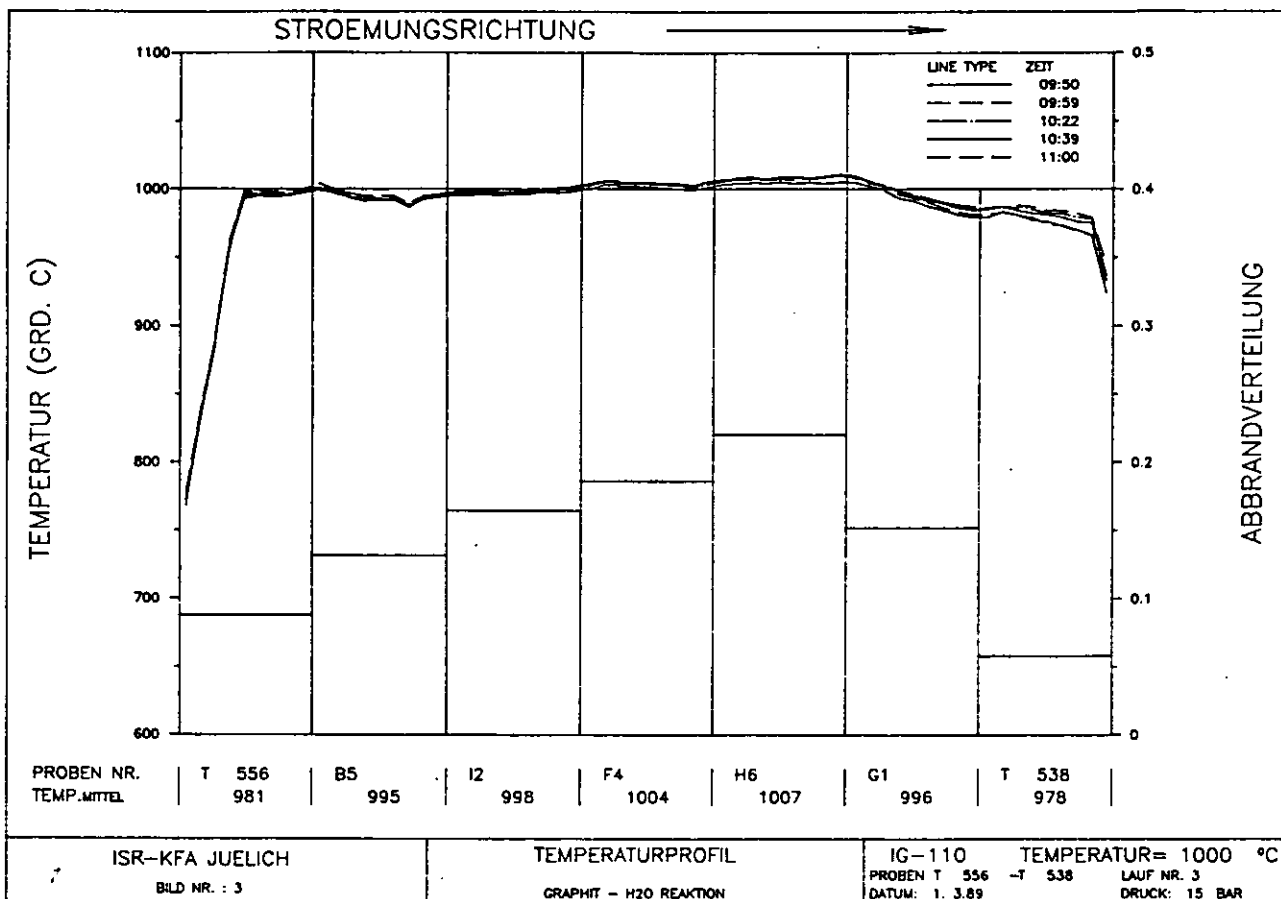


Fig. A.27:

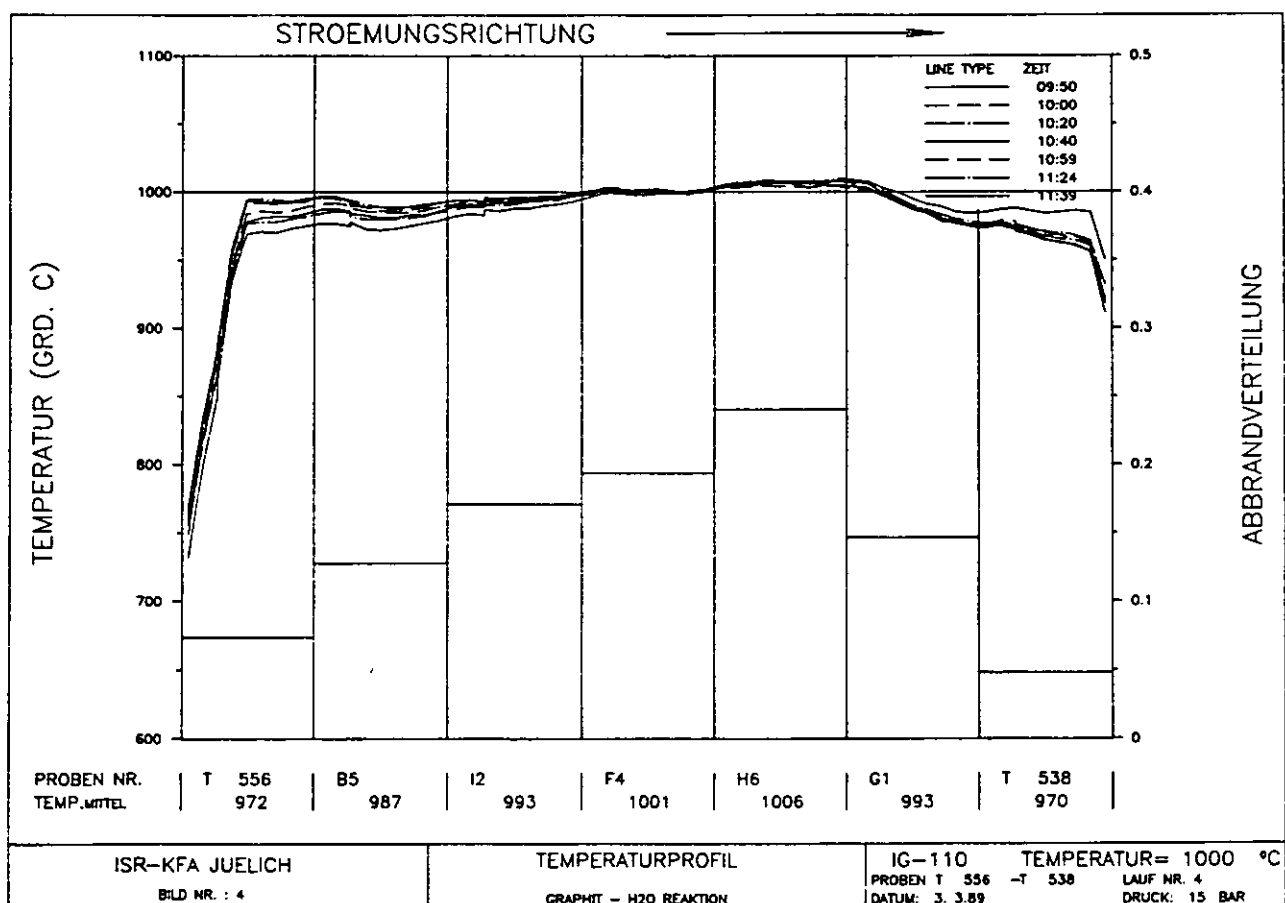


Fig. A.28:

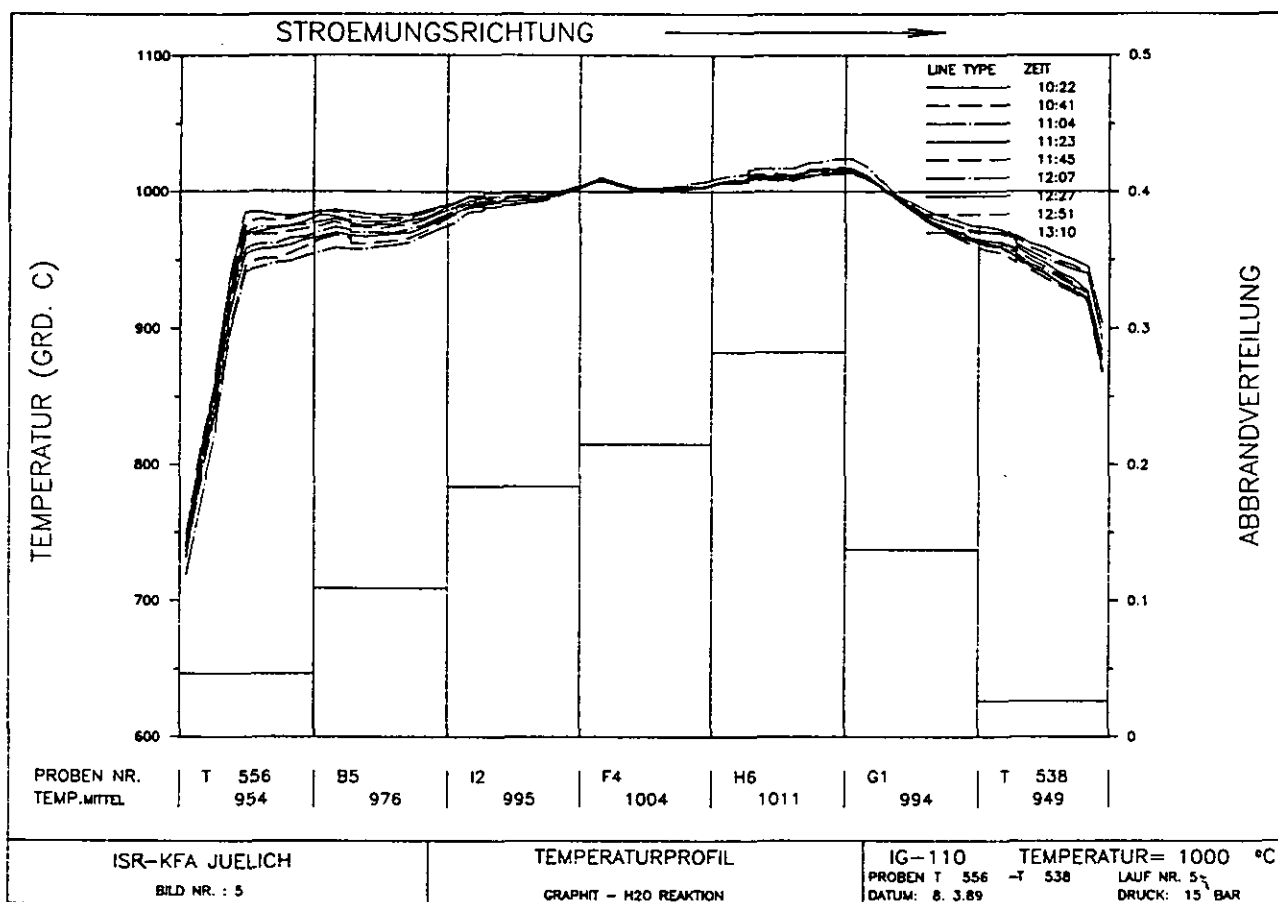


Fig. A.29:

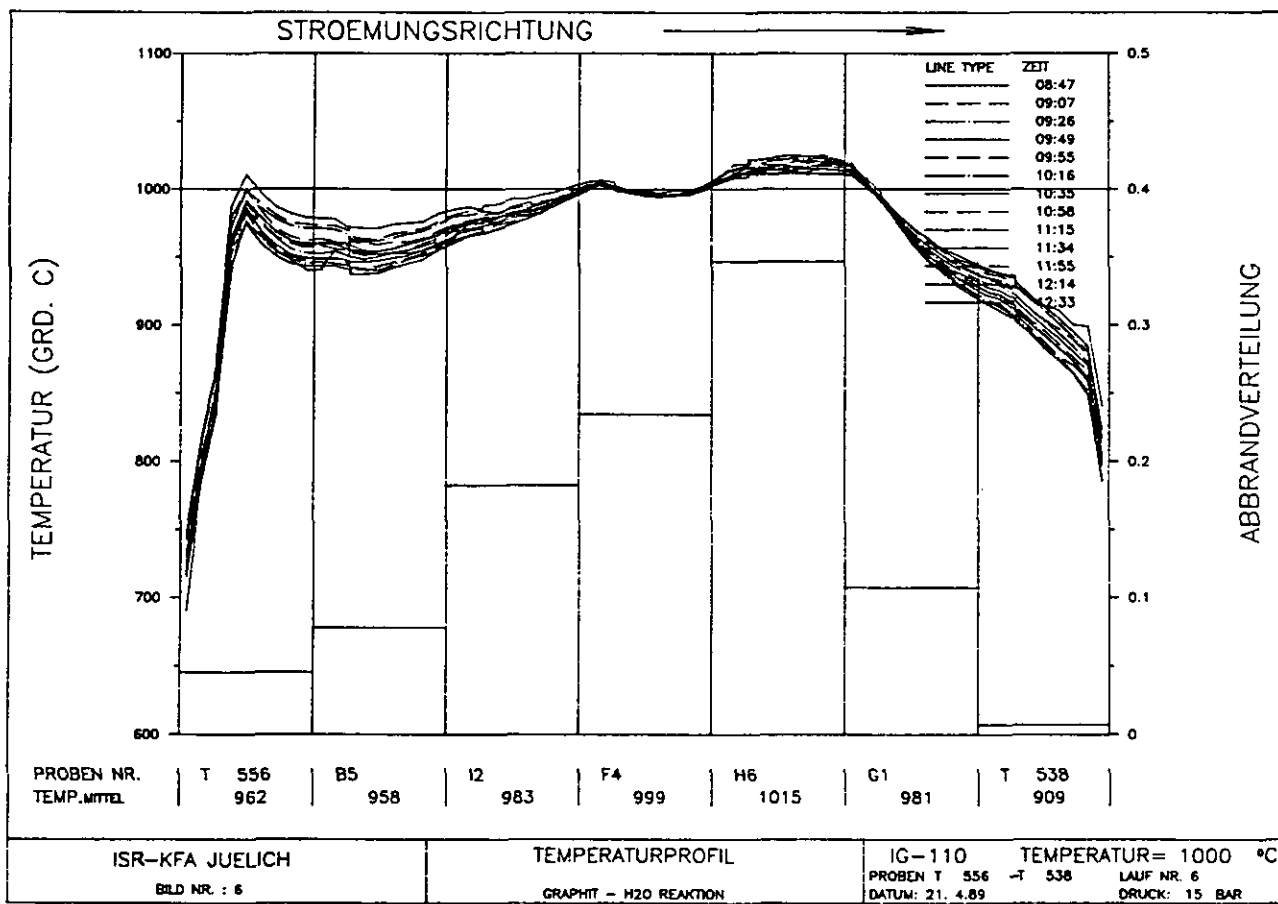


Fig. A.30:

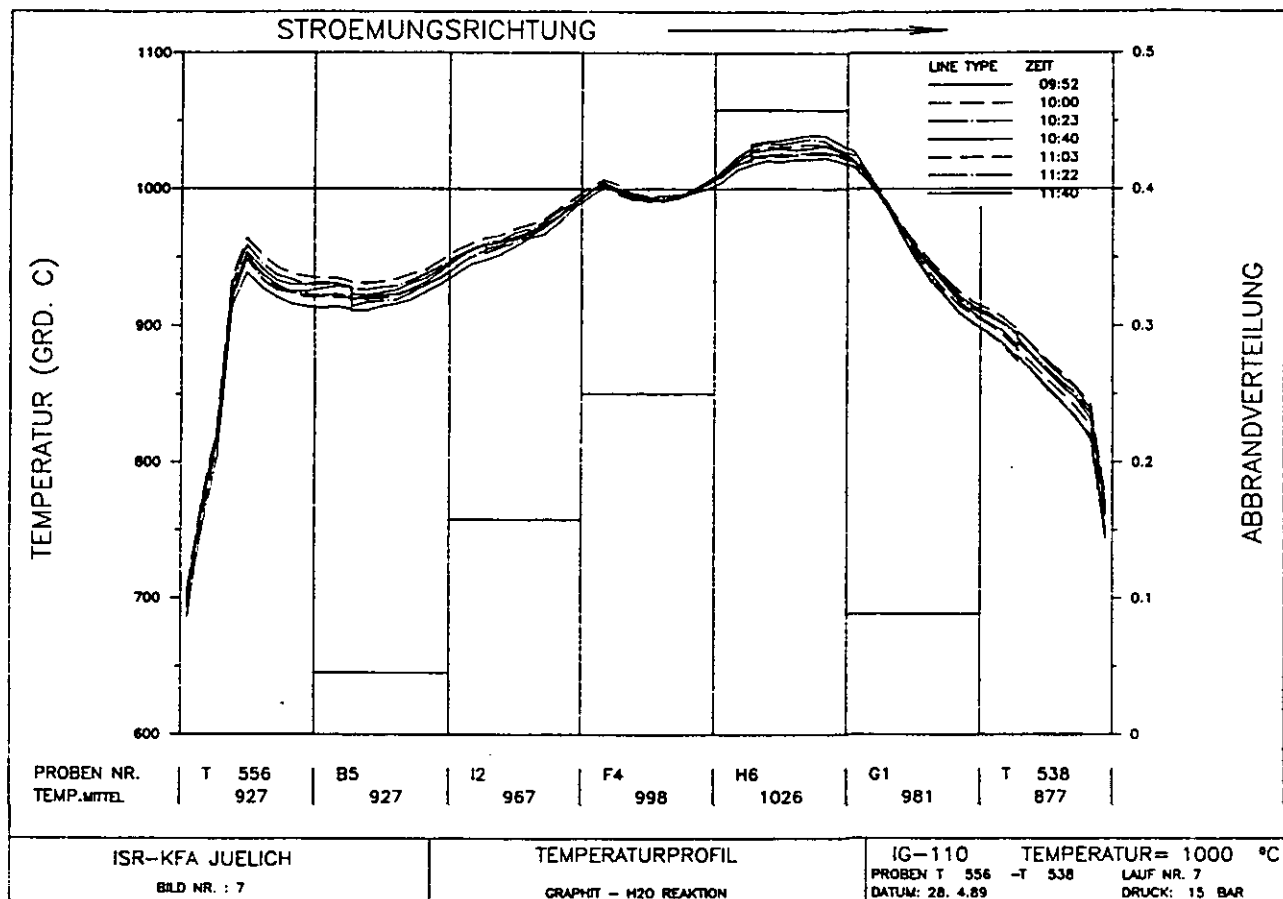


Fig. A.31:

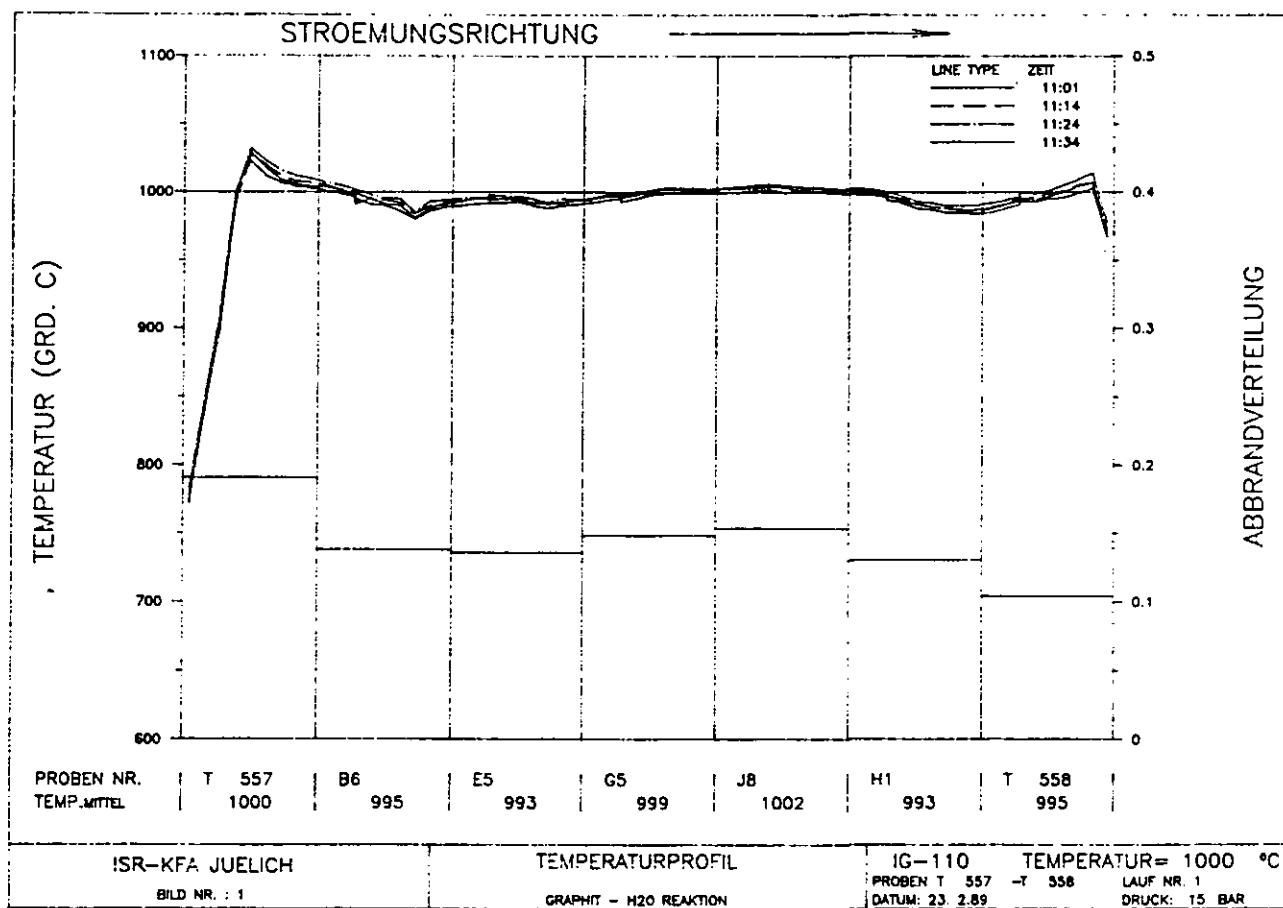


Fig. A.32:

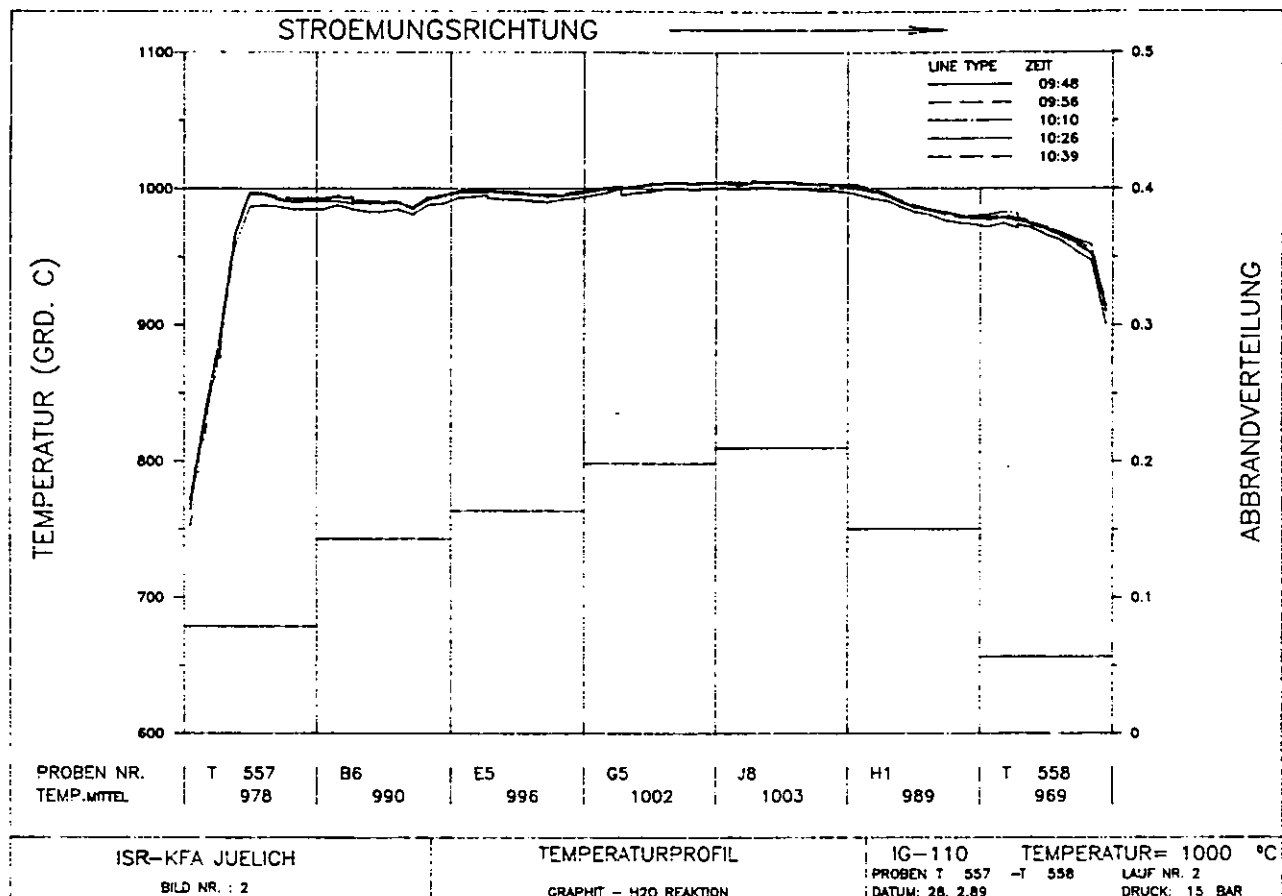


Fig. A.33:

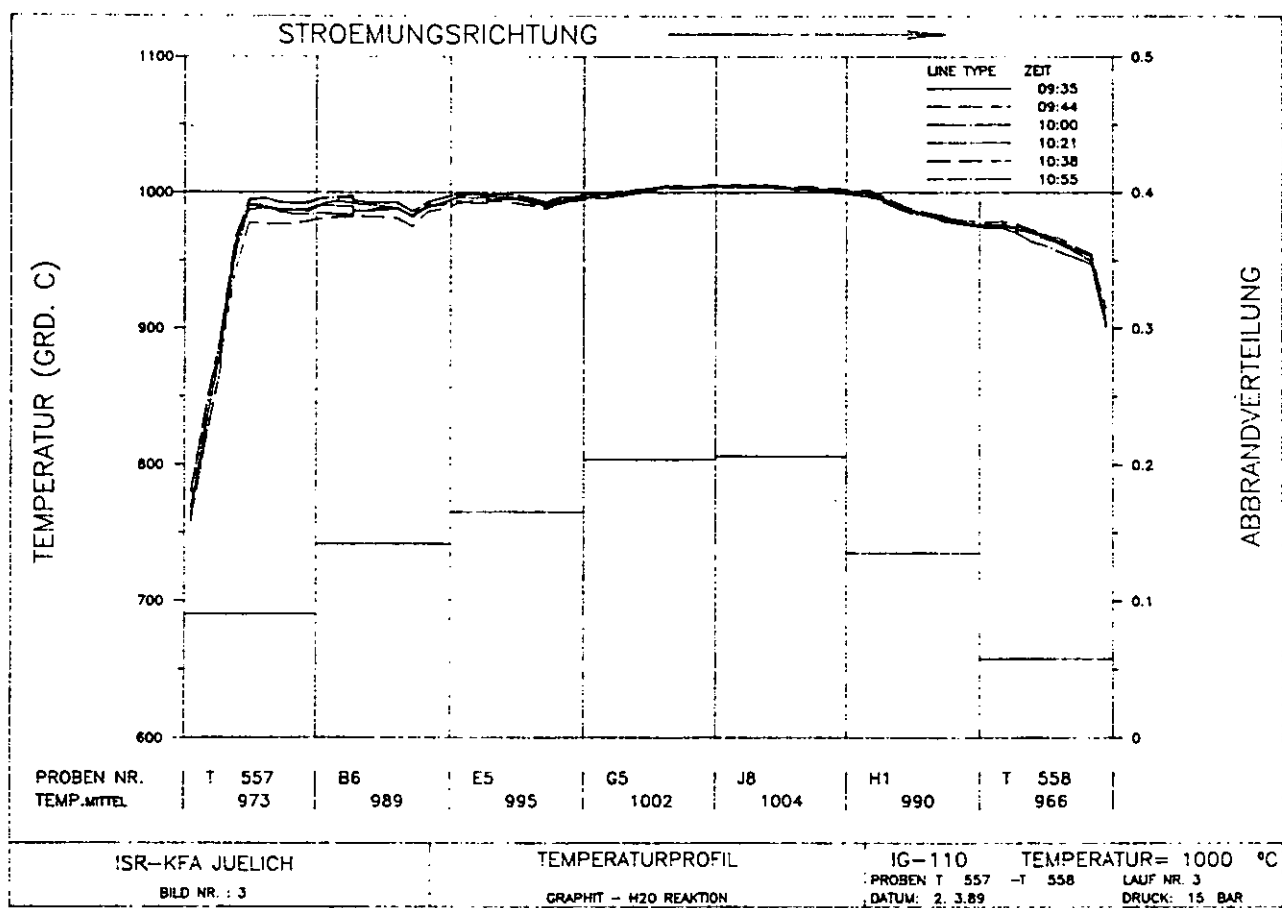


Fig. A.34:

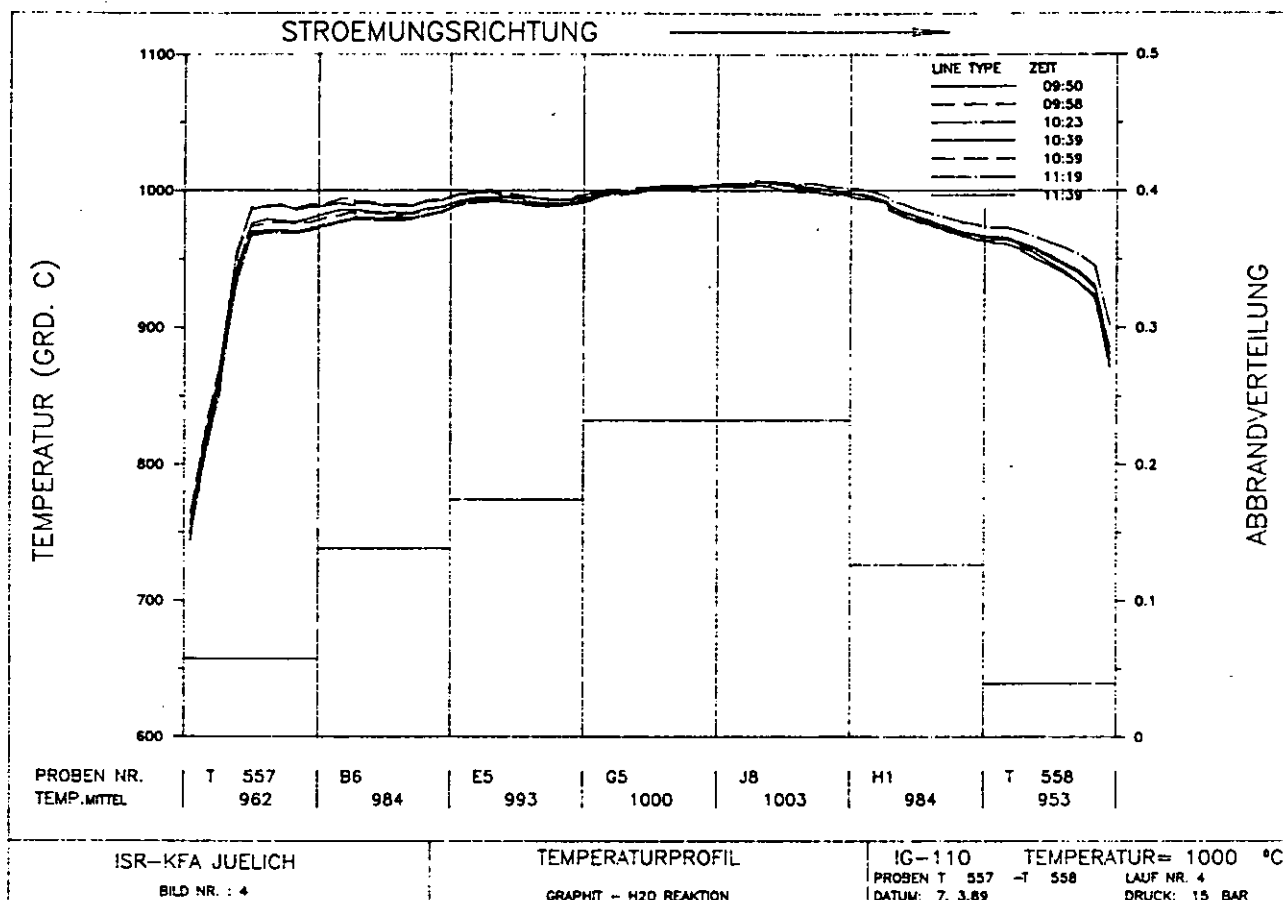


Fig. A.35:

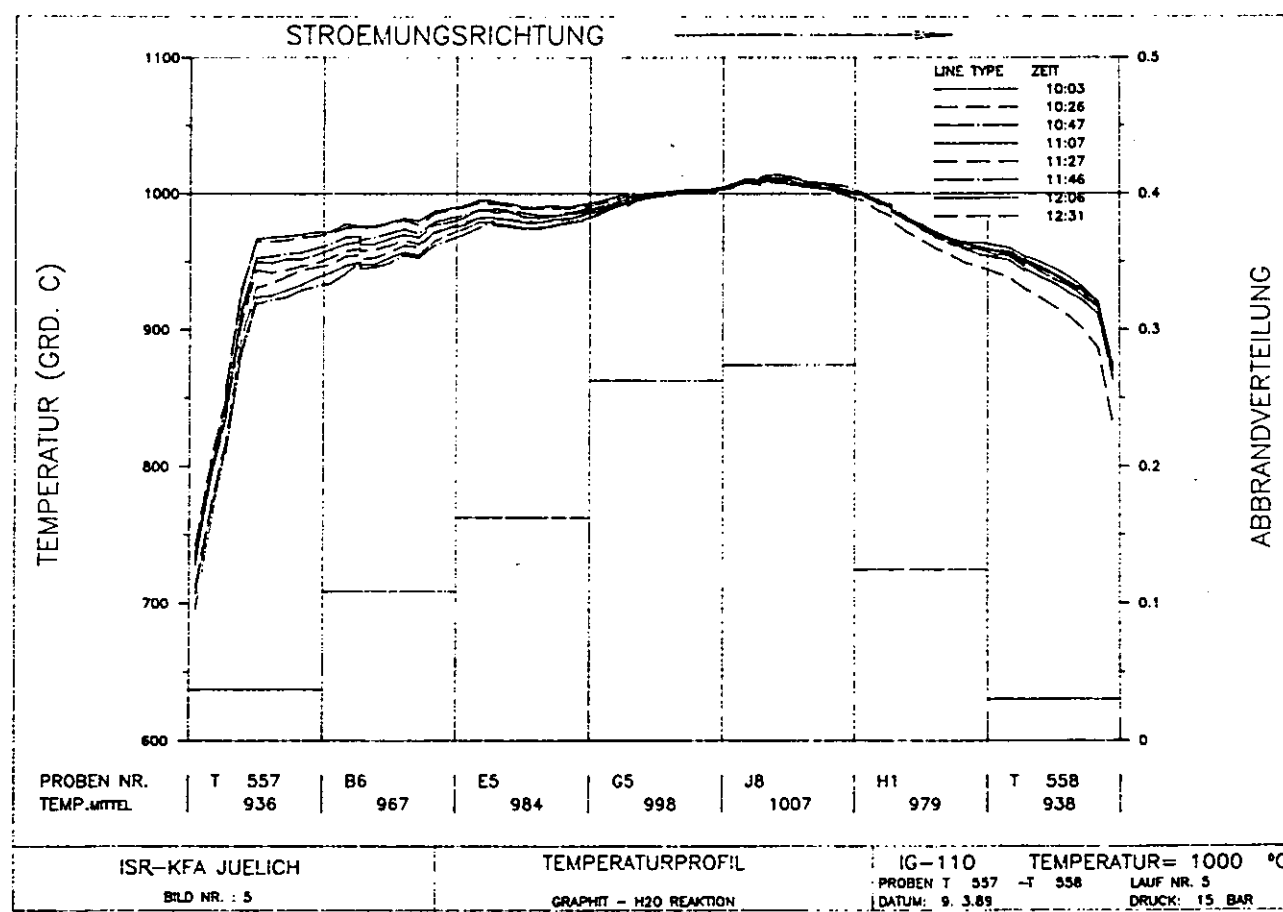


Fig. A.36:

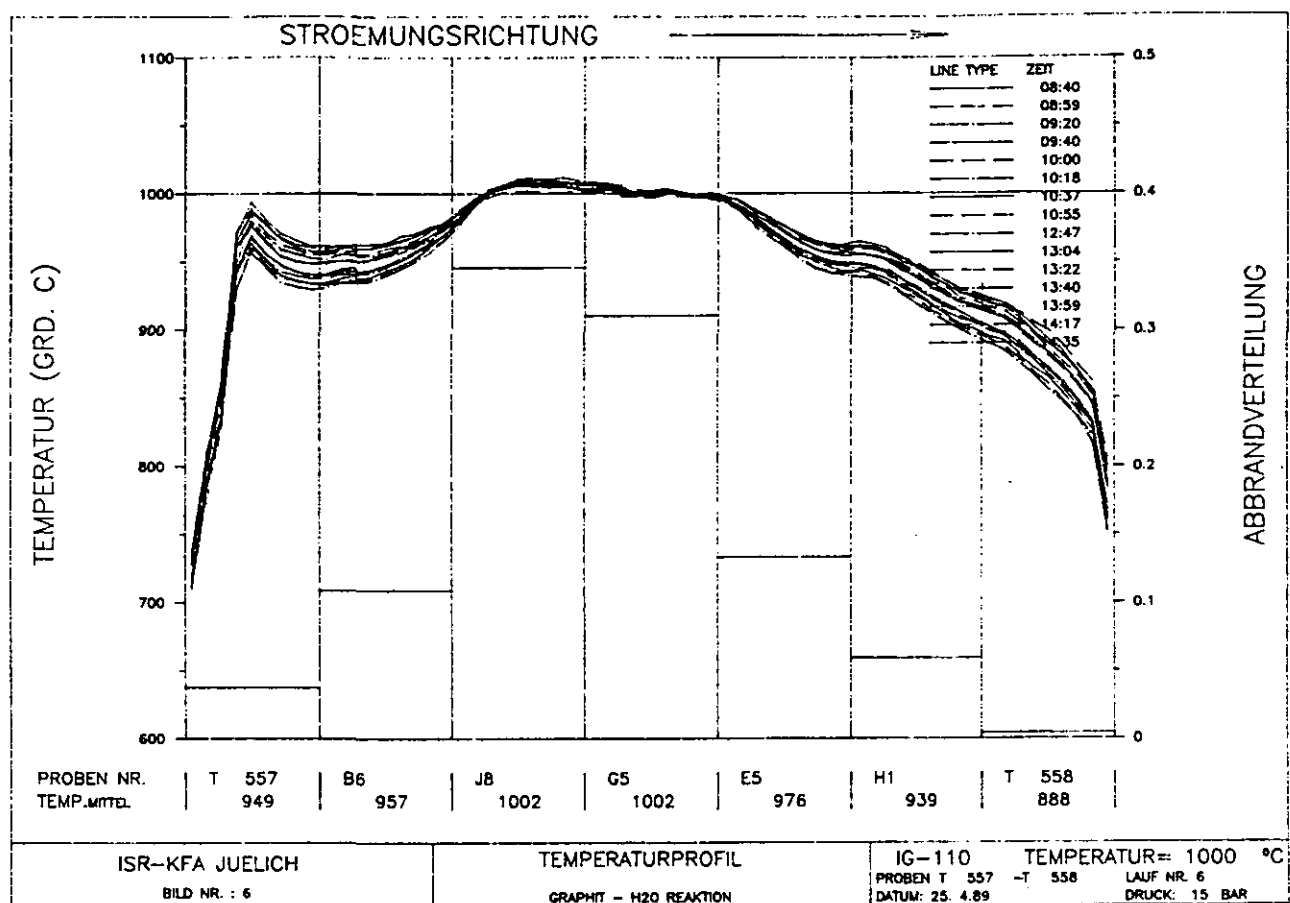
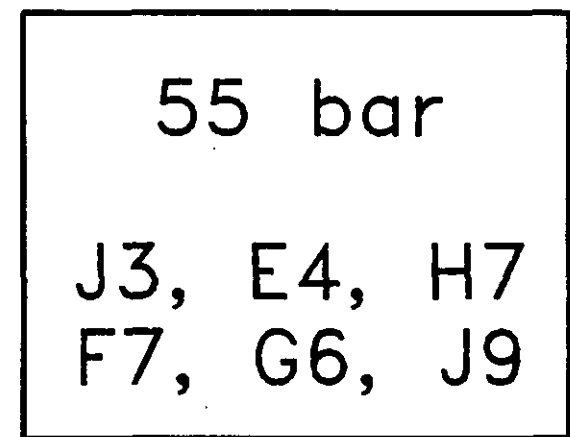


Fig. A.37:



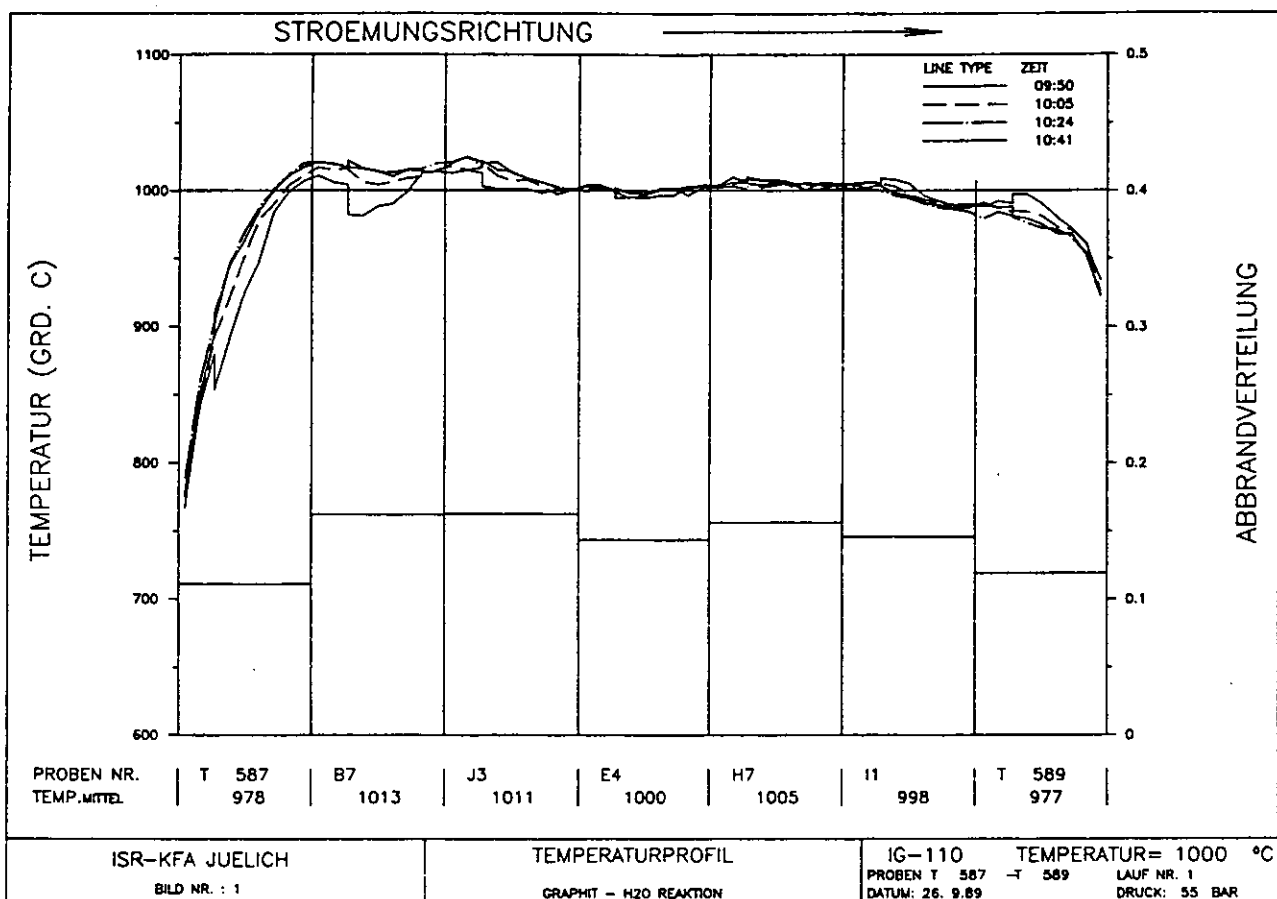


Fig. A.38:

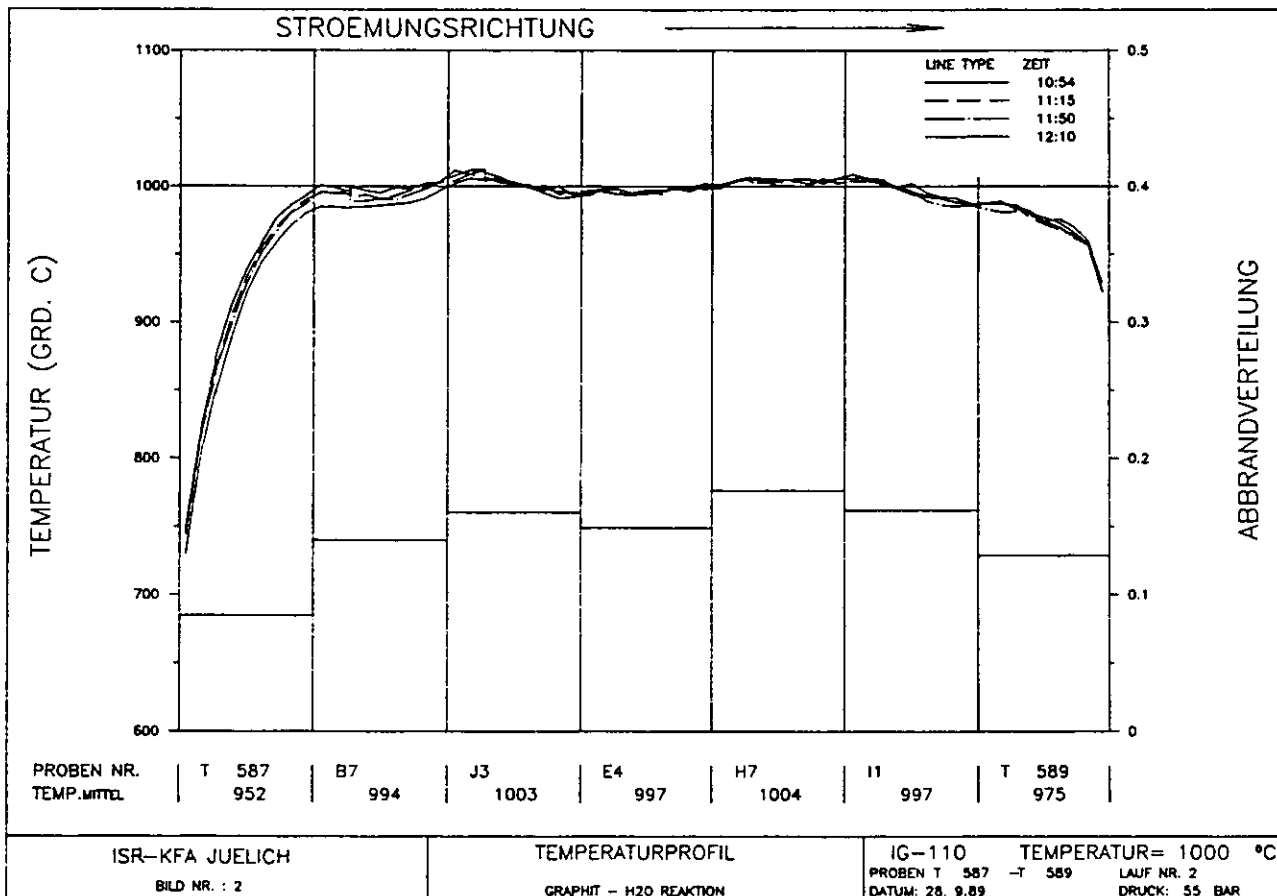


Fig. A.39:

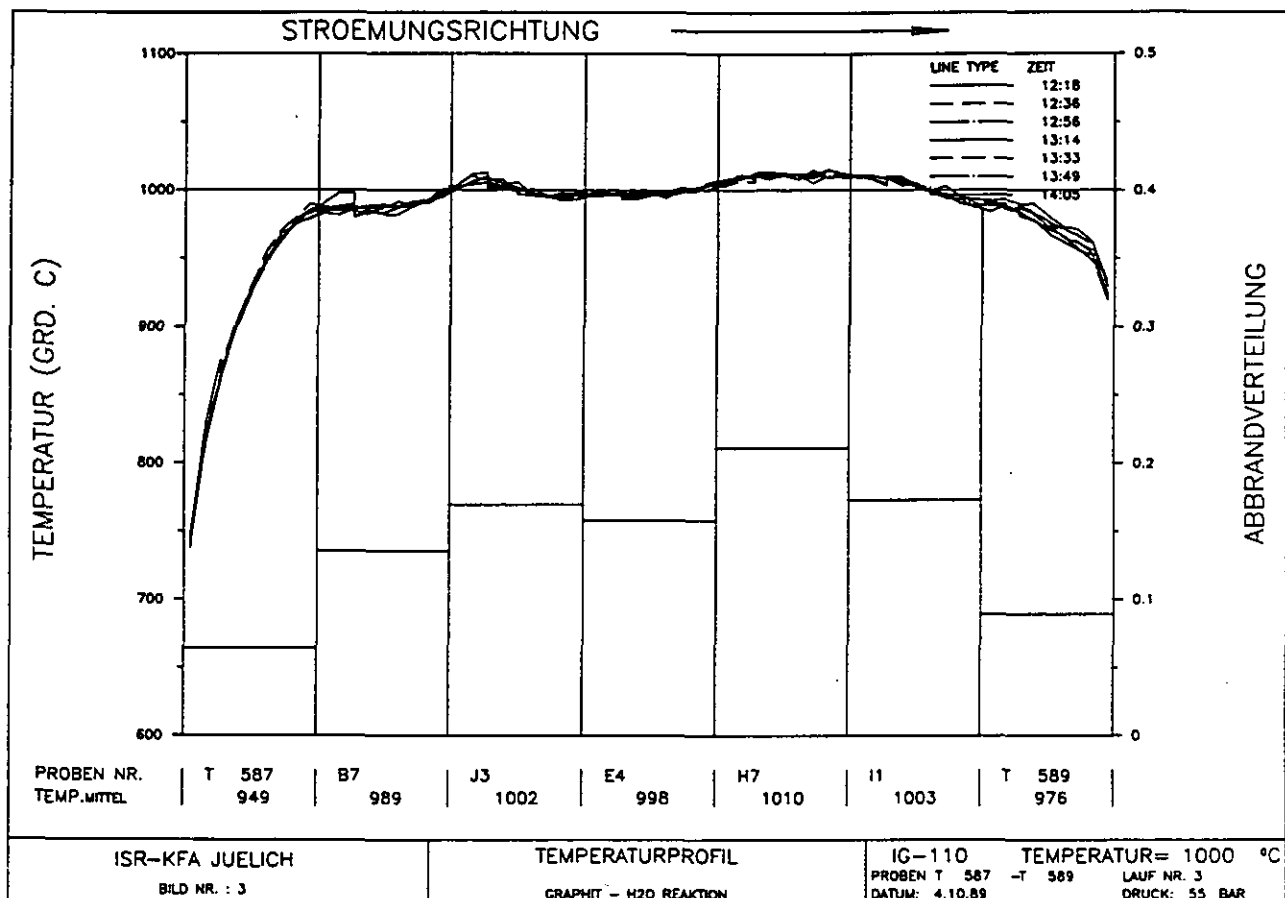


Fig. A.40:

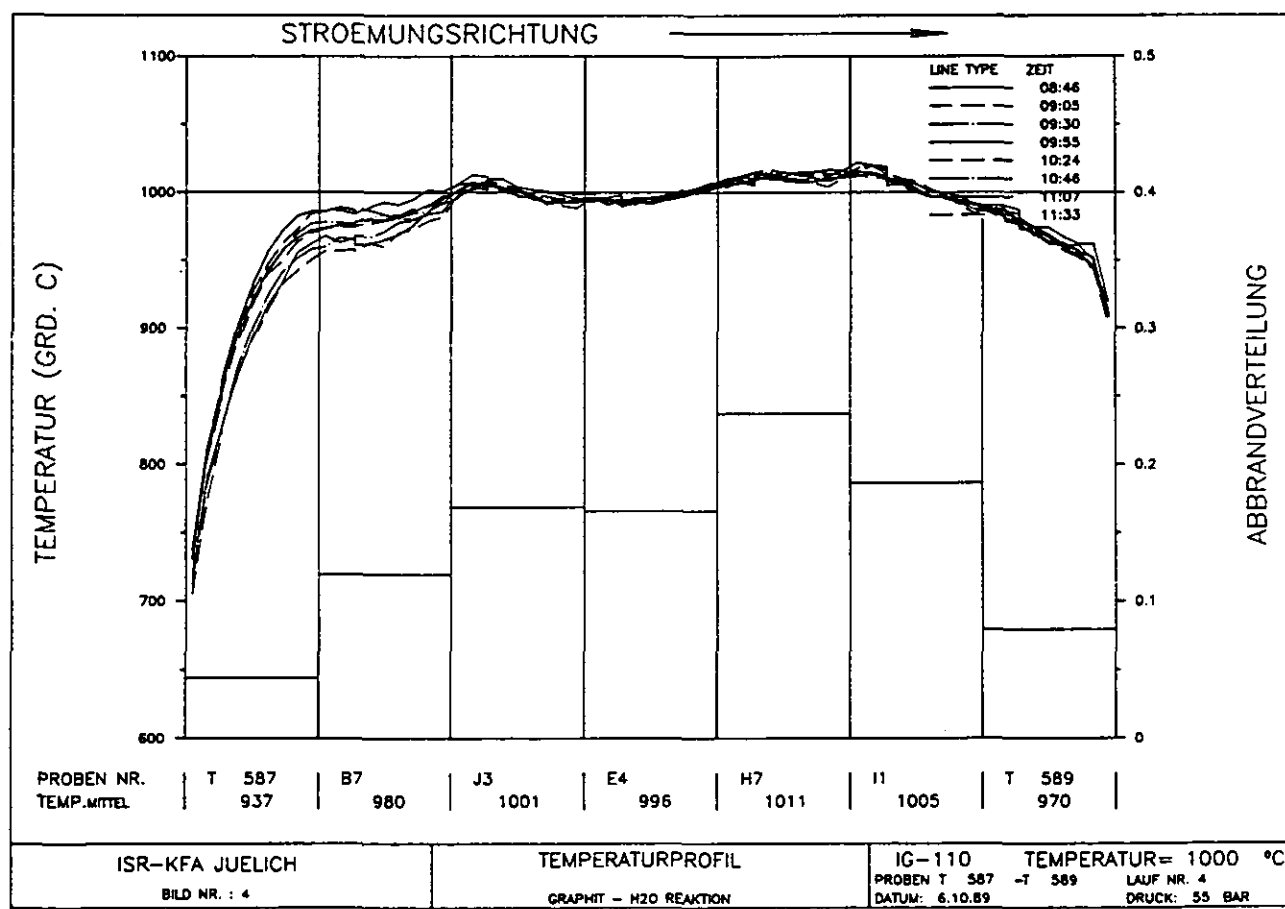


Fig. A.41:

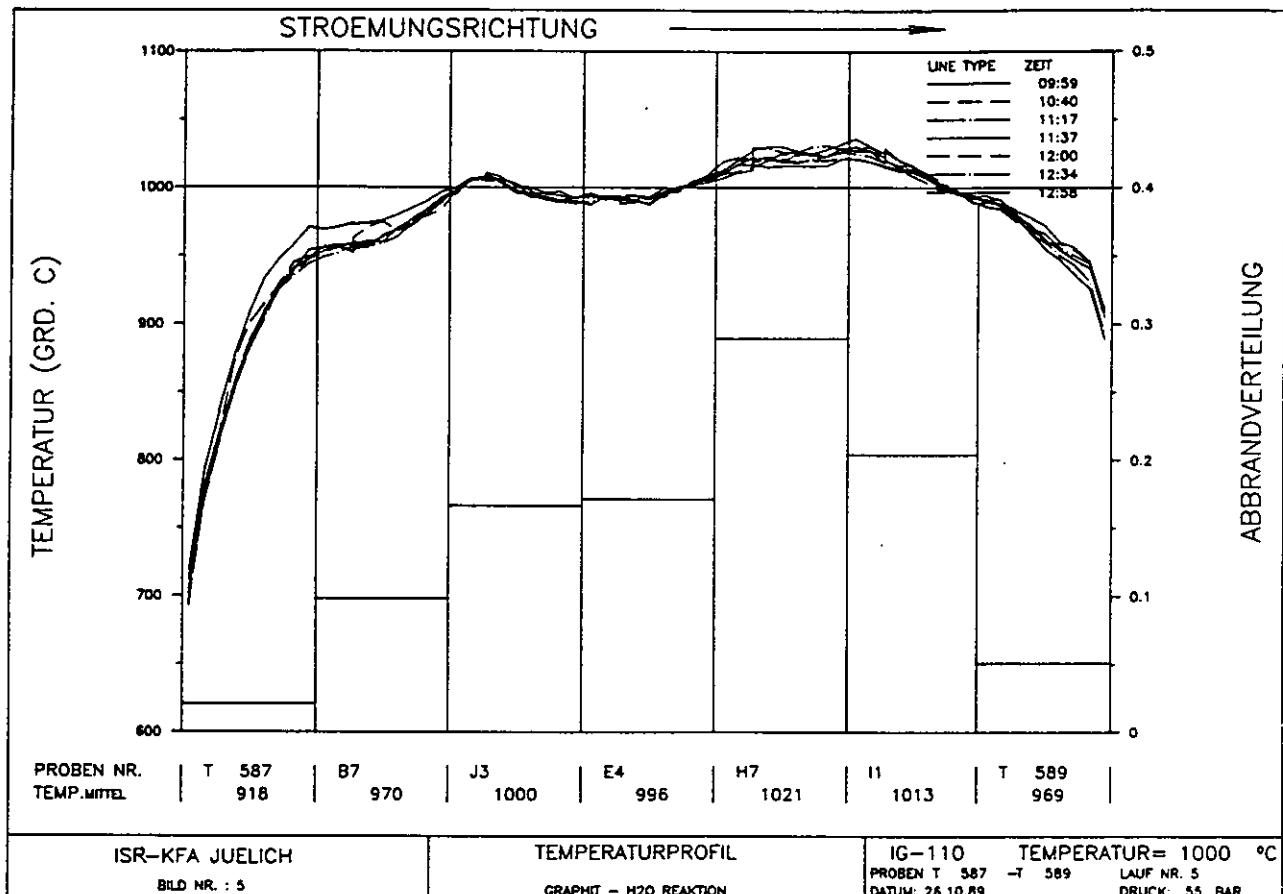


Fig. A.42:

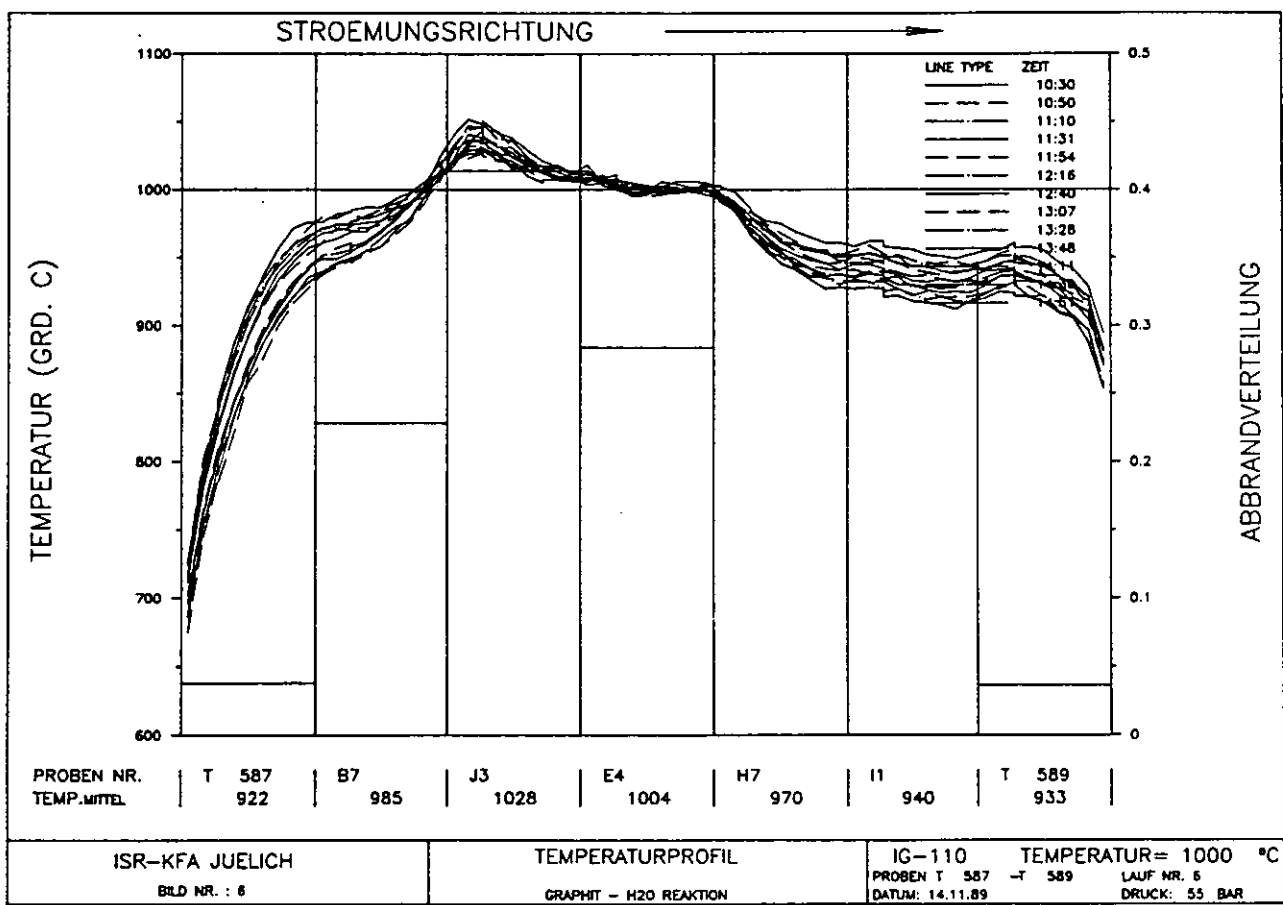


Fig. A.43:

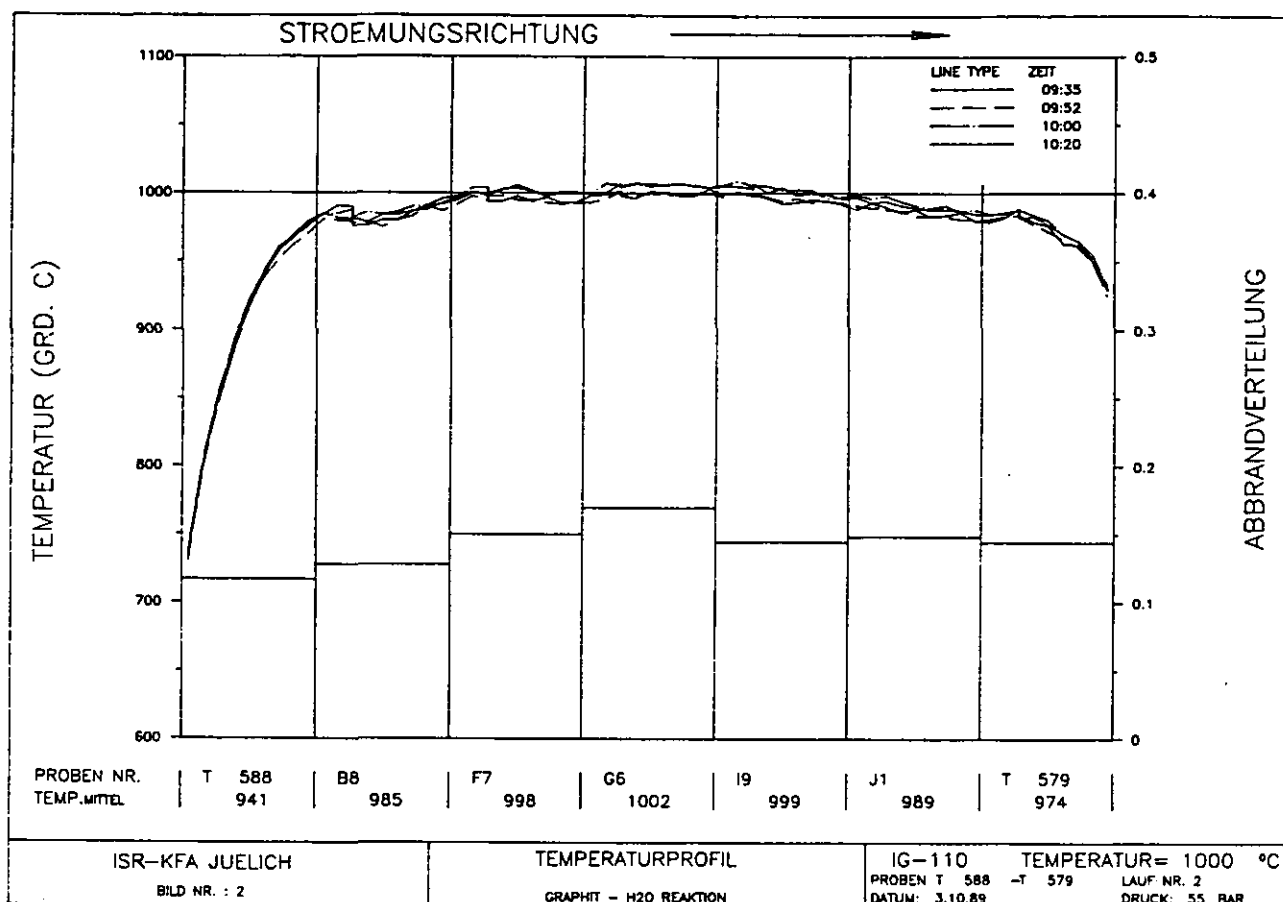


Fig. A.44:

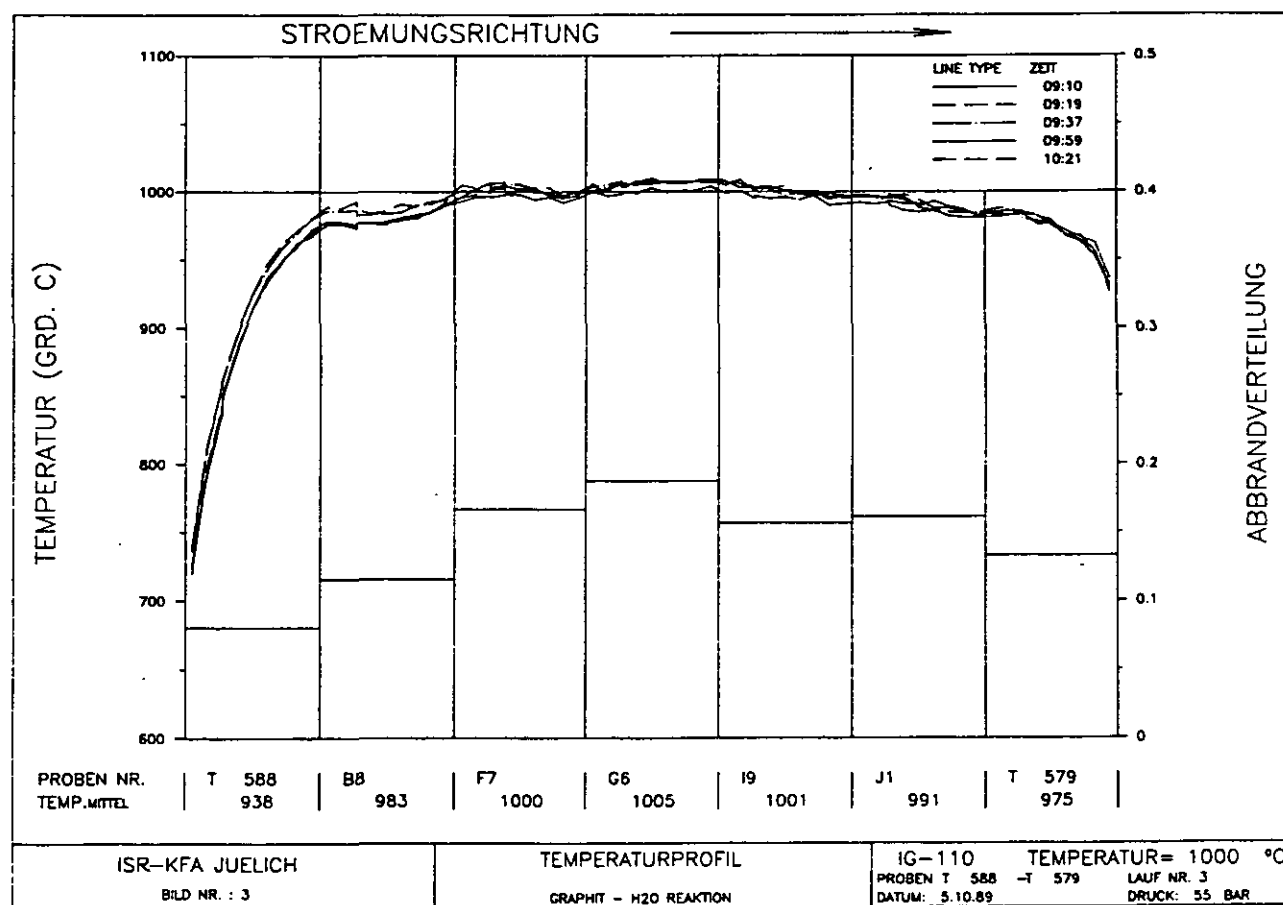


Fig. A.45:

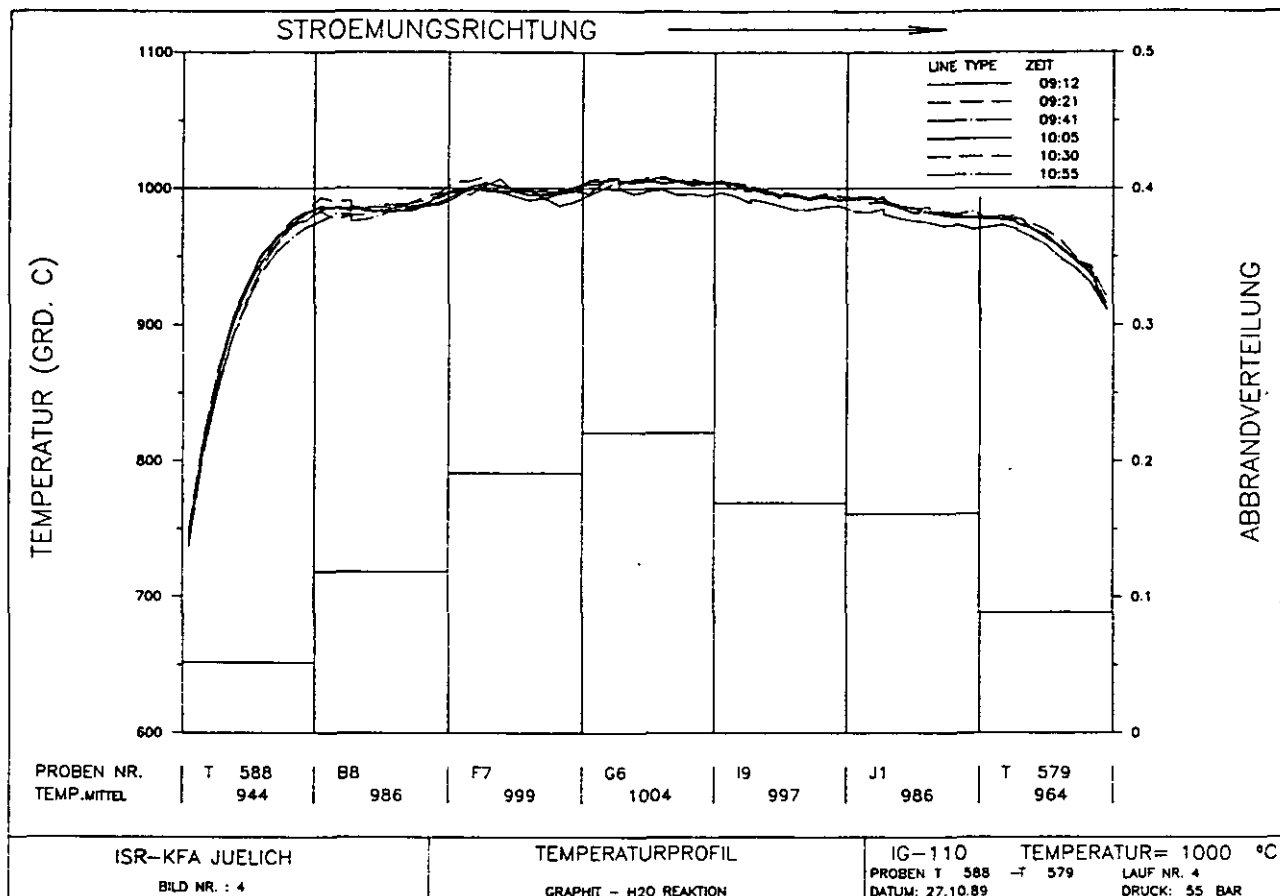


Fig. A.46:

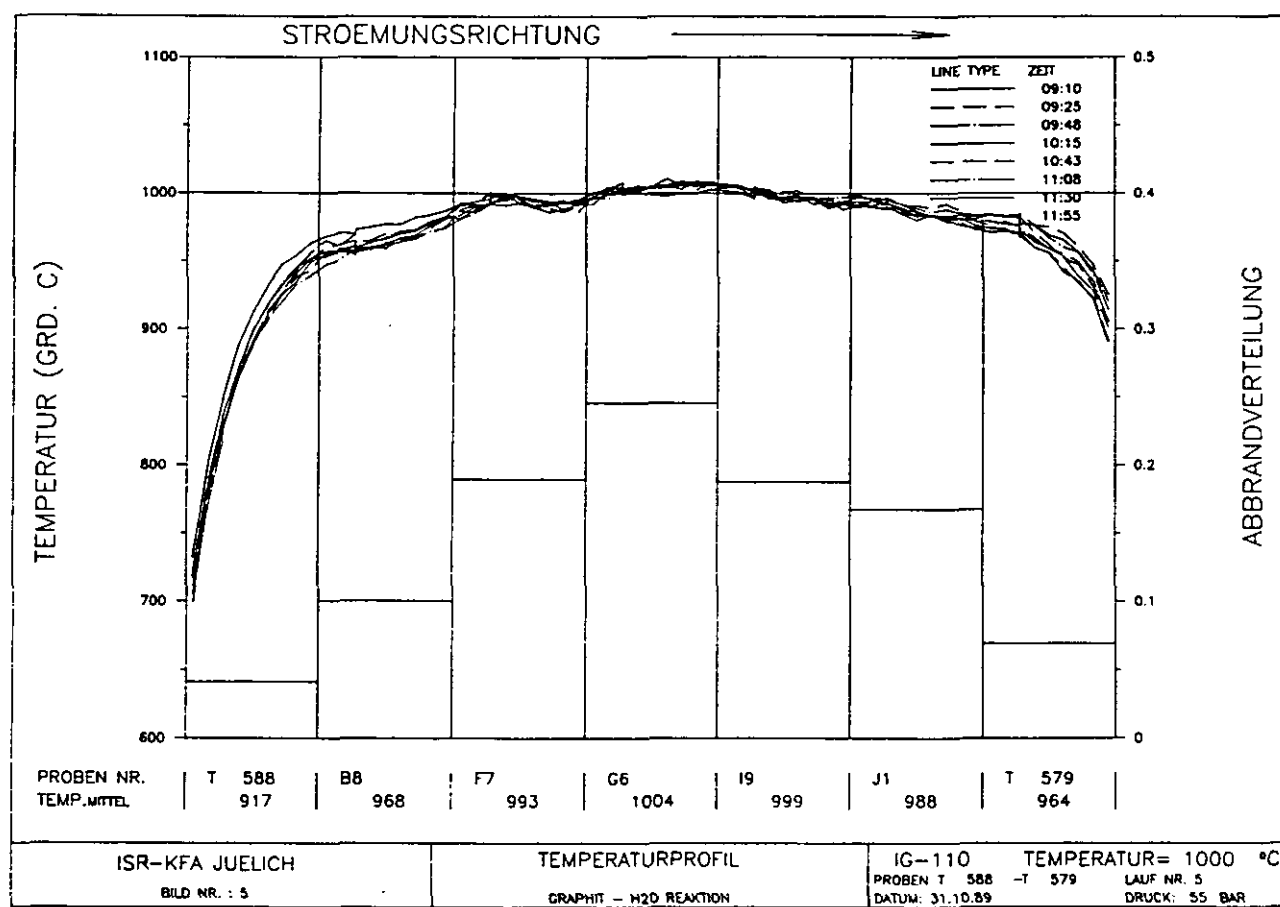


Fig. A.47:

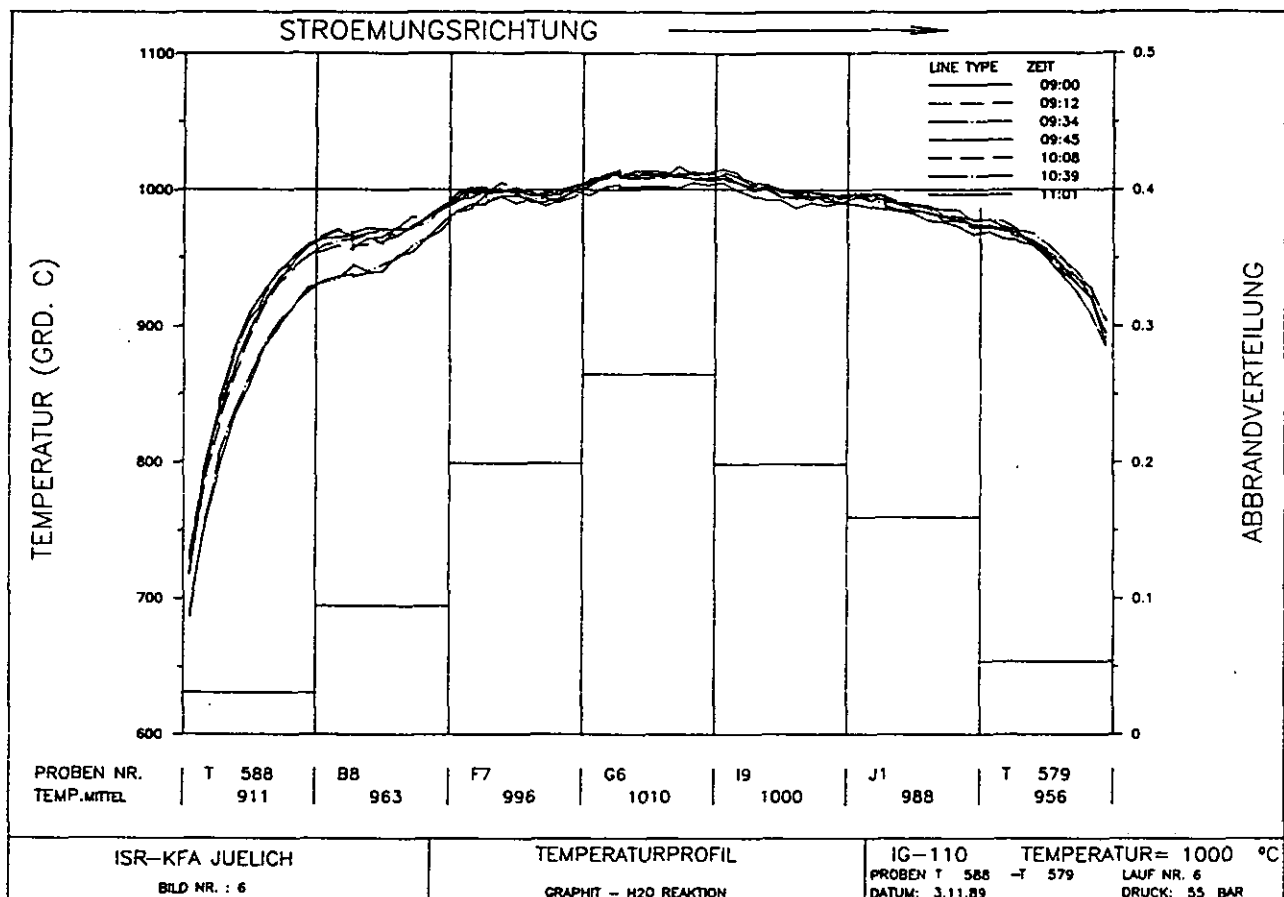


Fig. A.48: